Title
Role of iron oxide concentration and crystallinity on soil carbon distribution and composition

Author
Jin, Lixia

Publication Date
2019

Peer reviewed|Thesis/dissertation

UNIVERSITY OF CALIFORNIA, MERCED

Role of iron oxide concentration and crystallinity on soil carbon distribution and composition

A dissertation submitted in partial satisfaction of the
requirements for the degree of
Doctor of Philosophy

in

Environmental Systems

by

Lixia Jin

Committee in charge:
Professor Asmeret Asefaw Berhe, Chair
Professor Samuel J Traina
Professor Peggy A O`Day
Professor Steven J Hall

2019

The Dissertation of Lixia Jin is approved, and it is acceptable in quality and form for publication on microfilm and electronically:

Samuel J. Traina

Steven J. Hall

Peggy A. O'Day

Asmeret Asefaw Berhe, Chair

University of California, Merced

2019

Dedicated to

my amazing mother, Zhenyu, for inspiring me to be the very best I can be,

my beloved father, Long, for his unconditional trust,

the memory of my best grandparents, Chunzi and Kuifang, for giving me wonderful childhood memories,

my darling husband, Wenjun, for making everything possible,

and

our child, Denian Noah, for giving me hope and strength.

This humble work is my love to you!

TABLE OF CONTENTS

LIST OF TABLES

LIST OF FIGURES

ACKNOWLEDGEMENTS

I am tremendously fortunate to have my Ph.D. advisor, Prof. Asmeret Asefaw Berhe, without whom this piece of work would not be possible. I also greatly acknowledge my committee members, Prof. Peggy O`Day, Prof. Samuel Traina, and Prof. Steven Hall. I thank them for supporting this research and giving such thoughtful feedbacks.

I thank Dr. Fernanda Santos and Dr. Samuel Araya for their assistance with fieldwork. I also thank my colleagues, Prof. Rebecca Abney, Prof. Nate Bogie, Dr. Benjamin Sulman, Dr. Jing Yan, Morgan Barns, Kimber Moreland, Manisha Dolui, and Leila Wahab, with whom we had so many lab days and nights together, hard time together, and celebrated each accomplishment together.

I would like to thank Fredette, Domizio, and Wang families, Xiumin Shang, and Stefanie Helmrich for all of their kindness and encouragement on my life and work at UC Merced.

I would also like to express my gratitude to my M.S. and B.S. advisors, Prof. Yowhan Son, Prof. Haegeun Chung, and Prof. Weihong Zhu, for their professional guidance and advice for my scientific research and life.

This journey would not have been possible without the support of my family. I am especially grateful to Yingshu Jin, who has mentored me throughout my teenage years, and encouraged me in all my pursuits and inspired me to follow my dreams. I deeply thank my first mentor, Prof. Zhenai Zhang, who laid the foundation for my English language skills when I was just a kid.

Finally, I thank with my love to my parents, Zhenyu and Long Jin, my husband, Wenjun Ge, and our child, Denian Noah, for their unconditional trust and timely encouragement.

This work was funded by Startup funds from University of California, Merced, UC Merced Sierra Nevada Research Institute Seed Grant, and NSF award to Prof. Asmeret Asefaw Berhe (CAREER, EAR-1352627). Funding was also provided by Senate Research Grant to Profs. Berhe, Traina, and O'Day.

CURRICULUM VITAE

LIXIA JIN
School of Engineering, Environmental systems
University of California, Merced
5200 N. Lake Rd, Merced, CA, USA
kimryeoha@gmail.com; ljin3@ucmerced.edu

EDUCATION

2013-2019 **Ph.D.** in Environmental Systems, University of California, Merced, USA
Dissertation: Role of iron oxides concentrations and crystallinity on soil carbon storage and stability
Advisor: Dr. Asmeret Asefaw Berhe

2010-2012 **M.S.** in Division of Environmental Science and Ecological Engineering, Korea University, Korea
Thesis: Impact of single-walled carbon nanotubes on the soil enzyme activity and microbial biomass
Advisor: Dr. Yowhan Son

2006-2010 **B.S.** in Department of Geography, Yanbian University, China
Thesis: Changes of wetland soil nutrients along the environmental gradient in Changbai Mountain, China
Advisor: Dr. Weihong Zhu

2008-2010 **B.E.** in Department of Economics, Yanbian University, China
Double Degree

PROFESSIONAL EXPERIENCE

2012-2013 **Research fellow** - Department of Environmental Engineering, Konkuk University, Korea
Research title: Evaluation of environmental impacts of carbon nanotubes on soil ecosystem functions
Research advisor: Prof. Haegeun Chung

PUBLICATIONS

Abney, R. B., **Jin, L.** and Berhe, A. A. (2019). Soil properties and combustion temperature: Controls on the decomposition rate of pyrogenic organic matter. CATENA, 182, 104127.

Santos, F., Abney, R., Barnes, M., Bogie, N., Ghezzehei, T. A., **Jin, L.**, Moreland, K., Sulman, B. and Berhe, A. A. (2019). The role of the physical properties of soil in

determining biogeochemical responses to soil warming. In Ecosystem Consequences of Soil Warming (pp. 209-244). Academic Press.

Berhe, A. A., Arnold, C., **Jin, L.**, Kaiser, M. and Lever, R. 2017. Carbon Dynamics. In Oxford Bibliographies in Environmental Science. Ed. Ellen Wohl. New York: Oxford University Press.

Jin, L., Son, Y., DeForest J.L., Kang, Y.J., Kim, W. and Chung, H. 2014. Single-walled carbon nanotubes alter soil microbial community composition. Science of the Total Environment, 466-467, 533-538.

Jin, L., Son, Y., Yoon, T.K., Kang, Y.J., Kim, W. and Chung, H. 2013. High concentrations of single-walled carbon nanotubes lower soil enzyme activity and microbial biomass. Ecotoxicology and Environmental Safety, 88, 9-15.

- ***Highlighted article in Ecotoxicology and Environmental Safety***
- ***Featured in:***
  Life Science Weekly, "Studies from Korea University in the Area of Nanotechnology Described", January 15, 2013, page 493.

Park, C.W., Ko, S., Yoon, T.K., Han, S., Yi, K., Jo, W., **Jin, L.**, Lee, S.J., Noh, N.J., Chung, H. and Son, Y. 2012. Differences in soil aggregate, microbial biomass carbon concentration, and soil carbon between *Pinus rigida* and *Larix kaempferi* plantations in Yangpyeong, central Korea. Forest Science and Technology, 8, 38-46.

Jo, W., Son, Y., Chung, H., Noh, N.J., Yoon, T.K., Han, S., Lee, S.J., Lee, S.K., Yi, K. and **Jin, L.** 2011. Note: Effect of artificial warming on chlorophyll contents and net photosynthetic rate of *Quercus variabilis* seedlings in an open-field experiment. Journal of Korean Forest Society, 100, 733-737. (*in Korean with English abstract*)

Manuscript in preparation

Jin, L., O`Day, P. and Berhe, A. A. (*Expected submission in 2019*). Role of iron oxides on physical protection of soil organic matter inside aggregates.

Jin, L. and Berhe, A. A. (*Expected submission in 2019*). Characterization of organic matter in pedogenic iron-containing mineral fractions: Effect of iron phase crystallinity.

Jin, L., O`Day, P., Traina, S. and Berhe, A. A. (*Expected submission in 2019*). (De)sorption of soil organic matter by mineral soils with varying iron oxide concentrations.

Jin, L. and Berhe, A. A. (*Expected submission in 2019*). Iron oxide promotes soil organic matter storage in soil systems with varying weathering intensity-a review.

CONFERENCE PRESENTATIONS

Jin, L. and Berhe, A.A. Characterization of organic matter in pedogenic iron-containing mineral fractions: Effect of iron phase crystallinity. *Soil Science Society of America Annual Meeting 2019, San Antonio, Texas, USA, November 10-13, 2019.*

Jin, L. and Berhe, A.A. Effects of pedogenic Fe oxides on soil aggregate-associated carbon. *American Geophysical Union Fall Meeting 2017, New Orleans, Florida, USA, December 11-15, 2017.*

Abney, R., **Jin, L.** and Berhe, A.A. Landform position and combustion temperature as controls of decomposition of pyrogenic organic matter. *American Geophysical Union Fall Meeting 2016, San Francisco, California, USA,* December 12-16, 2016.

Jin, L. and Berhe, A.A. Stabilization of Organic Matter by Interactions with Iron Oxides: Relative Importance of Sorption vs. Aggregation. *American Geophysical Union Fall Meeting 2015, San Francisco, California, USA,* December 14-18, 2015.

Jin, L., Son, Y., Yoon, T.K., Kang, Y.J., Kim, W. and Chung, H. Surface-area-dependent effects of carbon nanotubes on soil enzyme activity and microbial biomass. *The Fourteenth International Conference on the Science and Application of Nanotubes, Aalto University, Espoo, Finland,* June 24-28, 2013.

Jin, L., Son, Y., DeForest J., Kang, Y.J., Kim W. and Chung, H. The impacts of single-walled carbon nanotubes on soil microbial communicaties. *The Fourteenth International Conference on the Science and Application of Nanotubes, Aalto University, Espoo, Finland,* June 24-28, 2013.

Jin, L., Chung, H., Son, Y., Noh, N.J., Yoon, T.K., Han, S., Jo, W., Yi, K. and Kang, Y.J. Effects of single-walled carbon nanotubes on soil microbial activities. *American Geophysical Union Fall Meeting 2011, San Francisco, California, USA,* December 5-9, 2011.

Jin, L., Chung, H. and Son, Y. Determining the soil microbial responses to single-walled carbon nanotubes. *The 66th Annual Meeting of the Korean Association of Biological Sciences, Chuncheon, Gangwon, Korea,* August 18-19, 2011.

Son, Y., Jo, W., Chung, H., Noh, N.J., Lee, S.K., Yoon, T.K., Yi, K. and **Jin, L.** Short-term effect of experimental warming on soil environment surrounding oak and pine seedlings. *The 58th Annual Meeting of the Ecological Society of Japan, Hokkaido, Sapporo, Japan,* March 8-12, 2011.

TEACHING EXPERIENCE

2013-2018 **UC Merced Teaching Assistant**
Contemporary Biology
General chemistry
Fundamentals of soil science (grader)

2013 **KU Lab Instructor**
Environmental Chemistry (taught in English)

2010-2011 **Science Camp Lab Instructor**
Teaching a method to determine of chlorophyll content of leaves for elementary school students

ACADEMIC AWARDS

2016-2017 **Academic Senate Research Grant**
University of California, Merced

2013-2019 **Environmental Systems Bobcat Awards**
University of California, Merced

2010-2012 **Foreign Student Scholarship**
Korea University, Seoul, Korea

2009 **Overseas Korean Scholarship**
Overseas Korean Foundation, Seoul, Korea

PREFERENTIAL AFFILIATION AND SERVICES

American Geophysical Union
Soil Science Society of America
Earth Science Women's Network
Peer reviewer for Journal of Mountain Science

ABSTRACT

Role of iron oxide concentration and crystallinity
on soil carbon distribution and composition

by

Lixia Jin

Doctor of Philosophy in Environmental Systems

University of California, Merced, 2019

Asmeret Asefaw Berhe - Chair

Pedogenic iron (Fe) oxides are important soil minerals that contribute to carbon (C) storage and stability in weathering soils around the world. Soil organic matter (SOM) associated with pedogenic Fe can persist in the soil systems for varying amount of time depending on Fe oxide crystallinity and concentration, chemical composition of SOM, and soil aggregation status. However, questions remain as to can the relationship between pedogenic Fe oxides and soil C storage be generalized in global scale, or how Fe oxide distribution in the soil profile responds to long-term processes of soil development and/or short-term exposure to changes in environmental conditions. Therefore, in this dissertation I addressed four research questions regarding the role of Fe oxides on soil carbon storage, distribution, and composition. First, I synthesized data from 15 representative studies conducted in soil systems with different weathering intensity to reveal the general relationships between pedogenic Fe oxides and soil development, and implications for soil C storage in variety of environments globally. Second, I evaluated the associations of Fe in different extractable pools of soil with C in distinct aggregate size classes along depth profiles in a landscape scale to evaluate the crystallinity of Fe oxides on distribution of SOM within soil aggregates. Third, I further determined the relationship of pedogenic Fe oxide crystallinity and chemical composition of C that is physically protected in soil aggregates. Finally, I evaluated the effects of Fe oxides concentrations on chemical vs. physical stabilization of SOM using sorption and desorption experiments with and without ultrasonication to determine the capacity of Fe oxides to selectively stabilize different organic C functional groups. My results show that Fe oxide concentrations and its crystallinity reflect soil weathering intensity and demonstrates a close relationship with soil C storage under a variety of soil types, including weakly weathered soils. At the landscape scale, I also found that pedogenic Fe oxides and amount of physically occluded SOM were closely related, where Fe oxides with varying crystallinity was distributed differently along soil aggregate size range. Preferential retention of different organic functional groups in pedogenic Fe oxides containing fraction was also observed. My results contribute to the growing body of literature that is highlighting the role of Fe oxides on soil C storage and stabilization in systems at varying stages of soil development (weathering environments) globally.

CHAPTER 1. INTRODUCTION: HOW DOES FE OXIDE PROMOTE SOIL ORGANIC MATTER STORAGE IN SOIL SYSTEMS WITH VARYING WEATHERING INTENSITY?

ABSTRACT

Strong relationship between pedogenic Fe oxides and soil C storage is often found in varying natural systems. However, we still have gaps in our understanding of how important pedogenic Fe oxides are for soil C storage in a global scale? In this review, we gathered data from 15 representative studies conducted in soil systems with different weathering intensity to determine the importance of Fe oxides on soil carbon storage. Sodium dithionite extractable total pedogenic Fe oxide concentrations increased from 4.15 g kg^{-1} in least weathered Entisol to 155.09 g kg^{-1} in most weathered Oxisol. The relative contribution of ammonium oxalate extractable poorly crystalline Fe oxides to total pedogenic Fe oxides decreased from 0.65 in least weathered Entisol to 0.08 in most weathered Oxisol. Total pedogenic Fe oxide concentration and Fe oxide crystallinity increased with soils from Entisol to Oxisol. Fe crystallinity also increased as total Fe oxide concentrations increased. Poorly crystalline Fe oxide concentrations increased with soil C content across varying environmental conditions. My dissertation research confirms that Fe oxide concentration and its crystallinity reflect soil weathering intensity, where poorly crystalline Fe oxides may play particularly important roles in soil C storage through their influences on chemical and physical stabilization of organic matter in soil.

1.1. INTRODUCTION

The soil system plays an important role in global C cycle as soil organic matter (SOM) represents the largest terrestrial carbon pool storing over 2700 Gt (Gt = 10^{15}g), more than twice the amount of carbon stored in the atmosphere (760 gigatons) and biosphere (560 gigatons) combined (Le Quere et al., 2018). Because of its large stock of C, small changes in SOM stock may affect atmospheric carbon dioxide concentrations and further influence the global climate (Lutzow et al., 2006; Stockmann et al., 2013). Associations between mineral and soil organic matter (SOM) have been intensively studied to understand their role on long-term SOM stabilization (Torn et al., 1997; Lutzow et al., 2006; Jastrow et al., 2007; Moni et al., 2010; Schmidt et al., 2011; Stockmann et al., 2013; Totsche et al., 2018).

Metal oxides play particularly important role by providing sorptive surfaces for SOM, and their important roles on soil C storage has been demonstrated in variety of soil and sediment systems (e.g. Dahlgren et al., 1997; Kaiser et al., 1997; Torn et al., 1997; Eusterhues et al., 2003; Lilienfein et al., 2003; Wagai and Mayer, 2007; Mikutta et al., 2006 and 2009; Moni et al., 2010; Sollins et al., 2009; Berhe et al., 2012; Lalonde et al., 2012; Wagai et al., 2013; Feng et al., 2014; Zhao et al., 2016; Coward et al., 2018a and 2018b; Hall et al., 2018; Heckman et al., 2018; Jin et al., chapter 2). However, question remains as to what extent the relationship between pedogenic Fe oxides and soil C storage can be generalizable in the global scale? To answer the questions, we gathered data from 15 relevant studies conducted globally in the last 20 years and determined the importance of Fe oxides on soil development and soil C storage.

1.2. PEDOGENIC IRON OXIDE AND SOIL DEVELOPMENT

As Fe-containing rocks that were uplifted to the Earth's surface through plate tectonic processes became unstable with interactions with oxygen, water, carbon dioxide, and organic compounds, Fe-containing materials were subjected to weathering and erosion, and eventually widely distributed throughout the Earth's surface, where the timing and the locations of uplift or types of rocks uplifted determined the distribution of different types of Fe-containing minerals across Earth's surface (Cornell and Schwertmenn, 2003; Charpin et al., 2011). With varying weathering intensity in soils, Fe-bearing primary minerals primarily in Fe^{2+} state can be oxidized and hydrolyzed to Fe^{3+} (oxides) when contact with water and atmospheric oxygen, or may further reduced back to Fe^{2+} under anaerobic conditions with microbial processes (Cornell and Schwertmenn, 2003; Hall and Huang, 2017; Figure 1-1). Fe as dust or volcanic ash, or Fe that leaches out from the soil systems, also travels further to aquatic system, where it is taken up by microorganisms or accumulates in sediments (Pérez-Guzmán et al., 2010). Depending on the physicochemical properties of the natural environments, a varying amount of Fe oxides may accumulate in different types of soil systems (e.g. Dahlgren et al., 1997; Kaiser et al., 1997; Torn et al., 1997; Eusterhues et al., 2003; Lilienfein et al., 2003; Wagai and Mayer, 2007; Mikutta et al., 2006 and 2009; Moni et al., 2010; Sollins et al., 2009; Berhe et al., 2012; Wagai et al., 2013; Feng et al., 2014; Zhao et al., 2016; Coward et al., 2018a

and 2018b; Hall et al., 2018; Heckman et al., 2018; Jin et al., chapter 2), as well as sediments of aquatic systems (Lalonde et al., 2012; Lawrence et al., 2015; Barber et al., 2017) (Figure 1-1).

Pedogenic Fe oxide concentration typically increases with increasing weathering intensity during soil development (Figure 1-2a). Figure 1-2a provided the sodium dithionite-citrate-bicarbonate, sodium dithionite-bicarbonate, or sodium dithionite hydrochloride extracted total pedogenic Fe concentrations from varying soil systems collected from literature (Table S1-1). Specifically, in least weathered soil, Entisol, total pedogenic Fe concentrations were about 3.90±0.46 g kg^{-1} in A horizon, 4.78±0.69 g kg^{-1} in B horizon, and 3.77±0.92 g kg^{-1} in C horizon (averaged data from Dahlgren et al., 1997; Zhao et al., 2016). In slightly weathered soil, Inceptisol, total pedogenic Fe concentrations of 8.65±2.57 g kg^{-1} in A horizon, 8.50 g kg^{-1} in in E horizon, and 17.69±5.38 g kg^{-1} in B horizon were reported (averaged data from Dahlgren et al., 1997; Kaiser et al., 1997; Sollins et al., 2009; Wagai and Mayer, 2007; Mikutta et al., 2006 and 2009; Wagai et al., 2013; Zhao et al., 2016; Coward et al., 2018). With intermediate degree of weathering, total pedogenic Fe concentrations of 7.42±1.58 g kg^{-1} in A horizon, 5.38±2.16g kg^{-1} in E horizon, 20.59±2.48g kg^{-1} in B horizon, and 16.45±8.21 g kg^{-1} in C horizon were reported in Alfisol, Mollisol, or Spodosol (averaged data from Dahlgren et al., 1997; Eusterhues et al., 2003; Mikutta et al., 2006; Wagai and Mayer, 2007; Sollins et al., 2009; Moni et al., 2010; Wagai et al., 2013; Feng et al., 2014; Zhao et al., 2016; Heckman et al., 2018). In more strongly weathered soil, Ultisol, 18.38±5.64 g kg^{-1} and 33.03±6.84g kg^{-1} of total pedogenic Fe concentration were founded in A and B horizons (averaged data from Wagai and Mayer, 2007; Mikutta et al., 2009; Feng et al., 2014; Zhao et al., 2016). On the other hand, in highly weathered Oxisol, 105.88±19.60 g kg^{-1} and 204.30±32.88 g kg^{-1} of total pedogenic Fe concentrations were recorded in A and B horizons (averaged data from Wagai and Mayer, 2007; Mikutta et al., 2009; Sollins et al., 2009; Wagai et al., 2013; Coward et al., 2018a and 2018b; Hall et al., 2018) (Figure 1-2a). Volcanic soil, Andisol, was grouped separately considering its potentially high Fe oxide content. The total pedogenic Fe concentration in Andisol were 114.17±33.80 g kg^{-1} in A horizon, and 147.1±38.84 g kg^{-1} in B horizon (averaged data from Mikutta et al., 2009; Heckman et al., 2018). Hence, we can generalize that there could be two orders of magnitude increase in Fe oxide concentrations in soil, across a weathering gradient ranging from Entisols to Oxisols.

Similarly, Fe crystallinity increases with increasing weathering intensity across the soil development continuum (Figure 1-2b). The ratio of oxalate- to dithionite (citrate) (bicarbonate)-extractable Fe (Fe_o/Fe_d) is routinely used as an index for transformation of poorly crystalline Fe oxides to better crystalline Fe oxides in soils and therefore the maturity of soils (Cornell and Schwertmann, 2003). Fe_o/Fe_d varies between almost 0 (when well crystalline Fe oxides dominated in a given soil system) up to close to 1 (when poorly crystalline Fe oxides predominated) (Cornell and Schwertmann, 2003). In the least weathered Entisol, Fe_o/Fe_d ratio was 0.70±0.05 g kg^{-1} in A horizon, 0.54±0.10 g kg^{-1} in B horizon, and 0.34±0.06 g kg^{-1} in C horizon (averaged data from Dahlgren et al., 1997). In

the less weathered Inceptisol, Fe_o/Fe_d ratio was 0.42±0.10 g kg^{-1} in A horizon and 0.34±0.06 g kg^{-1} in B horizon (averaged from Dahlgren et al., 1997; Kaiser et al., 1997; Eusterhues et al., 2003; Mikutta et al., 2009; Sollins et al., 2009; Wagai et al., 2013; Heckman et al., 2018). In the intermediately weathered Alfisol, Mollisol, or Spodozol, Fe_o/Fe_d ratio was 0.28±0.07 g kg^{-1} in A horizon, 0.27±0.10 g kg^{-1} in E horizon and 0.25±0.04 g kg^{-1} in B horizon, and 0.15±0.04 g kg^{-1} in C horizon (averaged from Dahlgren et al., 1997; Eusterhues et al., 2003; Sollins et al., 2009; Moni et al., 2010; Wagai et al., 2013; Heckman et al., 2018). In more intensely weathered Ultisol, Fe_o/Fe_d ratio was 0.30±0.09 g kg^{-1} in A horizon, and 0.27 g kg^{-1} in B horizon (averaged from Mikutta et al., 2009; Wagai et al., 2013). In the most intensely weathered Oxisol, Fe_o/Fe_d ratio was 0.13±0.03 g kg^{-1} in A horizon, and 0.02 g kg^{-1} in B horizon (averaged from Mikutta et al., 2009; Sollins et al., 2009; Wagai et al., 2013; Hall et al., 2018). In the volcanic Andisol, Fe_o/Fe_d ratio was 0.56±0.14 g kg^{-1} in A horizon, and 0.41±0.22 g kg^{-1} in B horizon. These results show that poorly crystalline Fe oxide tend to accumulate in less weathered Entisol, Inceptisol, or Andisol and their proportion decreases with increasing weathering intensity. In addition, the fraction of poorly crystalline Fe oxides to total pedogenic Fe globally varied from 0.65 in least weathered soils to ~0.08 in highly weathered soils.

Opposite trends of pedogenic Fe and Fe oxide crystallinity with soil weathering intensity and soil development may suggest that Fe oxide crystallinity may be strongly linked to the total pedogenic Fe oxide concentrations with lower fraction of poorly crystalline Fe oxides in more weathered soils (Figure 1-3). As biogeochemical weathering progresses, poorly crystalline Fe oxides may transform to more crystalline phases in soils (Torn et al., 1997; Porras et al., 2017). However, in some soil systems, the metastable lepidocrocite or ferrihydrite may stay in soils for a long period of time because they are kinetically favored, even though they are thermodynamically less stable by nature (Schwertmann and Fitzpatrick, 1993). On the other hand, goethite and hematite are widely spread in soils and sediments in weathered environments since they are thermodynamically most stable among Fe oxides (Schwertmann and Fitzpatrick, 1993; Cornell and Schwertmann, 2003). Therefore, Fe oxide concentration and crystallinity may reflect soil weathering intensity.

Major influences of climate, time, soil depth, and the topography on rates of soil weathering may also be mirrored on the Fe crystallinity (Table 1-1). In a study conducted along the Hawaiian substrate age gradient that spans from 300 yr to 4100 kyr old soils formed from volcanic parent material, Torn et al. (1997) showed the accumulation and the loss of crystalline and poorly crystalline Fe oxides in the soil profile with weathering (soil age). Along the Hawaiian chronosequence, poorly crystalline Fe accumulated in soil up to around 150 kyr and decreased afterwards with increasing weathering intensity up to 4,100 kyr (Torn et al., 1997; Mikutta et al., 2009). On the other hand, the authors found that as the stock of poorly crystalline minerals decreased after 150 kyr, the stock of the more stable crystalline Fe oxides continues to increase. A similar trend was also observed in soils located in southwestern (SW) Washington (Lawrence et al., 2015). In the Mt. Shasta Mudflow site in California, poorly crystalline Fe was observed to increase with

soil depth because deep soils that were limited with SOM allowed precipitation of secondary minerals, while mineral organic matter complexes in the surface soils limited the formation of secondary minerals (Lilienfein et al., 2003; Lawrence et al., 2015). In another study conducted along a climosequence along the western slope of the Sierra Nevada, Dahlgren et al. (1997) found that moderate climate conditions that were neither too cool (high elevation) nor too dry (lowest elevation) allowed for higher amount of crystallized Fe, along with highest SOM concentrations compared to any other points along the climosequence. Even at smaller spatial scales, different rates of soil weathering and the erosion along a hillslope profile in the Marin headlands in northern California were observed to have significant influence on Fe oxide stocks in the soil profile (Berhe et al., 2012). Berhe et al. (2012) found that summit or shoulder hillslope positions had higher stock of poorly crystallized Fe compared to the backslope or hollow (terrestrial depression) because of the relatively rapid weathering and subsequent lateral distribution of soil material in the latter two landform positions that exist at lower elevation than the gently sloping (or flat) summit and shoulder positions. At the bottom of the hillslope, the alluvial/colluvial plain landform position had the highest stock of poorly crystalline Fe as a result of deposition and long-term accumulation of transported soil (Berhe et al., 2008 and 2012). We conclude that the crystallinity of pedogenic Fe oxides, that varies across weathering and topographic gradients, is very likely to play important roles in regulating the capacity of soils to store and stabilize SOM.

1.3. PEDOGENIC FE OXIDE AND SOIL C STORAGE

Concentrations of poorly crystalline Fe oxides were strongly correlated to the soil C content, as was indicated by a strong positive relationship between ammonium oxalate or hydroxylamine hydrochloride extractable Fe oxides (mainly poorly crystalline Fe oxides) and soil C content in varying soil systems (Figure 4). Increasing availability of sorptive surface with increasing abundance of Fe oxides in soil is likely an important contributor to the relationship (Kleber et al., 2015). However, as SOM may partially or fully cover reactive surfaces of individual Fe minerals or aggregates with Fe oxides in sorption phase, additional association of OM with the Fe oxides may be limited (Kleber et al., 2015).

On the other hand, a large amount of SOM may be accumulated via coprecipitation of Fe oxides and SOM in soils (Figure 5). A general exponential increase of OC content of poorly crystalline Fe and Al-containing coprecipitates with decreasing molar ratio of poorly crystalline Fe and Al oxides to OC was revealed by Kleber et al. (2015), where he proposed a potential arrangement of poorly crystalline Fe oxides and SOM interactions as coprecipitates. Specifically, as organic ligands interact with hydrolyzed Fe, coprecipitates may form and Fe oxides in the coprecipitates may encapsulate in the organic matrix ("Embedded Fe oxide surface" in Figure 1-5). Coprecipitated Fe oxides will be smaller in size (when compare the size of Fe oxides aggregates in adsorption phase), and thus may allow more OC to adsorb on their surface, and consequently, enables further adsorption of SOM (Kleber et al., 2015). Compare to the patchy distribution of SOM on bulky Fe oxides aggregates during adsorption, evenly distributed patterns between SOM and Fe

oxides aggregates during coprecipitation may preserve a larger amount of SOM (Kleber et al., 2015). Here, I expanded the idea Kleber et al. (2015) has proposed. The regression line is obtained using the equation obtained from Figure 4. Kleber et al. (2015) has proposed that at a lower molar ratio of M/C (M=poorly crystalline Al and ferrihydrite)=0.1, Fe oxides in coprecipitates partially covered by SOM and large amount of surface area of Fe oxides may be still available for SOM sorption, whereas at M/C =1, more Fe oxides may be embedded in the coprecipitates and less amount of surface area may be available for additional sorption of SOC. Therefore, as poorly crystalline Fe oxide increases in amount, coprecipitation may become dominant and may increase the soil C storage in soils.

1.4. CONCLUSION

The important role of pedogenic Fe oxides on soil development and soil C storage was investigated using data collected from published studies. Our compiled results confirm that pedogenic Fe oxides and their crystallinity reflect soil weathering intensity and soil development, and poorly crystalline Fe oxides in particular play disproportionately large roles in soil C storage.

1.5. OBJECTIVES OF THE FOLLOWING CHAPTERS

Regarding the important role of pedogenic Fe oxides and their crystallinity on soil C stock, the role of pedogenic Fe oxides with varying crystallinity on physical protection of SOM inside aggregates were investigated in Chapter 2, characterization of organic matter in pedogenic Fe-containing mineral fractions was evaluated in Chapter 3, and sorption and desorption of soil organic matter by mineral soils with varying Fe oxide concentrations were assessed in Chapter 4. Chapter 5 presents synthesis of major findings from chapters 2 to 4.

REFERENCES

Barber, A., Brandes, J., Leri, A., Lalonde, K., Balind, K., Wirick, S., Wang, J. and Gélinas, Y. (2017). Preservation of organic matter in marine sediments by inner-sphere interactions with reactive iron. Scientific reports, 7(1), 366.

Berhe, A. A., Harden, J. W., Torn, M. S. and Harte, J. (2008). Linking soil organic matter dynamics and erosion-induced terrestrial carbon sequestration at different landform positions. Journal of Geophysical Research: Biogeosciences, 113(G4).

Berhe, A. A., Harden, J. W., Torn, M. S., Kleber, M., Burton, S. D. and Harte, J. (2012). Persistence of soil organic matter in eroding versus depositional landform positions. Journal of Geophysical Research: Biogeosciences, 117(G2).

Chapin III, F. S., Matson, P. A., & Vitousek, P. (2011). Principles of terrestrial ecosystem ecology. Springer Science & Business Media.

Cornell, R. M. and Schwertmann, U. (2003). The iron oxides: structure, properties, reactions, occurrences and uses. John Wiley & Sons.

Coward, E. K., Ohno, T. and Plante, A. F. (2018). Adsorption and molecular fractionation of dissolved organic matter on iron-bearing mineral matrices of varying crystallinity. Environmental science & technology, 52(3), 1036-1044.

Coward, E. K., Thompson, A. and Plante, A. F. (2018). Contrasting Fe speciation in two humid forest soils: Insight into organomineral associations in redox-active environments. Geochimica et Cosmochimica Acta, 238, 68-84.

Dahlgren, R. A., Boettinger, J. L., Huntington, G. L. and Amundson, R. G. (1997). Soil development along an elevational transect in the western Sierra Nevada, California. Geoderma, 78(3-4), 207-236.

Eusterhues, K., Rumpel, C., Kleber, M. and Kögel-Knabner, I. (2003). Stabilisation of soil organic matter by interactions with minerals as revealed by mineral dissolution and oxidative degradation. Organic Geochemistry, 34(12), 1591-1600.

Feng, W., Plante, A. F., Aufdenkampe, A. K. and Six, J. (2014). Soil organic matter stability in organo-mineral complexes as a function of increasing C loading. Soil Biology and Biochemistry, 69, 398-405.

Hall, S. J., Berhe, A. A. and Thompson, A. (2018). Order from disorder: do soil organic matter composition and turnover co-vary with iron phase crystallinity? Biogeochemistry, 140(1), 93-110.

Hall, S. J., & Huang, W. (2017). Iron reduction: a mechanism for dynamic cycling of occluded cations in tropical forest soils?. Biogeochemistry, 136(1), 91-102.

Heckman, K., Lawrence, C. R. and Harden, J. W. (2018). A sequential selective dissolution method to quantify storage and stability of organic carbon associated with Al and Fe hydroxide phases. Geoderma, 312, 24-35.

Jastrow, J. D., Amonette, J. E. and Bailey, V. L. (2007). Mechanisms controlling soil carbon turnover and their potential application for enhancing carbon sequestration. Climatic Change, 80(1-2), 5-23.

Jin, L., O'Day, P. and Berhe, A.A. Role of iron oxides on physical protection of soil organic matter inside aggregates. In preparation.

Kaiser, K., Guggenberger, G., Haumaier, L. and Zech, W. (1997). Dissolved organic matter sorption on sub soils and minerals studied by 13C-NMR and DRIFT spectroscopy. European Journal of Soil Science, 48(2), 301-310.

Kleber, M., Eusterhues, K., Keiluweit, M., Mikutta, C., Mikutta, R. and Nico, P. S. (2015). Mineral–organic associations: formation, properties, and relevance in soil environments. In Advances in agronomy (Vol. 130, pp. 1-140). Academic Press.

Lalonde, K., Mucci, A., Ouellet, A. and Gélinas, Y. (2012). Preservation of organic matter in sediments promoted by iron. Nature, 483(7388), 198.

Lawrence, C. R., Harden, J. W., Xu, X., Schulz, M. S. and Trumbore, S. E. (2015). Long-term controls on soil organic carbon with depth and time: A case study from the Cowlitz River Chronosequence, WA USA. Geoderma, 247, 73-87.

Le Quéré, C., Andrew, R. M., Friedlingstein, P., Sitch, S., Hauck, J., Pongratz, J., ... and Arneth, A. (2018). Global carbon budget 2018. Earth System Science Data (Online), 10(4).

Lilienfein, J., Qualls, R. G., Uselman, S. M. and Bridgham, S. D. (2003). Soil formation and organic matter accretion in a young andesitic chronosequence at Mt. Shasta, California. Geoderma, 116(3-4), 249-264.

Lützow, M. V., Kögel-Knabner, I., Ekschmitt, K., Matzner, E., Guggenberger, G., Marschner, B. and Flessa, H. (2006). Stabilization of organic matter in temperate soils: mechanisms and their relevance under different soil conditions–a review. European Journal of Soil Science, 57(4), 426-445.

Mikutta, R., Kleber, M., Torn, M. S. and Jahn, R. (2006). Stabilization of soil organic matter: association with minerals or chemical recalcitrance? Biogeochemistry, 77(1), 25-56.

Mikutta, R., Schaumann, G. E., Gildemeister, D., Bonneville, S., Kramer, M. G., Chorover, J., Chadwick, O.A. and Guggenberger, G. (2009). Biogeochemistry of mineral–organic associations across a long-term mineralogical soil gradient (0.3–4100 kyr), Hawaiian Islands. Geochimica et Cosmochimica Acta, 73(7), 2034-2060.

Moni, C., Rumpel, C., Virto, I., Chabbi, A. and Chenu, C. (2010). Relative importance of sorption versus aggregation for organic matter storage in subsoil horizons of two contrasting soils. European Journal of Soil Science, 61(6), 958-969.

Pérez-Guzmán, L., Bogner, K. R. and Lower, B. H. (2010). Earth's ferrous wheel. Nat. Educ. Knowl, 3, 32.

Porras, R. C., Pries, C. E. H., McFarlane, K. J., Hanson, P. J. and Torn, M. S. (2017). Association with pedogenic iron and aluminum: effects on soil organic carbon storage and stability in four temperate forest soils. Biogeochemistry, 133(3), 333-345.

Schmidt, M. W., Torn, M. S., Abiven, S., Dittmar, T., Guggenberger, G., Janssens, I. A., Kleber, M., Kogel-Knabner, I., Lehmann, J., Manning, D.A., Nannipiere, P., Rasse, D.P., Weiner, S. and Trumbore, S.E. (2011). Persistence of soil organic matter as an ecosystem property. Nature, 478(7367), 49.

Schwertmann, U. and Fitzpatrick, R. W. (1993). Iron minerals in surface environments. Catena Supplement, 21, 7-7.

Sollins, P., Kramer, M. G., Swanston, C., Lajtha, K., Filley, T., Aufdenkampe, A. K., Wagai, R. and Bowden, R. D. (2009). Sequential density fractionation across soils of contrasting mineralogy: evidence for both microbial-and mineral-controlled soil organic matter stabilization. Biogeochemistry, 96(1-3), 209-231.

Stockmann, U., Adams, M. A., Crawford, J. W., Field, D. J., Henakaarchchi, N., Jenkins, M., ... and Wheeler, I. (2013). The knowns, known unknowns and unknowns of sequestration of soil organic carbon. Agriculture, Ecosystems & Environment, 164, 80-99.

Torn, M. S., Trumbore, S. E., Chadwick, O. A., Vitousek, P. M. and Hendricks, D. M. (1997). Mineral control of soil organic carbon storage and turnover. Nature, 389(6647), 170.

Totsche, K. U., Amelung, W., Gerzabek, M. H., Guggenberger, G., Klumpp, E., Knief, C., Lehndorff, E., Mikutta, R., Peth, S., Prechtel, A., Ray, N. and Kogel-Knabner, I. (2018). Microaggregates in soils. Journal of Plant Nutrition and Soil Science, 181(1), 104-136.

Wagai, R. and Mayer, L. M. (2007). Sorptive stabilization of organic matter in soils by hydrous iron oxides. Geochimica et Cosmochimica Acta, 71(1), 25-35.

Wagai, R., Kishimoto-Mo, A. W., Yonemura, S., Shirato, Y., Hiradate, S. and Yagasaki, Y. (2013). Linking temperature sensitivity of soil organic matter decomposition to its molecular structure, accessibility, and microbial physiology. Global Change Biology, 19(4), 1114-1125.

Zhao, Q., Poulson, S. R., Obrist, D., Sumaila, S., Dynes, J. J., McBeth, J. M. and Yang, Y. (2016). Iron-bound organic carbon in forest soils: quantification and characterization.

TABLE

Table 1-1. Studies on effects of climate, time, soil depth and topography on Fe oxide crystallinity.

Series	Location	Experimental site	Soil order/details	Factors	Fe_o/Fe_d	References
			Year (kyr)			
Chronosequence	Vocanic soil on Island of Hawaii	Thurston	Inceptisol	0.3	0.9	Torn et al., 1997
		Laupahoehoe	Andisol	20	0.8	
		Kohala	Andisol	150	1.1	Mikutta et al., 2009
		Pololu		400	0.5	
		Kolekole	Ultisol	1400	0.3	
		Kokee	Oxisol	4100	0	
	Cowlitz River, Washington	Latest pleistocene outwash	Quaternary deposit	11	0.19 ± 0.03	Lawrence et al., 2015
		Evans creek drift	Quaternary deposit	24	0.75 ± 0.18	
		Pre-evans creek outwash	Quaternary deposit	60	0.20 ± 0.05	
		Late Hayden creek outwash	Quaternary deposit	150	0.12 ± 0.02	
		Middle Hayden creek outwash	Quaternary deposit	225	0.15 ± 0.04	
		Early Hayden creek outwash	Quaternary deposit	300	0.13 ± 0.06	
		Wingate hill outwash	Quaternary deposit	500	0.09 ± 0.01	
		Logan hill formation	Quaternary deposit	1200	0.05 ± 0.00	
			Depths (cm)			
Soil depths	Mt. Shasta Mudflow research natural area in California		Volcanic mudflow	0-10	0.67 ± 0.18	Lilienfein et al., 2003
			Volcanic mudflow	10-20	0.84 ± 0.12	
			Volcanic mudflow	30-40	0.79 ± 0.07	
			Volcanic mudflow	70-80	0.85 ± 0.07	
			Volcanic mudflow	140-150	0.89 ± 0.03	

Table 1-1 (cont.). Studies on effects of climate, time, soil depth and topography on Fe oxide crystallinity.

Series	Location	Experimental site	Soil order/details	Factors	Fe_o/Fe_d	References
			Elev/Temp/Prep (m, C, cm)			
Climosequence	Elevational transect in the western Sierra Nevada, California	Chiquito	Inceptisol	2865/3.9/127	0.78	Dahlgren et al., 1997
		Sirretta	Entisol	2195/7.2/108	0.54 ± 0.18	
		Shaver	Entisol	1800/9.1/101	0.55 ± 0.04	
		Musick	Alfisol	1390/11.1/91	0.06 ± 0.004	
		Auberry	Alfisol	794/14.4/62	0.09 ± 0.02	
		Ahwahnee	Alfisol	561/15.0/57	0.10 ± 0.002	
		Vista	Inceptisol	198/16.7/33	0.13 ± 0.01	
			Slope			
Toposequence	Tennessee Valley (TV) in Marin County, California		Mollisol	Summit	~ 0.27	Berhe et al., 2008 and 2012
			Mollisol	Slope	~ 0.18	
			Mollisol	Hollow	~ 0.20	
			Entisol	Plain	~ 0.68	

FIGURES

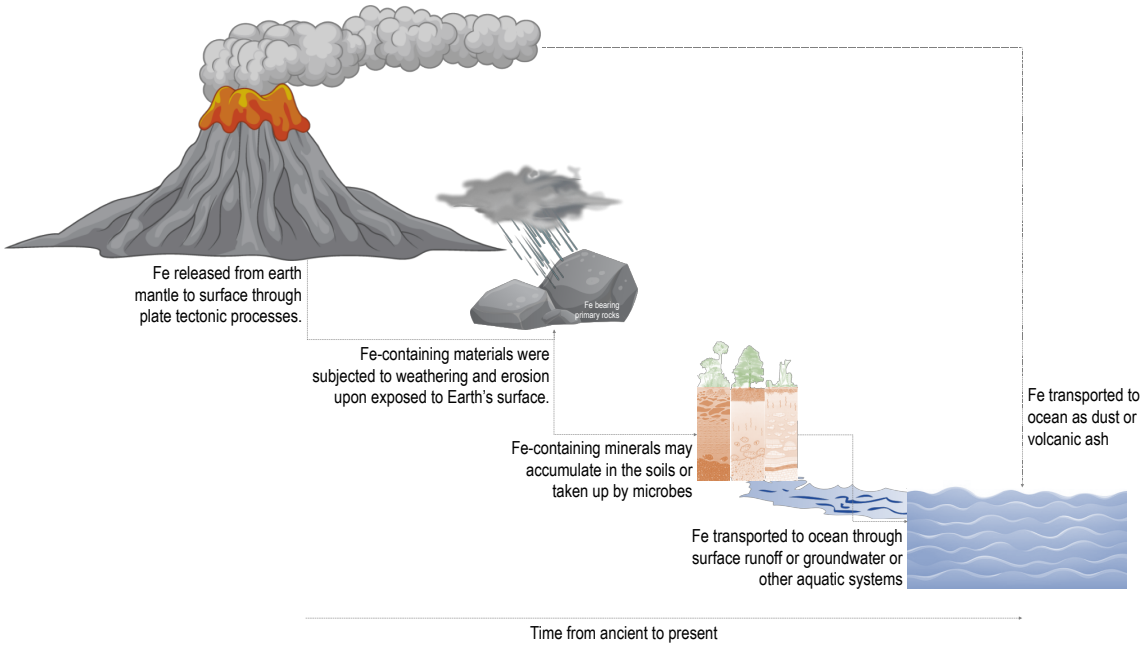

Figure 1-1. The biogeochemical cycling of pedogenic Fe on Earth surface environment. Note that individual images are from online sources. As Fe-containing rocks that were uplifted to the Earth's surface through plate tectonic processes became unstable with interactions with oxygen, water, carbon dioxide, and organic compounds, Fe-containing materials were subjected to weathering and erosion, and eventually widely distributed throughout the Earth's surface, where the timing and the locations of uplift or types of rocks uplifted determined the distribution of different types of Fe-containing minerals across Earth's surface (Cornell and Schwertmenn, 2003; Charpin et al., 2011). With varying weathering intensity in soils, Fe-bearing primary minerals primarily in Fe^{2+} state can be oxidized and hydrolyzed to Fe^{3+} (oxides) when contact with water and atmospheric oxygen, or may further reduced back to Fe^{2+} under anaerobic conditions with microbial processes (Cornell and Schwertmenn, 2003; Hall and Huang, 2017). Fe as dust or volcanic ash, or Fe that leaches out from the soil systems, also travels further to aquatic system, where it is taken up by microorganisms or accumulates in sediments (Pérez-Guzmán et al., 2010).

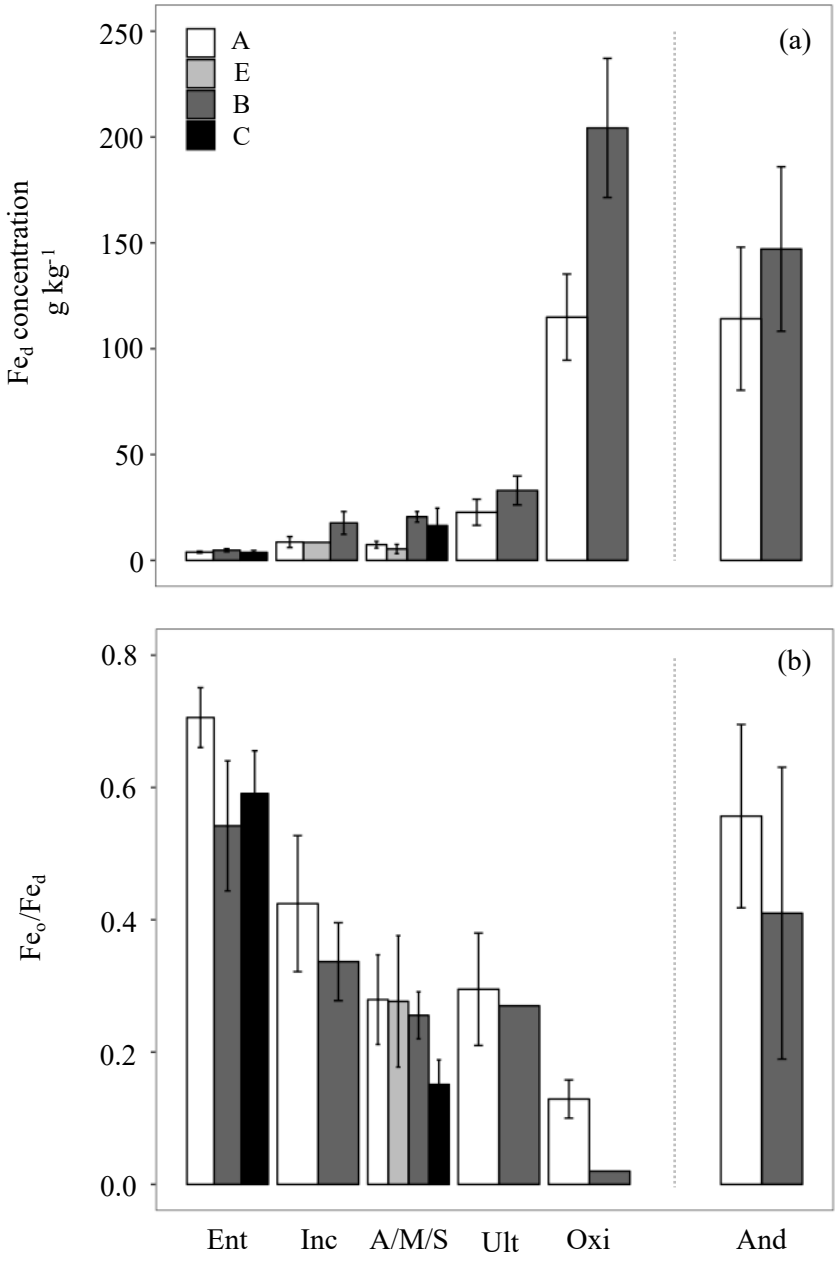

Figure 1-2. Sodium dithionite (citrate) (bicarbonate) extractable total pedogenic Fe concentration and the ratio of ammonium oxalate extractable poorly crystalline Fe concentration to total pedogenic Fe concentration with soil development with increasing weathering intensity. “Ent”, “Inc”, “A/M/S”, “Ult”, “Oxi”, and “And” indicate Entisol, Inceptisol, Alfisol/Mollisol/Spodozol, Ultisol, Oxisol, and Andisol. Data is showing the mean and standard error. Detailed data can be found in the text or Table S1-1.

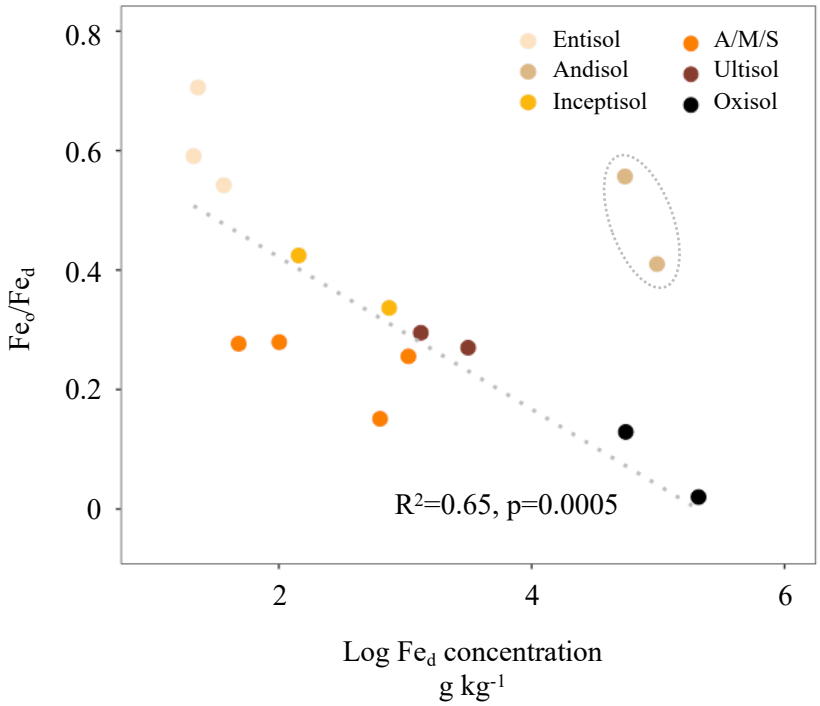

Figure 1-3. Correlation between the ratio of ammonium oxalate-extractable poorly crystalline Fe concentration and sodium dithionite (citrate) (bicarbonate) extractable-total pedogenic Fe concentration in varying weathering environments. Data from Andisol (circled) was not included for linear regression.

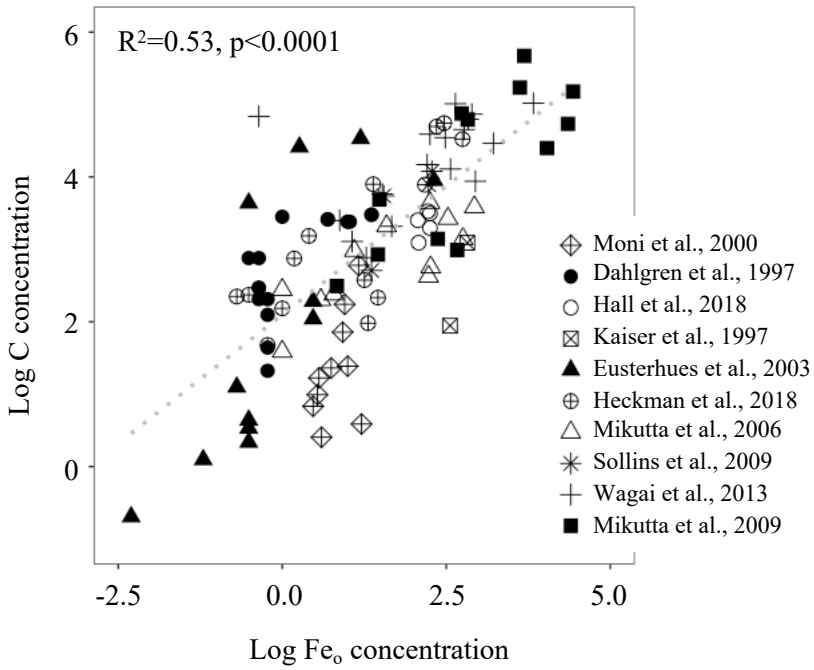

Figure 1-4. Correlation between ammonium oxalate extractable poorly crystalline Fe concentration and soil OC concentration in varying weathering environments.

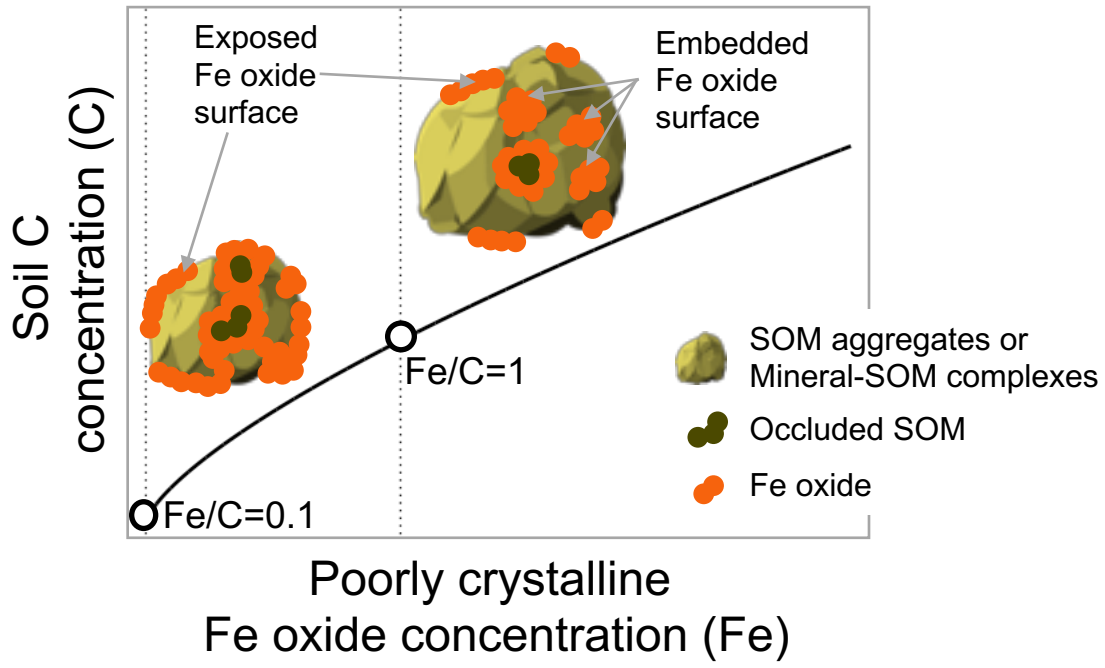

Figure 1-5. Possible associations between poorly crystalline Fe oxides and soil C content in coprecipitation. The idea is expanded from Kleber et al. 2015 (Figure 12). The regression line is obtained using the equation obtained from Figure 1-4.

CHAPTER 2. ROLE OF IRON OXIDES ON PHYSICAL PROTECTION OF SOIL ORGANIC MATTER INSIDE AGGREGATES

ABSTRACT

Soil carbon (C) storage and stability are highly influenced by soil structure, in particular soil aggregation that physically protects C from loss. Organic matter (OM) and pedogenic iron (Fe) are major binding agents that facilitate soil aggregate formation and stability. However, few studies have investigated relationships among pedogenic Fe, Ca, and C in different sized aggregates. We sequentially extracted pedogenic Fe and determined the amount of C associated with macroaggregates (2000-250 μm), microaggregates (250-53 μm), and two silt and clay fractions (53-20 μm, and <20 μm) in an Alfisol from Sierra Nevada in California. Results revealed that sodium pyrophosphate (PP)-extracted Fe was the major pedogenic Fe pool associated with C in soils, especially in smaller soil aggregates. PP-extractable calcium (Ca) was strongly correlated with PP-extractable Fe and C, possibly suggesting that both polyvalent cations (Fe and Ca) contribute to C storage in the soil. Fe extracted by hydroxylamine hydrochloride (i.e. poorly crystalline Fe oxides) was consistently low compared to PP-extractable Fe but was higher in largest soil aggregate size range (250-2000 μm). With increasing soil depth, the proportions of PP-extracted Fe decreased and dithionite hydrochloride-extracted Fe (i.e. crystalline Fe oxides) increased, likely due to the translocation of Fe oxides along the soil profile through illuviation process, or because high concentrations of organic matter in surface soils limited Fe crystallization. Our results showed that pedogenic Fe and Ca plays important roles in preservation of OM inside soil aggregates.

2.1. INTRODUCTION

Soil organic matter (SOM) is the largest stock of terrestrial carbon (C) and plays an important role in the global C cycle. Since a small change in SOM storage may significantly influence atmospheric C concentration (Stockmann et al., 2013), there has been a growing interest in improving our understanding of the mechanisms that promote increase in stock and stability of OM in soil, and SOM's stabilization mechanism (Schmidt et al., 2011). Carbon storage and stabilization in soil principally depend on physical and chemical associations of organic matter (OM) with soil minerals (Lutzow et al., 2006; Jastrow and Bailey, 2007; Moni et al., 2010; Stockmann et al., 2013). Generally, SOM is stabilized either physically by occlusion within soil aggregates or chemically by sorption on mineral surfaces, such as metal oxide surfaces. Evidence from natural soil samples has highlighted that OM in natural soils is typically observed to be preferentially stabilized by association with silt and clay-size aggregates and can be encrusted by soil minerals (Chenu and Plante, 2006; Moni et al., 2010), where metal oxides are critical for formation and the stability of soil aggregates (Barral et al., 1998; Cornell and Schwertmann, 2003; Six et al., 2004; Bronick and Lal, 2005; Totsche et al., 2018).

Pedogenic metal oxides, especially Fe and Al oxides, in weathered soils have been recognized as important soil minerals that play disproportionally high role in SOM stabilization (Torn et al., 1997; Kalbitz et al., 2000; Eusterhues et al., 2005; Wagai and Mayer, et al., 2007; Moni et al., 2010; Eglinton, 2012; Lalonde et al., 2012; Wissing et al., 2014; Porras et al., 2017; Heckman et al., 2018). SOM can be often associated with Fe oxides by forming chemical association with oxide coatings on soil mineral surface (Cornell and Schwertmann, 2003; Kleber et al., 2007), by entering into the porous structure within Fe oxide clusters (Kaiser and Guggenberger, 2007), where Fe oxides regulate the formation and the stability of soil aggregates (Cornell and Schwertmann, 2003; Kleber et al., 2015), or provide sorptive surfaces for SOM adsorption to mineral surfaces or form aqueous complexation or coprecipitation (Kaiser and Guggenberger, 2000; Eusterhues et al., 2003; Mikutta et al., 2006;Wagai and Mayer, 2007; Wagai et al., 2009; Wissing et al., 2014). Though the sorptive reactions of SOM on Fe oxide surfaces were extensively studied, the impacts of Fe oxides on physically occluded SOM by Fe oxides were not studied in a same level, especially considering that OC stabilized by physical associations with soil minerals, such as Fe oxides, was found to have longer mean residence time compared to OC in free fraction (Rasmussen et al., 2005; Moni et al., 2010), and slowed decay of OM (e.g. Kaiser et al., 2002; Kaiser and Guggenberger, 2003 and 2007). Concentration of exchangeable cations in soils may also regulate the attachment of organic molecules involved in organo-mineral complexes in soil aggregates (Bronick and Lal, 2005; Lutzow et al., 2006; Kleber et al., 2007; Ellerbrock and Gerke, 2013; Chen et al., 2014). Kleber et al. (2007) proposed a zonal structure of organo-mineral interactions with three distinct zones, namely, contact zone, zone of hydrophobic interactions, and kinetic zone. In the outermost kinetic zone, cations may help to attract additional organic compound to this region allowing for the formation of a supramolecule-colloid. Alternatively, exchangeable cations may attach on negatively

charged mineral surface and promote SOM accumulations (Ellerbrock and Gerke, 2013). Therefore, higher concentrations of SOM and exchangeable cations in soils may contribute to a thicker kinetic zone, and/or a greater attachment to mineral surfaces, and thus preserve a large amount of SOC in organo-mineral associations (Kleber et al., 2007). These findings suggest that investigating the impacts of Fe oxides on soil aggregate protected SOM may further our knowledge on the effects of Fe oxides on C stabilization.

The effectiveness of Fe oxides on their associated soil C storage and stabilization depends on their nature, concentration, and oxide crystallinity (Schwertmann, 1986; Cornell and Schwertmann, 2003; Coward et al., 2017 and 2018; Hall et al., 2018; Heckman et al., 2018). Relative concentrations of Fe and C in soils, for example, affect Fe oxide crystallinity and the types of SOM-Fe oxide associations that may form in soils (Schwertmann et al., 1986; Adhikari et al., 2017). Schwertmann et al. (1986) proposed that, with high SOM content, most of the Fe ion is organically associated and oxide formation is hindered, whereas both relatively high SOM content and high Fe content promote ferrihydrite formation (i.e. poorly crystalline Fe oxide) and impede the formation of crystalline Fe oxides. On the other hand, with relatively low SOM content, formation of crystalline Fe oxides (e.g. hematite or goethite) are favored. Wagai and Mayer (2007) observed the shift of Fe phases involved in SOM-Fe complexes from Fe oxides to organically associated Fe with increasing C supply. Similarly, Lawrence et al. (2015) have found that the formation of crystalline Fe oxides may be hindered due to the formation of organo-metal complexes in deposit soils from Cowlitz River. Most recently, Heckman et al. (2018) reported that the stability of organo-mineral complexes varied with the degree of crystallinity of the mineral phases, especially metal oxides. Coward et al. (2018) found that most of poorly crystalline Fe oxide with high specific surface areas is more resistant to be reductant released from Oxisol. Hall et al. (2018) proposed that more disordered Fe oxides may be associated with faster-cycling, plant-derived SOM, whereas more crystalline Fe oxides may be associated with older, microbe-derived SOM. These studies have shown that crystallinity of Fe oxides influences soil C storage and their relative abundance may regulate the persistence of SOM (Coward et al., 2017 and 2018; Hall et al., 2018; Heckman et al., 2018). However, there has been no extensive studies on how the relative contribution of different Fe pools (i.e. organically associated, poorly crystalline, and crystalline Fe) is related to C distribution and presumably C persistence in soil aggregates.

In this study, we determined the association of Fe in different extractable pools of soil with C within distinct aggregate size ranges along depth profiles in an Alfisol from Sierra Nevada in California (Musick soil series) using a sequential Fe dissolution extraction approach. Our main objectives were: (i) to quantify the amount of C in extractable Fe containing fractions in different soil aggregate size fractions, and (ii) to determine the relative contribution of different Fe pools within soil aggregates or along soil depths to soil C storage.

2.2. METHODS

2.2.1. Sample collection and particle size fractionation

Soils were collected from A and B horizons (0-29 cm, 29-38 cm, 38-54 cm, and 54-69 cm) of the Musick soil series that have amongst the highest concentrations of both C and Fe oxides in soils along western slope of the Sierra Nevada (Dahlgren et al., 1997). Two pits apart within 30 feet were collected in the sites. The site (located at 37.06073 N, 119.37348 W) is located at 1390 m above sea level and has mean annual air temperature of 11.1 ^{O}C and mean annual precipitation of 91 cm (Dahlgren et al., 1997). The site is dominated by forest, made up of ponderosa pine, incense cedar, and manzanita (Dahlgren et al., 1997; Castanha et al., 2012). Soil was formed from Jurassic granodiorite and classified as a Fine-loamy, mixed, semiactive, mesic, Ultic Haploxeralf, and the dominant clay minerals found at this site include kaolinite, mica and vermiculite (Dahlgren et al., 1997; Figure S2-1). The soil texture, pH, particle size distribution and C concentration in different aggregate size ranges in Musick soil are reported in Table 2-1.

After collection, the soil samples were dry-sieved through 2 mm, 250 μm, 53 μm, and 20 μm sieves representing macroaggregate (2 mm-250 μm), microaggregate (250-53 μm), and silt and clay fractions (53-20 μm and <20 μm). Fractions of total sample mass recovered during physical size fractionation were between 0.95 and 1 (data not shown). Total C concentrations of bulk soil and each aggregate size range were determined with a Costech ECS 4010 CHNSO Analyzer (Costech Analytical Technologies, Valencia, CA, USA).

2.2.2. Characterization of soil Fe phases by X-ray Absorption Spectroscopy (XAS)

Major Fe phases in bulk soil samples from A (0-29cm) and B horizons (54-69cm) were determined by XAS. Fe K-edge X-ray absorption near edge structure (XANES) and extended X-ray absorption fine structure (EXAFS) were collected at Stanford Synchrotron Radiation Lightsource (SSRL) on wiggler-magnet beamline 4-1. Energy of each X-ray absorption spectrum was calibrated using a metallic Fe foil with the first inflection point set to 7112 eV (Berger and Hubbell, 1987). Replicate spectra were averaged with the Sixpack program (Webb, 2005) and then analyzed in the ATHENA program (Ravel and Newville, 2005). Background was subtracted separately for XANES and EXAFS regions for a uniform normalization and a better match in combination fits (Leven et al., 2018). The normalization range for XANES was between 7165 and 7325 eV, and that for EXAFS was between 7250 and 7625 eV. Linear combination fits (LCF) were performed with the normalized data using ATHENA program. The constrains were set to force the weights of reference spectra between 0 and 1, but the component sum was not forced to 1. The spectra were initially fit to a larger set of reference spectra with a variety of Fe oxides and Fe-containing minerals (11 reference spectra), and then narrowed down to a smaller set of 4 spectra (Table S2-1, Figure S2-2) that best matched the unknown samples. The same set of reference spectra was used for both soil samples for consistency. Specifically, XANES and EXAFS spectra were fit independently using

same set of reference spectra of smectite (SAz-1), mixed illite/smectite (IMt-1), both from the Clay Minerals Society Source Clay Repository, ferrihydrite, and hematite (O'Day et al., 2004) (Table S2-1, Figure S2-2). However, combinations with three reference minerals were identified as the best fit for EXAFS spectra for Musick B soils. Numerical fit results are reported in the Table 2-2. The practical detection limit for Fe phases in this study was ~ 5% Fe by atomic mass and thus Fe phases under this detection limit were considered minor and statistically insignificant (Leven et al., 2018).

2.2.3. Sequential dissolution extraction

To isolate different pools of pedogenic Fe in both bulk soil and separated aggregate size ranges, each soil size range or bulk soils from different soil depths were extracted with a sequential, selective extraction protocol according to the methods of Heckman et al. (2018), who adapted the approach from Parfitt and Childs (1988), Dahlgren (1994), Wagai and Mayer (2007), and Lawrence et al. (2015). Specifically, 1 g of sample was extracted sequentially with 0.1 M sodium pyrophosphate solution (PP), 0.25 M hydroxylamine hydrochloride solution (HH), and 0.05 M sodium dithionite solution (DH). Samples were shaken for 16 h and centrifuged at 10000 rpm for 30 min after each extraction. The PP, HH, and DH extracts were then filtered through a 0.2 μm filter and analyzed for the concentrations of elemental Fe and Ca, and total organic carbon (TOC) using ICP-OES (Perkin-Elmer Optima 5300 DV Inductively Coupled Plasma Optical Emission Spectrometer with detection limits of 0.020 ppm for Ca and 0.022 ppm for Fe) and TOC (Shimadzu TOC-Vcsh Total Organic Carbon Analyzer with detection limit of 0.5 $\mu g\ l^{-1}$) analyzer, respectively. Other than Fe, only Ca is discussed in this study because the Musick soil contained a much higher amount of Ca than other common cations (except Al) (data not shown). Correlations between Al and C were also included in the supplementary information as a comparison to correlations between Fe, Ca, and C. Total C measured from solid samples before extraction was compared to C extracted from each of the three extraction steps and residues after DH extraction (last extraction in sequential extraction) to calculate the fraction of C recovered, which was between 0.5 to 1.2 (Table S2-2). The discrepancies may be due to the small amount of C in these samples or C loss from physical size fractionation process through sieving (Heckman et al., 2018). The mass fractions of Fe and C in each extraction were calculated by multiplying the mass proportion with their concentrations in individual fraction, and the mass balance of C and Fe is reported in Table S2-2.

2.2.4. Statistical analyses

R software 3.5.3 (R Foundation for Statistical Computing) and Rstudio (Rstudio Inc.) were used to perform statistical analyses. All data were tested for normality and analysis of variance (ANOVA) was used to test for significance ($p \leq 0.05$) of relationships between different variables. Linear regression model was used to evaluate the significant linear relationships between different Fe pools and their associated C or soil C concentrations in different soil horizons.

2.3. RESULTS

2.3.1. Distribution of extractable C in soil

For the whole profile, macroaggreates represented 61.7-67.8% of the horizon's mass, but contained the lowest concentration of C compared to other aggregates size ranges (Table 2-1). In contrast, silt and clay fractions (<20 μm) represented only 5.3-6.9% of the horizon's mass but contained the highest concentrations of C compared to other aggregates size fractions.

Generally, the concentration of C in A horizon was much higher than B horizon in all soil aggregate sizes (Figure 2-1, Table S2-2). PP-extractable fraction, especially, showed the greatest differences in C concentrations from A to B horizons, where the highest concentrations of C in silt and clay fractions with more than 2 mol kg^{-1} in the surface decreased to 0.6 mol kg^{-1} in the subsoil. C concentration in HH- and DH-extractable fractions also declined to nearly half of their amount from A to B horizons.

The distribution of C along soil depths was similar among soil aggregates, where the C concentration increased with decreasing aggregate size ranges (Figure 2-1, Table S2-2). For example, C concentrations in silt and clay fractions, especially in <20 μm fraction, typically contained the highest amount of C in all soil depths, compared to other size aggregates. C contents in bulk soils were similar to that in macro- and micro-aggregates, whereas silt and clay fractions generally contained up to two times of C compared to that in larger aggregate size ranges.

The majority of extractable C was found in the PP-extractable fraction, in particular in near-surface soil layers, whereas the concentrations of HH- and DH- extractable C with much lower concentrations were higher in deeper soil layers (Figure 2-2, Table S2-3). For example, the concentrations of PP-, HH-, and DH-extractable C were around 2 mol kg^{-1}, 0.1 mol kg^{-1} and 0.2 mol kg^{-1} in < 20 μm size range in A horizon, where more than 90% of extractable C was related to PP extractable fraction. The values decreased to 0.6 mol kg^{-1} of PP extractable C, 0.05 mol kg^{-1} of HH extractable C, and 0.1 mol kg^{-1} of DH extractable C in the same aggregate size range in B horizon, where only 61% of extractable C was related to PP extractable fraction.

2.3.2. Distribution of Fe in soil

The concentrations of extractable Fe were ~1 or 2 magnitude lower than those of extractable C (Figure 2-1, Table S2-4). For example, the concentration of Fe ranged from 0.003 to 0.05 mol kg^{-1} in the PP extractable fraction, whereas C concentration was ranged from 0.3 to 2 mol kg^{-1} in the same fraction. Similarly, the concentrations of HH- and DH-extractable C were typically 20 and 10 times higher than the concentrations of HH- and DH-extractable Fe, respectively.

The absolute amount of PP-extractable Fe and the relative amount of PP-extractable Fe to total Fe extracted with this sequential extraction decreased as soil aggregate size increased, whereas those of HH-extractable Fe decreased as soil aggregate size decreased (Figure 2-1, Table S2-4). The amount of DH-extractable Fe slightly decreased as soil aggregate size increased.

Similar to C distribution, the extractable concentration of Fe was generally higher in surface soil than in the lower horizons (Figure 2-1, Table S2-4). Iron concentration in PP-extractable fraction was up to 0.05 mol kg^{-1} in the A horizon and declined to 0.003 mol kg^{-1} in the B horizon. Fe concentrations in HH- and DH-extractable fractions were generally low, ranging from 0.003 mol kg^{-1} and 0.02 mol kg^{-1} in the A horizon to 0.001 mol kg^{-1} and 0.009 mol kg^{-1} in the B horizon.

Relative proportions of PP-extractable Fe decreased with increasing soil depths, whereas HH- and DH-extractable Fe, especially DH-extractable Fe became more profound in deeper soils (Figure 2-2, Table S2-5). PP-extractable Fe concentrations were higher than DH-extractable Fe concentrations in A horizon, but the opposite trend was observed in B horizon, which also lead to the decrease in the proportion of PP-extractable Fe along soil depths (Figure 2-1 and 2-2, Table S2-4 and S2-5). For example, PP-extractable Fe that accounted for 88% of extractable Fe in < 20 μm in A horizon declined to 32% in same fraction in B horizon, whereas DH-extractable Fe increased its proportion from 11% in A horizon to 62% in B horizon.

Iron X-ray Absorption Spectroscopy

Major Fe phases in bulk soil samples from A (0-29 cm) and B horizons (54-69 cm) were determined by XANES and EXAFS to evaluate the Fe environment in Musick soil. Hematite and ferrihydrite were identified as the major Fe oxides, whereas smectite and/or illite were identified as the major Fe-containing clay minerals, in Musick soils. Detailed measurement parameters can be found in Table S2-1. The proportion of hematite increased from 7.5±0.3% in the bulk surface soil to 17.1±2.8% in subsoil, whereas the proportion of ferrihydrite was 37.1±4.3% in surface and 36.1±7.2% in subsoil as shown in Fe-XANES/EXAFS spectra (Figure 2-3, Table 2-2). Smectite and/or illite generally accounted for around 50% of Fe mass regardless of the soil horizon. The results from XANES and EXAFS were slightly different may due to the differences in signal to noise and background subtraction relative to reference compound spectra in the two spectral regions.

2.3.3. Extractable Calcium

Only PP-extractable Ca was discussed in this study because the concentrations of HH and DH-extractable Ca were below detection and thus negligible for Musick soil (data not shown). Similar to the distributions of extractable Fe and C, the concentration of Ca was higher in A horizon and/or smaller size aggregates (Figure 2-1, Table S2-6). Ca concentration was up to ~0.1 mol kg^{-1} in the < 20 μm size class in A horizon, and

declined to ~ 0.02 mol kg^{-1} in B horizon, and the overall distribution of Ca along soil depths was similar to Fe and C in the same dissolved fraction (Figure 2-4). The concentration of PP-extractable Ca was higher than Fe but is much lower than C in the same pool.

2.3.4. Correlations of Fe, Ca, and C

Concentrations of C in PP and DH extractions were positively correlated with extracted Fe in the A horizon with R^2 values of 0.68 ($p < 0.0001$) and 0.55 ($p < 0.0001$), respectively (Figure 2-5). However, the correlations became weaker in the B horizon with R^2 values of 0.36 ($p < 0.0001$) and 0.19 ($p < 0.0001$), respectively (Figure 2-5). Concentration of PP-extractable Fe was also closely correlated to the PP-extractable Ca (R^2=0.77, p<0.0001) in the A horizon (Figure 2-4). In addition, we observed a positive linear association of soil C concentration with proportion of PP-extractable Fe ($R^2 = 0.87$, p<0.0001), whereas we observed a negative correlation of soil C concentration with increasing proportion of HH- and DH-extractable Fe with R^2 values of 0.46 (p=0.0006) and 0.86 (p<0.0001) in Musick soils (Figure 2-6).

2.4. DISCUSSION

2.4.1. Linkages between pedogenic Fe, soil aggregates, and soil C storage

Pyrophosphate (PP) solution is presumed to selectively extract Fe in organo-mineral associations, including chelated organo-metal ions (such as Fe) or organo-cation complexes (e.g. Masiello et al., 2004; Kaiser et al. 2011; Berhe et al., 2012; Lopez-Sangil and Rovira, 2013; Lawrence et al., 2015; Coward et al., 2018; Hechman et al., 2018). But PP solution may also dissolve Fe minerals that were entrapped inside organic matter colloids (Coward et al., 2017). Previous studies have pointed out that a small amount of poorly crystalline Fe oxides may also be dissolved with this extraction (e.g. Masiello et al., 2014; Lawrence et al., 2015; Heckman et al., 2018; Berhe et al. 2012). Hydroxylamine hydrochloride (HH), as a common alternative to ammonium oxalate, is used to extract mostly poorly crystalline Fe oxides (e.g. Land et al., 1999; Laveuf et al., 2012; Vazquez-Ortega et al., 2016; Coward et al., 2017) and sodium dithionite hydrochloride (DH) is used to target extraction of total pedogenic Fe (e.g. Wagai and Mayer, 2007). Since poorly crystalline Fe oxide was removed by the PP and HH extractions in the sequential extraction procedure we followed, DH extraction liberates Fe from crystalline Fe oxides, including crystalline hematite and goethite (Lawrence et al., 2015). Note that extractants used in this study were carbon-free replacement to traditional extractants to avoid C contamination from chemicals used in the procedure (Wagai and Mayer, 2007; Heckman et al., 2018). The effectiveness of parallel (or single) vs. sequential extraction procedures was tested using pure Fe oxides and natural soils/sediments samples in previous studies. Results of previous studies showed that sequential extractions procedure (PP → HH → DH) can be used to infer the concentrations of Fe associated with organic matter, Fe associated with poorly crystalline or short-range order minerals, and crystalline pedogenic Fe oxides, respectively; and also

allow targeting of C that is extracted from the same procedures to infer the amount of C associated with different Fe phases (Poulton and Canfield, 2005; Wagai et al., 2013; Heckman et al., 2018). It is also possible that HH- and DH-extractable Fe under acidic conditions may preserve some of SOM possibly by precipitation and underestimate soil C that is associated to HH- and DH-extractable Fe (Coward et al., 2017).

The concentration of PP-extractable Fe may significantly influence the amount of PP-extractable C and SOC, especially in A horizon in Musick soil, as is shown by the higher relative contribution of PP-extractable Fe to C compared to the other two Fe pools (Figure 2-2), by the strong correlations between the concentrations of PP-extractable Fe and C (Figure 2-5), as well as by the correlations between the proportions of PP-extractable Fe and SOC content (Figure 2-6). The finding is consistent with the recent studies by Wagai et al. (2013), Coward et al. (2017) and Heckman et al. (2018), who found that PP-extractable C accounted for the largest pool in their soils. Stronger correlations between the concentrations of PP-extractable Fe and SOC, compared to HH- and DH-extractable fractions, may also indicate that PP-extractable Fe may better predict the SOC concentrations (Porras et al., 2017). The contribution of PP-extractable Fe to C storage is highest in silt and clay size fraction of soil aggregates as was shown by the higher concentrations of the PP-extractable Fe and C in smaller soil size aggregates (Figure 2-1). Similarly, Wissing et al. (2014) also found that Fe oxides and their associated C (SOC removed from Fe oxide surface with hydrogen peroxide) was protected primarily in clay-sized fraction in paddy soil. Thus, organically associated Fe may improve C storage in soil aggregates, especially in silt and clay fractions. Organically associated aluminum (Al) may also promote OC in this fraction as a close relationship between PP-extractable Al and C was also found (Figure S2-4). Higher surface area in smaller aggregate size fractions may partially contribute to the strong relationships between PP-extractable Fe and soil C storage.

HH-extractable Fe, representing mostly poorly crystalline Fe oxides, had no significant correlations with HH-extractable C, and proportions of HH-extractable Fe was negatively correlated to HH-extractable C. The importance of poorly crystalline metal oxides on C storage is not as significant as previous findings (e.g. Torn et al., 1997, Kleber et al., 2009). This is likely because: (1) poorly crystalline mineral phases may not always provide effective surface for C sorption (Heckman et al., 2018), (2) low abundance of poorly crystalline Fe oxides in Musick soils (Dahlgren et al., 1997), (3) poorly crystalline Fe oxide may catalize microbial metabolism (Hall et al., 2015), and/or (4) in soils with low concentration of Fe phases, other mineral phases, such as poorly crystalline Al may be more strongly interact with SOM, compared to poorly crystalline Fe minerals (Masiello et al., 2004). Our results may favor the last explanation since HH-extractable C strongly positively correlated to HH-extractable Al (Figure S2-4). Additionally, the concentration of HH-extractable Fe concentration was higher in macroaggregates and microaggregates than in silt and clay fractions, suggesting that the poorly crystalline Fe oxides may be enriched in larger aggregate size fractions (Huang et al., 2016). The SOC preserved by Fe oxides inside aggregates may also exhibit longer residence time and may be more stable compared to the free C, and prevent desorption or decomposition (Kaiser,

2002; Kaiser and Guggenberger, 2003 and 2007; Rasmussen et al., 2005; Moni et al., 2010; Regelink et al., 2015; Huang et al., 2016). Special microenvironment due to enzyme productions and their activities, and/or soil pore structures may also slow the microbial decomposition (McCarthy et al., 2008). Since ferrihydrite has been identified as a major poorly crystalline Fe oxide in Musick soil (Figure 2-3, Table 2-2), our results suggest that the HH-extractable Fe oxide, mainly ferrihydrite, may mostly preserve soil C in the large aggregate size classes, despite of the limited concentration of poorly crystalline Fe oxides presented in the Musick soil. In addition, comparing to poorly crystalline Fe oxides, poorly crystalline Al oxides may play a bigger role on poorly crystalline mineral associated C in Musick soils. It is possible that poorly crystalline Fe oxides, such as ferrihydrite, may be heavily Al-substituted in Musick soils, which may affect surface composition, structures and overall reactivity with pollutants in soils (Schulze and Schwertmann, 1984; Jentzsch and Penn, 2006; Ekstrom et al., 2010; Masue et al., 2011; Cismasu et al., 2012). However, the exact mechanism on how poorly crystalline metal oxides regulate the formation and the stability of macroaggregates warrants further investigation.

DH-extractable Fe, representing crystalline Fe oxides in the sequential extraction series in this study, was significantly correlated to soil C associated in this fraction as indicated by the close correlations between DH-extractable Fe oxides and DH-extractable C or soil C storage (Figure 2-5 and 2-6). We found that the concentration of DH-extractable Fe had a significant positive correlation with C concentration in the same pool. DH-extractable Fe oxides had much lower C:Fe ratio compared to PP- or HH-extractable pools, and the proportion of DH extractable Fe was significantly negatively correlated with SOC content, suggesting that DH-extractable Fe oxide may not as important as PP-extractable Fe pools on soil C accumulation (Kleber et al., 2005; Heckman et al., 2018). Low C:Fe ratio may indicate that sorption may be the dominant C stabilization mechanism in DH-extractable Fe pool (Lalonde et al. 2012; Zhao et al., 2016). Since the relative importance of DH-extractable Fe increases with soil depths, the relative importance of sorption may also increase with soil depths (Moni et al., 2010). Moreover, the SOC that is associated to DH-extractable Fe may also be considered as slow-cycling “old” C as indicated by radiocarbon(^{14}C) analysis in previous studies (Hall et al., 2018; Heckman et al., 2018). Therefore, although DH-extractable Fe oxides, mainly hematite in this soil as indicated by Fe-XAS analysis, may not promote high amount of SOC, the portions sorbed on to this fraction may persist for long periods of time (Hall et al., 2018; Heckman et al., 2018). On the other hand, DH-extractable Al was not correlated with DH-extractable C (Figure S4), which may indicate that crystalline Fe oxide may play a bigger role in soil C persistence in Musick soils compared to crystalline Al oxide.

2.4.2. Relationship between organically associated Fe and Ca cation

PP-extractable Fe was strongly correlated with PP-extractable Ca and C in Musick soils (Figure 2-4), which may indicate that Ca regulates the Fe-OM associations in this soil. Carbonate was not found in the soil as was found in previous studies in the same area (Dahlgren et al., 1997; Castanha and Trumbore, 2012), and thus Ca may mostly be

involved in the formation of organo-mineral associations in Musick soil, where Ca facilitated the accumulation of organic molecules (Oades, 1988). The role of Ca on accumulating organic molecules in organo-mineral associations in PP-extractable Fe pool may be similar to the role of Ca in zonal structure of organo-mineral associations proposed by Kleber et al. (2007). According to Kleber et al. (2007), polyvalent cations (such as Ca) may mediate the thickness of outer region of organo-mineral associations by connecting negatively charged organic fragments, such as carboxyl group or microbial residues (e.g. Chen et al., 2014; Kleber et al., 2015) or negatively charged mineral surface, and thus the overall size of organo-mineral associations. It is possible because kaolinite and carboxyl group may exert negative charge in Musick soil since soil pH is over 5. It is also possible that Ca cation may be occluded within Fe-C associations, which may be released with reduction extraction process (Hall and Huang et al., 2017). Similar to organically associated Fe, organically associated Al was also closely correlated to Ca (Figure S2-3). A strong correlation between metal oxide, C, and Ca was also evident from scanning transmission X-ray microscope-NEXAFS spectroscopy previously (Cheng et al., 2014; Hall and Huang, 2017). Therefore, with high input of SOM and exchangeable Ca content, large amount of C may be preserved by organically associated Fe and/or Al in A horizon, which is also supported by much higher concentrations of SOC and Ca found in A horizon in Musick soil compared to B horizon in this study (Figure 2-1). Additionally, since Ca may enhance soil aggregate stability (Six et al., 2004), we suggest that it is likely to be partly responsible for higher aggregate stability in silt and clay sized fractions. Therefore, Ca in PP-extractable pool, especially in silt and clay fractions, may influence the overall soil aggregate formation and stability, and further influence soil C persistence in Musick soil.

2.4.3. Relationship between Fe crystallinity and soil development

Fe oxide crystallinity shifted along soil depths as indicated by the decrease in proportion of PP-extractable Fe as a result of an increase in proportion of DH-extractable Fe (Figure 2-2). The finding was also supported by Fe-XANES/EXAFS spectra in this study, where we found that the relative proportion of pedogenic Fe was shifted from less crystalline Fe oxide (i.e. ferrihydrite) to more crystalline Fe oxide (i.e. hematite) in B horizon (Figure 2-3). This may likely due to the translocation of Fe oxides along the soil profile through illuviation processes. It is also possible that high amount of PP-extractable Fe and C may limit the precipitation of crystalline Fe oxides in surface soils, whereas low supply of C in the subsoil may allow the precipitation of crystalline Fe oxides in subsoil (Lawrence et al., 2015). These results support the conceptual model, as proposed by Schwertmann's group (1986), that SOM-Fe oxide associations with high OC supply inhibited the precipitation of Fe oxide mineral phases. Similar findings were also reported by previous groups. For example, Wagai and Mayer (2007) observed the shift of Fe phases in SOM-Fe complexes from Fe oxides (sodium dithionite-citrate extraction) to precipitated Fe-OM associations with increasing C supply. Lawrence and his coworkers (2015) found that organo-metal complexes (PP-extractable fraction) in surface soil limited the precipitation of secondary minerals (such as oxides), whereas lower input of SOM in subsoil allowed the formation of secondary minerals (ammonium oxalate- and dithionite-

citrate-extractable fractions). Therefore, we suggest that Fe crystallinity and soil C content are closely linked in Musick soil.

2.4.4. Application of sequential extraction methodology

To assess the effectiveness of sequential extraction methodology in Musick soil, our results were compared to the previous study by Dahlgren et al. (1997), who conducted parallel Fe extractions in the same area. In their study, the authors used PP to extract organically associated Fe, ammonium oxalate (Fe_o) to extract poorly-crystalline Fe oxides and organically associated Fe, and sodium dithionite-citrate (Fe_d) to extract crystalline Fe oxides, poorly-crystalline Fe oxides, and organically associated Fe, individually (i.e. parallel extraction) to bulk soil in different soil depths as was described in their paper (Dahlgren et al., 1997). To compare Fe concentrations with varying crystallinity between two studies, we took differences among each extraction to obtain the concentrations of different types of Fe.

Concentrations of PP-extractable Fe and HH-extractable Fe in surface soils were around 30% higher in our study compared to Dahlgren's work, whereas the concentrations of poorly crystalline Fe oxide (i.e. $Fe_{O\text{-}P}$ = oxalate extractable Fe – PP extractable Fe in their study vs. HH extractable Fe in this study) in subsoils and crystalline Fe oxides (i.e. $Fe_{D\text{-}O}$ = DC extractable Fe – oxalate extractable Fe in their study vs. DH extractable Fe in this study) were found more than ten times higher in Dahlgren's study. This discrepancy was highly likely due to the grinding process through 100-mesh (< 149 μm) sieve prior to Fe extraction that was performed in Dahlgren's study (e.g. McKeague et al., 1967; McKeague et al., 1977; Ross and Wang, 1993; Dahlgren et al., 1997), whereas, on the contrary, bulk soil samples in this study were passed through 2 mm sieve (e.g. Wagai and Mayer, 2007; Wagai et al., 2013; Lawrence et al., 2015). Fe extractaions on sieved or non-sieved soils may yield different amount of Fe since some portion of soil aggregates may be solvent-stable. The findings indicate that a certain amount of poorly-crystalline and crystalline (HH and DH extraction) Fe oxides in Musick soil may benot released and detected during our procedures without grinding process. PP-extractable Fe was not affected much by usage of different size sieves in two studies, suggesting that most of the organically associated Fe may reside in the smaller size class aggregates in Musick soil, which was also supported by the concentrations of PP-extractable Fe found in this study (see discussion above). Additionally, the trend of degree of crystallinity indices (i.e. Fe_d/Fe_o in Dahlgren's study was compared to $(Fe_{PP} + Fe_{HH} + Fe_{DH})/(Fe_{HH} + Fe_{PP})$ in our study) were generally in agreement with previous work by Dahlgren et al. (1997), and were increased with soil depths in both studies, which was supported by Fe-XANES/EXAFS in our study (see discussion above). It should be noted that the time and the chemical differences between two studies may also partially contribute to the differences in results reported by two studies. Considering these (dis)similarities between two studies, we suggest that grinding process may affect the effectiveness of sequential extractions and is recommended to use in the future studies to obtain more accurate concentrations of Fe oxides in macroaggregate.

2.5. CONCLUSION

To understand the importance of pedogenic Fe on the distribution of SOC that is occluded in soil aggregates, sequential selective extraction procedure was applied to the Musick soil in different aggregate size fractions. Distribution of extractable C pedogenic Fe with varying crystallinity on soil C, presumably soil C persistence, were determined. Organically associated Fe (PP-extractable Fe) may promote organically associated C, presumably their persistence, especially in smaller soil aggregate size fractions. Polyvalent cation (Ca) may possibly also contribute to soil C storage in organically associated fractions (PP-extractable fraction). Poorly crystalline Fe oxides (HH-extractable Fe) may be enriched in larger soil aggregate size fractions, but poorly crystalline Al oxides (HH-extractable Al) may play a bigger role in promoting C presumable their persistence in poorly crystalline mineral containing fraction (HH-extractable fraction). Crystalline Fe oxides may promote crystalline mineral associated C, presumably their persistence, in smaller soil aggregate size fraction or deeper soils.

ACKNOWLEDGEMENTS

The authors thank Liying Zhao at the Environmental Analytical Lab at UC Merced for assistance with lab analyses, and Samuel Negusse Araya and Randy Dahlgren for information about field sites and the Musick soil. This work was funded by Startup funds from University of California, Merced, UC Merced Sierra Nevada Research Institute Seed Grant, and NSF award to AAB (CAREER, EAR-1352627).

REFERENCES

Adhikari, D., Zhao, Q., Das, K., Mejia, J., Huang, R., Wang, Poulson, S., Tang, Y., Roden, E., & Yang, Y. (2017). Dynamics of ferrihydrite-bound organic carbon during microbial Fe reduction. Geochimica et Cosmochimica Acta, 212, 221-233.

Barral, M. T., Arias, M., & Guerif, J. (1998). Effects of iron and organic matter on the porosity and structural stability of soil aggregates. Soil and Tillage Research, 46(3-4), 261-272.

Berger, M. J. and Hubbell, J. H. (1987). XCOM: Photon cross sections on a personal computer (No. NBSIR-87-3597). National Bureau of Standards, Washington, DC (USA). Center for Radiation Research.

Berhe, A. A., Harden, J. W., Torn, M. S., Kleber, M., Burton, S. D. and Harte, J. (2012). Persistence of soil organic matter in eroding versus depositional landform positions. Journal of Geophysical Research: Biogeosciences, 117(G2).

Bronick, C. J. and Lal, R. (2005). Soil structure and management: a review. Geoderma, 124(1-2), 3-22.

Castanha, C., Trumbore, S. E. and Amundson, R. (2012). Mineral and Organic Matter Characterization of Density Fractions of Basalt-and Granite-Derived Soils in Montane California. In An Introduction to the Study of Mineralogy. IntechOpen.

Cismasu, A. C., Michel, F. M., Stebbins, J. F., Levard, C., & Brown Jr, G. E. (2012). Properties of impurity-bearing ferrihydrite I. Effects of Al content and precipitation rate on the structure of 2-line ferrihydrite. Geochimica et Cosmochimica Acta, 92, 275-291.

Chen, C., Dynes, J. J., Wang, J., Karunakaran, C. and Sparks, D. L. (2014). Soft X-ray spectromicroscopy study of mineral-organic matter associations in pasture soil clay fractions. Environmental science & technology, 48(12), 6678-6686.

Chenu, C., & Plante, A. F. (2006). Clay-sized organo-mineral complexes in a cultivation chronosequence: revisiting the concept of the ‘primary organo-mineral complex’. European Journal of Soil Science, 57(4), 596-607.

Cornell, R. M. and Schwertmann, U. (2003). The iron oxides: structure, properties, reactions, occurrences and uses. John Wiley & Sons.

Coward, E. K., Thompson, A. T. and Plante, A. F. (2017). Iron-mediated mineralogical control of organic matter accumulation in tropical soils. Geoderma, 306, 206-216.

Coward, E. K., Thompson, A. and Plante, A. F. (2018). Contrasting Fe speciation in two humid forest soils: Insight into organomineral associations in redox-active environments. Geochimica et Cosmochimica Acta, 238, 68-84.

Dahlgren, R. A. (1994). Quantification of allophane and imogolite. Quantitative methods in soil mineralogy, (quantitativemet), 430-451.

Dahlgren, R. A., Boettinger, J. L., Huntington, G. L. and Amundson, R. G. (1997). Soil development along an elevational transect in the western Sierra Nevada, California. Geoderma, 78(3-4), 207-236.

Eglinton, T. I. (2012). Geochemistry: A rusty carbon sink. Nature, 483(7388), 165.

Ekstrom, E. B., Learman, D. R., Madden, A. S., & Hansel, C. M. (2010). Contrasting effects of Al substitution on microbial reduction of Fe (III)(hydr) oxides. Geochimica et Cosmochimica Acta, 74(24), 7086-7099.

Ellerbrock, R. H. and Gerke, H. H. (2013). Characterization of organic matter composition of soil and flow path surfaces based on physicochemical principles—A review. In Advances in agronomy (Vol. 121, pp. 117-177). Academic Press. Chicago

Eusterhues, K., Rumpel, C., Kleber, M. and Kögel-Knabner, I. (2003). Stabilisation of soil organic matter by interactions with minerals as revealed by mineral dissolution and oxidative degradation. Organic Geochemistry, 34(12), 1591-1600.

Eusterhues, K., Rumpel, C. and Kögel-Knabner, I. (2005). Organo-mineral associations in sandy acid forest soils: importance of specific surface area, iron oxides and micropores. European Journal of Soil Science, 56(6), 753-763.

Hall, S. J., Berhe, A. A. and Thompson, A. (2018). Order from disorder: do soil organic matter composition and turnover co-vary with iron phase crystallinity? Biogeochemistry, 140(1), 93-110.

Hall, S. J., & Huang, W. (2017). Iron reduction: a mechanism for dynamic cycling of occluded cations in tropical forest soils?. Biogeochemistry, 136(1), 91-102.

Hall, S. J., & Silver, W. L. (2015). Reducing conditions, reactive metals, and their interactions can explain spatial patterns of surface soil carbon in a humid tropical forest. Biogeochemistry, 125(2), 149-165.

Heckman, K., Lawrence, C. R. and Harden, J. W. (2018). A sequential selective dissolution method to quantify storage and stability of organic carbon associated with Al and Fe hydroxide phases. Geoderma, 312, 24-35.

Huang, X., Jiang, H., Li, Y., Ma, Y., Tang, H., Ran, W. and Shen, Q. (2016). The role of poorly crystalline iron oxides in the stability of soil aggregate-associated organic carbon in a rice–wheat cropping system. Geoderma, 279, 1-10.

Jastrow, J. D., Amonette, J. E. and Bailey, V. L. (2007). Mechanisms controlling soil carbon turnover and their potential application for enhancing carbon sequestration. Climatic Change, 80(1-2), 5-23.

Jentzsch, T. L., & Penn, R. L. (2006). Influence of aluminum doping on ferrihydrite nanoparticle reactivity. The Journal of Physical Chemistry B, 110(24), 11746-11750.

Kaiser, K. and Guggenberger, G. (2000). The role of DOM sorption to mineral surfaces in the preservation of organic matter in soils. Organic geochemistry, 31(7-8), 711-725.

Kaiser, K., Eusterhues, K., Rumpel, C., Guggenberger, G. and Kögel-Knabner, I. (2002). Stabilization of organic matter by soil minerals—investigations of density and particle-size fractions from two acid forest soils. Journal of Plant Nutrition and Soil Science, 165(4), 451-459.

Kaiser, K. and Guggenberger, G. (2003). Mineral surfaces and soil organic matter. European Journal of Soil Science, 54(2), 219-236.

Kaiser, K. and Guggenberger, G. (2007). Sorptive stabilization of organic matter by microporous goethite: sorption into small pores vs. surface complexation. European Journal of Soil Science, 58(1), 45-59.

Kaiser, M., Walter, K., Ellerbrock, R. H. and Sommer, M. (2011). Effects of land use and mineral characteristics on the organic carbon content, and the amount and composition of Na-pyrophosphate-soluble organic matter, in subsurface soils. European Journal of Soil Science, 62(2), 226-236.

Kalbitz, K., Solinger, S., Park, J. H., Michalzik, B. and Matzner, E. (2000). Controls on the dynamics of dissolved organic matter in soils: a review. Soil science, 165(4), 277-304.

Kleber, M., Eusterhues, K., Keiluweit, M., Mikutta, C., Mikutta, R. and Nico, P. S. (2015). Mineral–organic associations: formation, properties, and relevance in soil environments. In Advances in agronomy (Vol. 130, pp. 1-140). Academic Press.

Kleber, M., Mikutta, R., Torn, M. S., & Jahn, R. (2005). Poorly crystalline mineral phases protect organic matter in acid subsoil horizons. European Journal of Soil Science, 56(6), 717-725.

Kleber, M., Sollins, P., & Sutton, R. (2007). A conceptual model of organo-mineral interactions in soils: self-assembly of organic molecular fragments into zonal structures on mineral surfaces. Biogeochemistry, 85(1), 9-24.

Lalonde, K., Mucci, A., Ouellet, A. and Gélinas, Y. (2012). Preservation of organic matter in sediments promoted by iron. Nature, 483(7388), 198.

Land, M., Öhlander, B., Ingri, J., & Thunberg, J. (1999). Solid speciation and fractionation of rare earth elements in a spodosol profile from northern Sweden as revealed by sequential extraction. Chemical Geology, 160(1-2), 121-138.

Laveuf, C., Cornu, S., Guilherme, L. R. G., Guerin, A. and Juillot, F. (2012). The impact of redox conditions on the rare earth element signature of redoximorphic features in a soil sequence developed from limestone. Geoderma, 170, 25-38.

Lawrence, C. R., Harden, J. W., Xu, X., Schulz, M. S. and Trumbore, S. E. (2015). Long-term controls on soil organic carbon with depth and time: A case study from the Cowlitz River Chronosequence, WA USA. Geoderma, 247, 73-87.

Leven, A., Vlassopoulos, D., Kanematsu, M., Goin, J., & O'Day, P. A. (2018). Characterization of manganese oxide amendments for in situ remediation of mercury-contaminated sediments. Environmental Science: Processes & Impacts, 20(12), 1761-1773.

Lützow, M. V., Kögel-Knabner, I., Ekschmitt, K., Matzner, E., Guggenberger, G., Marschner, B. and Flessa, H. (2006). Stabilization of organic matter in temperate soils: mechanisms and their relevance under different soil conditions–a review. European Journal of Soil Science, 57(4), 426-445.

Masiello, C. A., Chadwick, O. A., Southon, J., Torn, M. S. and Harden, J. W. (2004). Weathering controls on mechanisms of carbon storage in grassland soils. Global Biogeochemical Cycles, 18(4).

Masue-Slowey, Y., Loeppert, R. H., & Fendorf, S. (2011). Alteration of ferrihydrite reductive dissolution and transformation by adsorbed As and structural Al: Implications for As retention. Geochimica et Cosmochimica Acta, 75(3), 870-886.

McCarthy, J. F., Ilavsky, J., Jastrow, J. D., Mayer, L. M., Perfect, E. and Zhuang, J. (2008). Protection of organic carbon in soil microaggregates via restructuring of aggregate porosity and filling of pores with accumulating organic matter. Geochimica et Cosmochimica Acta, 72(19), 4725-4744.

McKeague, J. A. (1967). An evaluation of 0.1 M pyrophosphate and pyrophosphate-dithionite in comparison with oxalate as extractants of the accumulation products in podzols and some other soils. Canadian Journal of Soil Science, 47(2), 95-99.

McKeague, J. A., & Sheldrick, B. H. (1977). Sodium hydroxide-tetraborate in comparison with sodium pyrophosphate as an extractant of “complexes” characteristic of spodic horizons. Geoderma, 19(2), 97-104.

Mikutta, R., Kleber, M., Torn, M. S. and Jahn, R. (2006). Stabilization of soil organic matter: association with minerals or chemical recalcitrance? Biogeochemistry, 77(1), 25-56.

Moni, C., Rumpel, C., Virto, I., Chabbi, A. and Chenu, C. (2010). Relative importance of sorption versus aggregation for organic matter storage in subsoil horizons of two contrasting soils. European Journal of Soil Science, 61(6), 958-969.

Oades, J. M. (1988). The retention of organic matter in soils. Biogeochemistry, 5(1), 35-70.

O’Day, P. A., Rivera Jr, N., Root, R. and Carroll, S. A. (2004). X-ray absorption spectroscopic study of Fe reference compounds for the analysis of natural sediments. American Mineralogist, 89(4), 572-585.

Parfitt, R. L. and Childs, C. W. (1988). Estimation of forms of Fe and Al-a review, and analysis of contrasting soils by dissolution and Mossbauer methods. Soil Research, 26(1), 121-144.

Porras, R. C., Pries, C. E. H., McFarlane, K. J., Hanson, P. J. and Torn, M. S. (2017). Association with pedogenic iron and aluminum: effects on soil organic carbon storage and stability in four temperate forest soils. Biogeochemistry, 133(3), 333-345.

Poulton, S. W. and Canfield, D. E. (2005). Development of a sequential extraction procedure for iron: implications for iron partitioning in continentally derived particulates. Chemical geology, 214(3-4), 209-221.

Rasmussen, C., Torn, M. S., & Southard, R. J. (2005). Mineral assemblage and aggregates control carbon dynamics in a California conifer forest. Soil Science Society of America Journal, 69(6), 1711-1721.

Ravel, B. and Newville, M. (2005). ATHENA and ARTEMIS: interactive graphical data analysis using IFEFFIT. Physica Scripta, 2005(T115), 1007.

Regelink, I. C., Stoof, C. R., Rousseva, S., Weng, L., Lair, G. J., Kram, P., Nikolaidis, N.P., Kercheva, M., Banwart, S. and Comans, R. N. (2015). Linkages between aggregate formation, porosity and soil chemical properties. Geoderma, 247, 24-37.

Ross, G. J., & Wang, C. (1993). Extractable Al, Fe, Mn, and Si. Soil sampling and methods of analysis, 1993, 239-246.

Schmidt, M. W., Torn, M. S., Abiven, S., Dittmar, T., Guggenberger, G., Janssens, I. A., Kleber, M., Kogel-Knabner, I., Lehmann, J., Manning, D.A., Nannipiere, P., Rasse, D.P., Weiner, S. and Trumbore, S.E. (2011). Persistence of soil organic matter as an ecosystem property. Nature, 478(7367), 49.

Schulze, D. G., & Schwertmann, U. (1984). The influence of aluminium on iron oxides: X. Properties of Al-substituted goethites. Clay Minerals, 19(4), 521-539.

Schwertmann, U., Kodama, H. and Fischer, W. R. (1986). Mutual Interactions Between Organics and Iron Oxides 1. Interactions of soil minerals with natural organics and microbes, (interactionsofs), 223-250.

Six, J., Bossuyt, H., Degryze, S. and Denef, K. (2004). A history of research on the link between (micro) aggregates, soil biota, and soil organic matter dynamics. Soil and Tillage Research, 79(1), 7-31.

Stockmann, U., Adams, M. A., Crawford, J. W., Field, D. J., Henakaarchchi, N., Jenkins, M., ... & Wheeler, I. (2013). The knowns, known unknowns and unknowns of sequestration of soil organic carbon. Agriculture, Ecosystems & Environment, 164, 80-99.

Torn, M. S., Trumbore, S. E., Chadwick, O. A., Vitousek, P. M. and Hendricks, D. M. (1997). Mineral control of soil organic carbon storage and turnover. Nature, 389(6647), 170.

Totsche, K. U., Amelung, W., Gerzabek, M. H., Guggenberger, G., Klumpp, E., Knief, C., Lehndorff, E., Mikutta, R., Peth, S., Prechtel, A., Ray, N., & Kogel-Knabner, I. (2018). Microaggregates in soils. Journal of Plant Nutrition and Soil Science, 181(1), 104-136.

Vázquez-Ortega, A., Huckle, D., Perdrial, J., Amistadi, M. K., Durcik, M., Rasmussen, C., McIntosh, J. and Chorover, J. (2016). Solid-phase redistribution of rare earth elements in hillslope pedons subjected to different hydrologic fluxes. Chemical Geology, 426, 1-18.

Wagai, R. and Mayer, L. M. (2007). Sorptive stabilization of organic matter in soils by hydrous iron oxides. Geochimica et Cosmochimica Acta, 71(1), 25-35.

Wagai, R., Mayer, L. M., & Kitayama, K. (2009). Extent and nature of organic coverage of soil mineral surfaces assessed by a gas sorption approach. Geoderma, 149(1-2), 152-160.

Wagai, R., Mayer, L. M., Kitayama, K. and Shirato, Y. (2013). Association of organic matter with iron and aluminum across a range of soils determined via selective

dissolution techniques coupled with dissolved nitrogen analysis. Biogeochemistry, 112(1-3), 95-109.

Webb, S. M. (2005). SIXpack: a graphical user interface for XAS analysis using IFEFFIT. Physica scripta, 2005(T115), 1011.

Wissing, L., Kölbl, A., Schad, P., Bräuer, T., Cao, Z. H., & Kögel-Knabner, I. (2014). Organic carbon accumulation on soil mineral surfaces in paddy soils derived from tidal wetlands. Geoderma, 228, 90-103.

TABLES

Table 2-1. Properties of Musick soil in different soil depths.

Horizon[a]	Depths[a] (cm)	Texture[a]	pH (water)	Particle size distribution (%)				C (wt%)				
				2000-250μm	250-53μm	53-20μm	<20μm	2000-250μm	250-53μm	53-20μm	<20μm	BS[b]
AE	0-29	SL	5.70±0.04	67.8±2.0	26.9±1.7	4.0±0.4	1.3±0.1	2.71±0.05	4.13±0.05	4.64±0.00	5.24±0.01	3.15±0.01
EBt	29-38	SL	5.74±0.06	67.2±2.5	27.2±1.8	4.3±0.6	1.3±0.2	0.63±0.03	0.98±0.02	1.37±0.00	1.75±0.08	0.81±0.08
Bt1	38-54	SCL	5.59±0.05	65.7±1.2	27.4±1.0	5.5±0.2	1.4±0.1	0.45±0.04	0.79±0.02	1.08±0.00	0.98±0.00	0.52±0.01
Bt2	54-69	SCL	5.51±0.01	61.7±0.5	32.6±0.4	4.5±0.1	1.2±0.1	0.25±0.00	0.54±0.0	0.87±0.00	1.14±0.00	0.38±0.01

[a]Values from Dahlgren et al. (1997). SL: sandy loam; SCL: sandy clay loam.

[b]Abbreviate of bulk soil (BS).

Table 2-2. Results of linear combination fits of Fe-XANES and Fe-EXAFS spectra of Musick soil samples from A (0-29cm) and B (54-69cm) horizons.

Soil sample	Spectra	Hematite (%)	Ferrihydrite (%)	Smectite (%)[a]	Illite (%)[b]	Total (%)	Reduced χ^{2}[c]	R-factor[d]
Musick A horizon	XANES	7.2	32.8	39.1	19.9	99.0	1.69×10^{-4}	6.34×10^{-4}
	EXAFS	7.8	41.4	23.4	22.2	94.8	1.20×10^{-1}	2.08×10^{-2}
Musick B horizon	XANES	14.3	28.9	49.7	4.7	97.6	4.83×10^{-4}	1.75×10^{-3}
	EXAFS	19.9	43.3	34.9		98.1	1.04×10^{-1}	1.62×10^{-2}

[a] Fit with reference smectite (SAz_1), analyzed by O'Day (O'Day et al., 2004).

[b] Fit with reference illite (IMt_1), a mixed illite/smectite, analyzed by O'Day (O'Day et al., 2004).

[c] Reduced χ^{2} : statistical goodness-of-fit equal to (F-factor) / (# of points - # of variables)

[d] R-factor: statistical goodness-of-fit equal to ($\sum$ (data-fit)^{2} / $\sum$ (data)^{2})

FIGURES

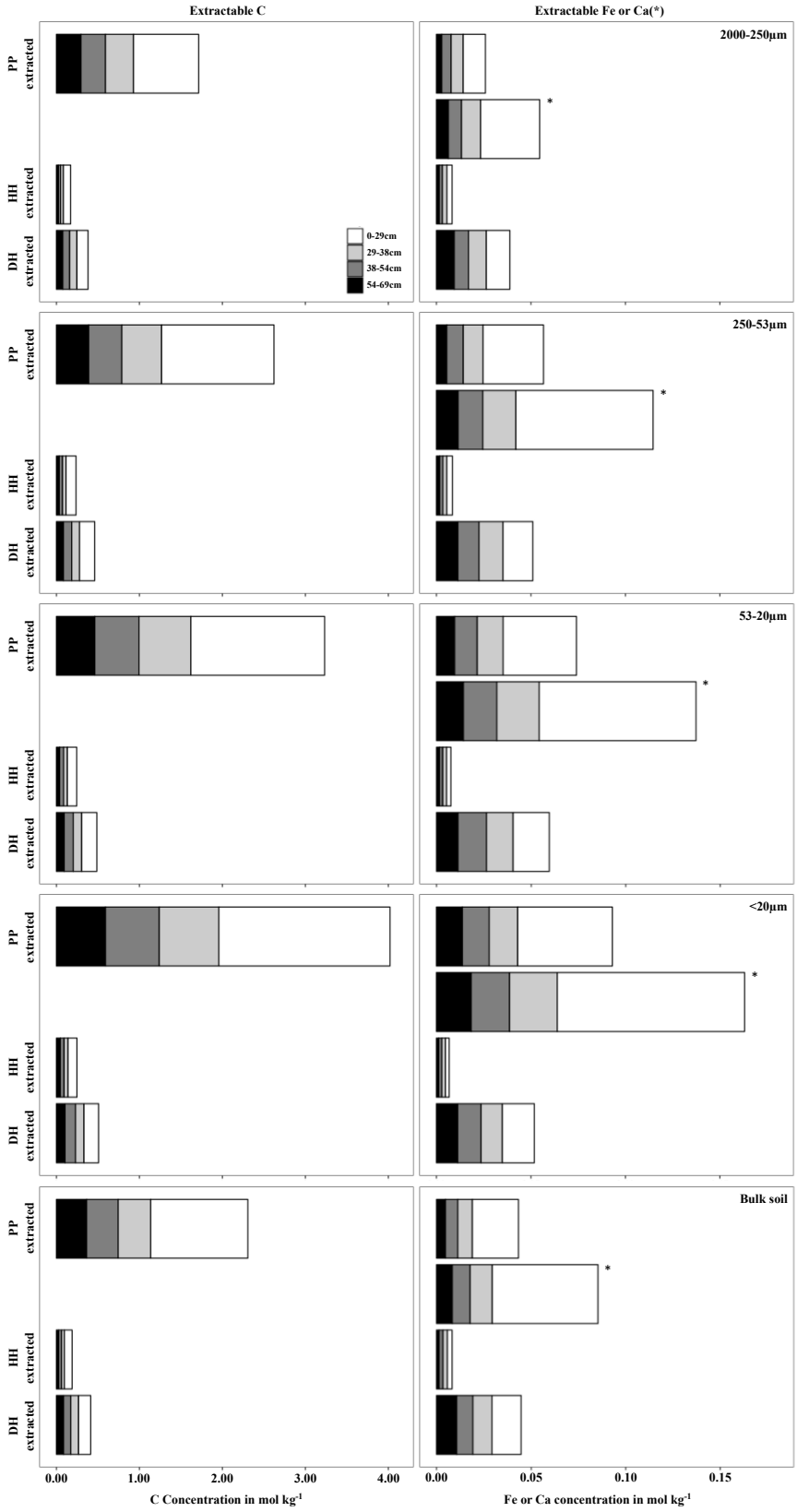

Figure 2-1. Concentrations of sequentially extracted C (left panel) and Fe or Ca (right panel, Ca concentration was indicated with *) in soil aggregate size ranges or bulk soil along soil depth profile. Values are reported in the supplementary document (Table S2-2, S2-4, and S2-6).

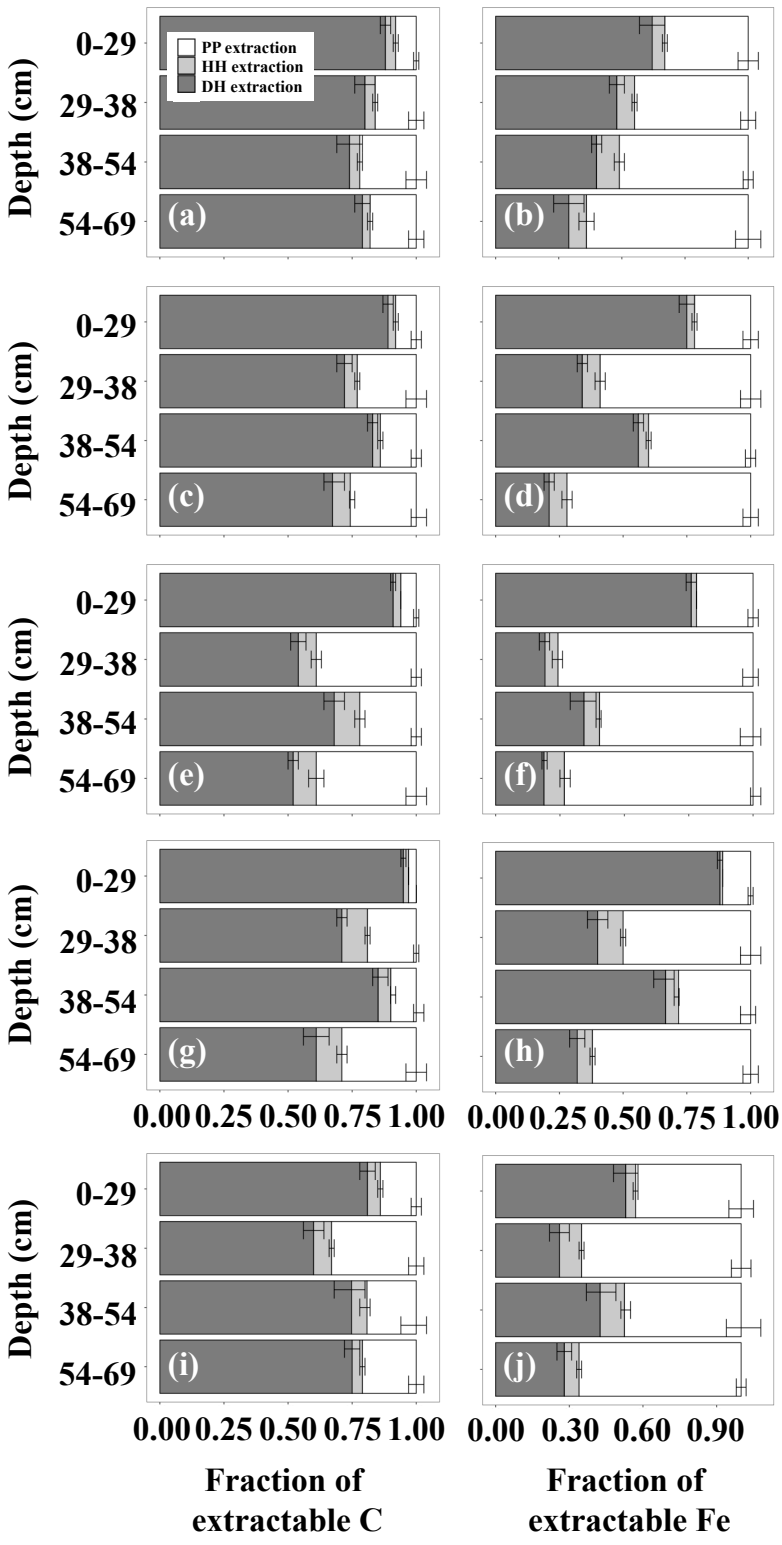

Figure 2-2. Mass distribution of sequentially extracted C (left panel) and Fe (right panel) in bulk soil and each aggregate class along soil depths (a and b: 2000-250 μm, c and d: 250-53 μm, e and f: 53-20 μm; g and h: <20 μm) (normalized to extracted C or Fe). Averaged data and standard error are reported in the supplementary document (Table S2-3 and S2-5).

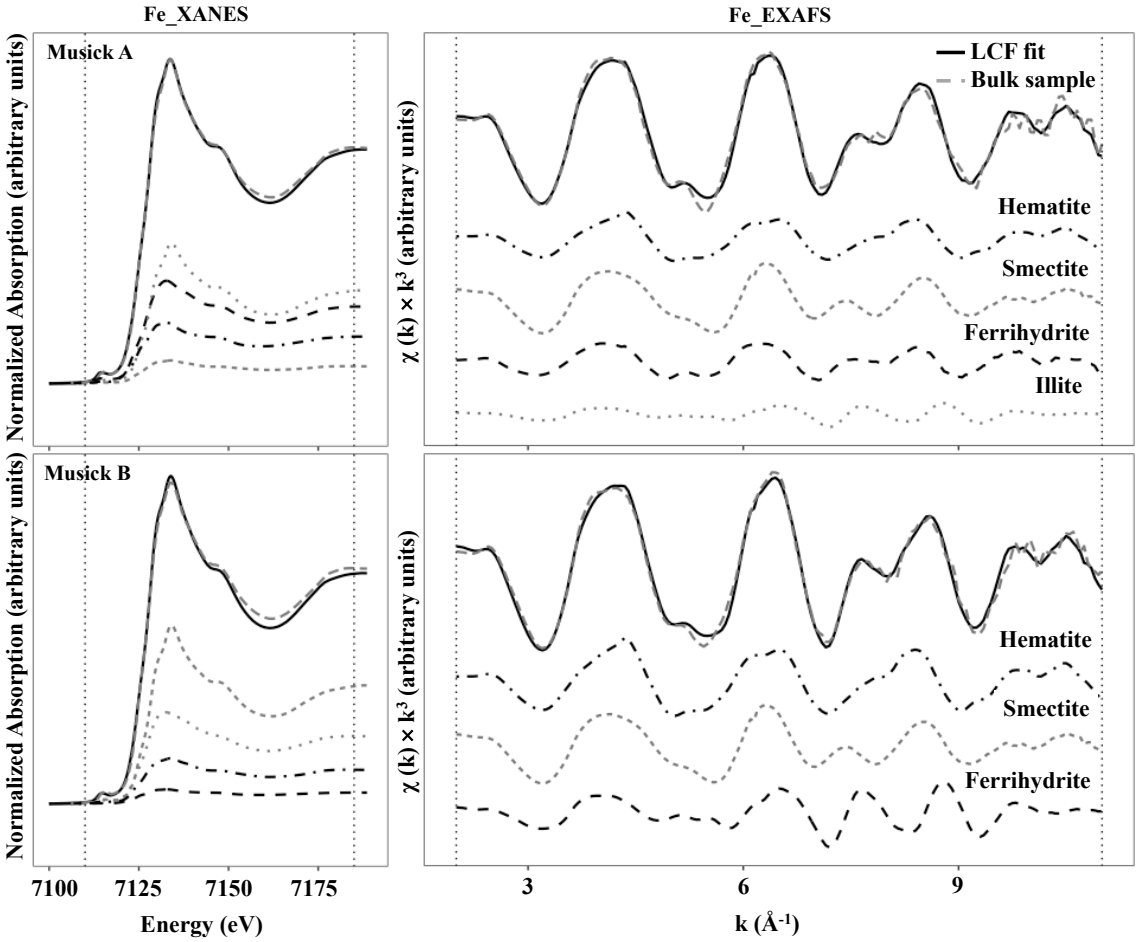

Figure 2-3. Iron K-edge XANES and EXAFS spectra of Musick A and B horizons, spectral deconvolution, and their linear combination fits using the reference spectra provided in the material section. Four minerals were used to fit all the sample spectra. However, combinations with three reference minerals were identified as the best fit for EXAFS spectra for Musick B soils. Vertical gray lines show the fitted regions of the spectra. Numerical fit results are reported in Table 2-2. Sample collection conditions and reference mineral information are reported in Table S2-1.

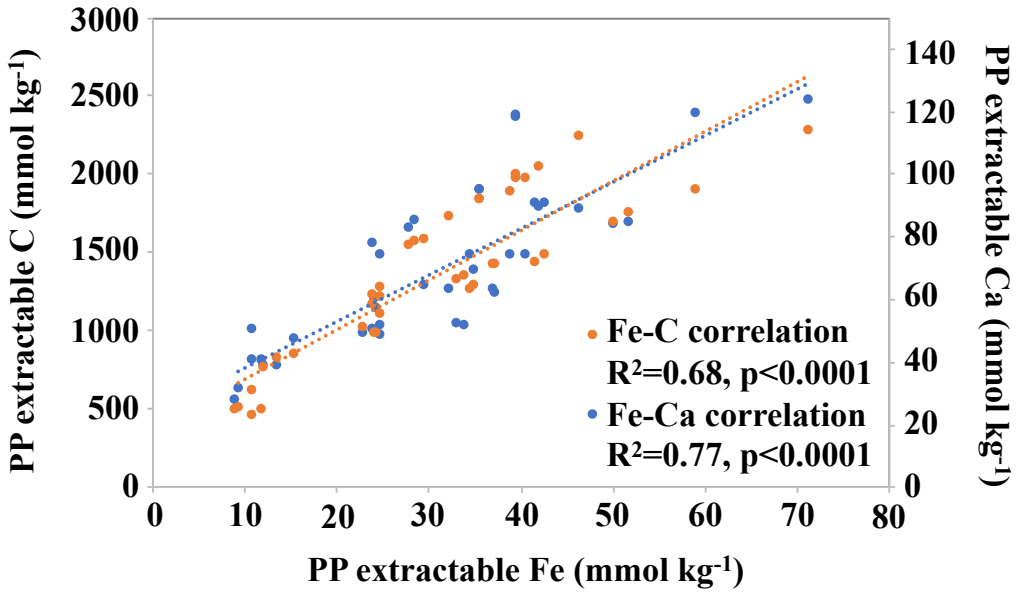

Figure 2-4. Correlations between concentrations of PP-extractable Fe and Ca (data in blue) or C (data in orange) in musick soil. Regression lines are significant at $p<0.0001$.

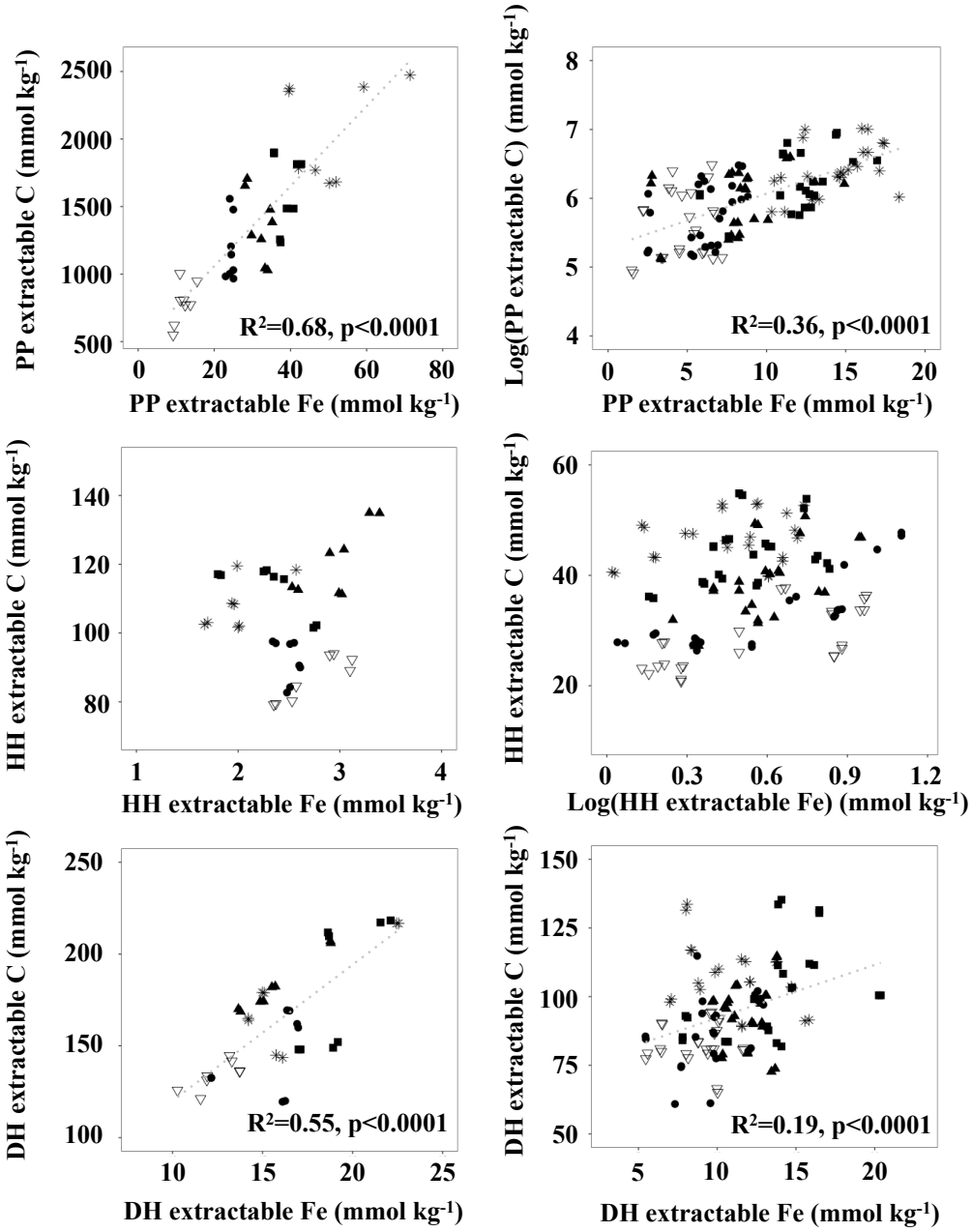

Figure 2-5. Correlations between concentrations of PP-, HH-, and DH- extractable Fe and extractable C in different size aggregates in A (left) and B horizon (right).

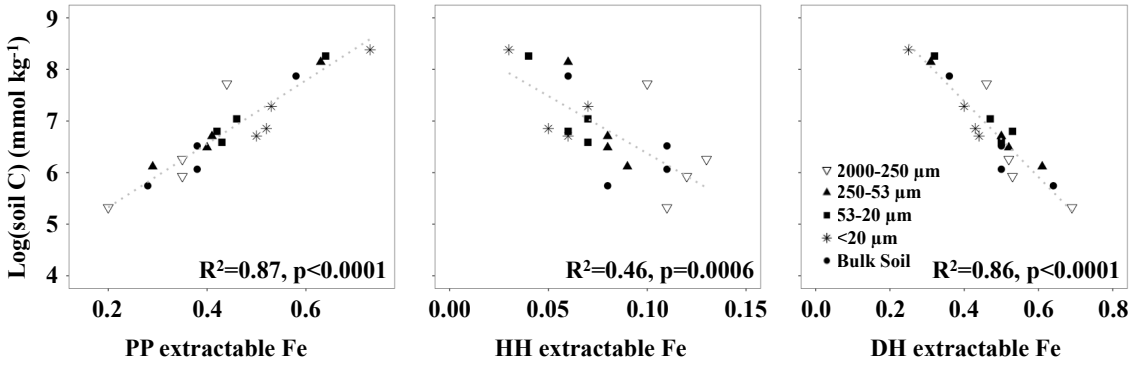

Figure 2-6. Correlations between proportions of PP-, HH-, and DH-extractable Fe and soil C content in different size aggregates along soil depths.

CHAPTER 3. CHARACTERIZATION OF ORGANIC MATTER IN PEDOGENIC IRON-CONTAINING MINERAL FRACTIONS

ABSTRACT

Soil organic matter (SOM) associated with pedogenic iron (Fe) can be preserved in the soil system depending on Fe crystallinity, chemical composition of SOM, and soil aggregation status. However, questions remain about how different organic functional groups in soil aggregate associated SOM may be retained in chemical extracted pedogenic Fe, and if this relationship varies with soil aggregate size. We analyzed Fe extracted with sodium pyrophosphate (PP), hydroxylamine hydrochloride (HH), and sodium dithionite hydrochloride (DH), which was then referred to PP-extractable organically associated Fe, HH-extractable poorly crystalline Fe oxides, and DH-extractable crystalline Fe oxides. C functional groups and stable C isotopic composition in extractable fractions determined and stability of soil organic carbon (SOC) was presumed. Peak area of each C functional group calculated from DRIFT spectra was divided by total peak area of all C functional groups to obtain relative peak area. Results showed that relative peak area of aliphatic C increased with increasing concentrations of PP-extractable Fe along decreasing size fractions. However, relative peak areas of aromatic and carboxyl C tended to increase as the concentrations of HH- and DH-extractable Fe increased with decreasing soil size fractions. The ratios of aliphatic/carbonyl and/or aliphatic /carboxyl increased with increasing PP-extractable Fe concentration, whereas it tended to decrease with increasing HH- and DH-extractable Fe concentrations. In addition, stable isotopic carbon composition of extractable C tended to be enriched as relative contribution of DH-extractable Fe to HH- and DH-extractable Fe increased. These findings suggest that organically associated Fe may contribute to the abundance of aliphatic C in organically associated mineral fraction, whereas poorly crystalline and crystalline Fe oxides may contribute to the abundance of aromatic and carboxyl C in the Fe oxide containing fractions. The extent of processing C was higher as relative Fe oxide crystallinity increased. Our findings suggest that preferential association of different organic functional groups with pedogenic Fe-containing mineral fractions may play an important role in composition of OM preserved in soils.

3.1. INTRODUCTION

Associations between pedogenic Fe and soil organic matter (SOM) are important for promoting soil aggregate formation and stability (Barral et al., 1998; Cornell and Schwertmann, 2003; Six et al., 2004; Bronick and Lal, 2005; Yang et al., 2016; Regelink et al., 2015; Totsche et al., 2018). Soil aggregation, concentrations of Fe minerals, and SOM have also been linked to soil fertility and quality, i.e. structural stability and water and nutrient retention in soil (Six et al., 2004; Bronick and Lal, 2005). Among their many roles in soil, Fe oxides may prevent dispersion of soil particles by forming coatings on minerals that have low surface area and thereby providing extra adsorption sites for SOM and binding the soil particles into the stable soil aggregates (Redelink et al., 2015). Soils with high pedogenic Fe and SOM concentrations tend to have low soil porosity and textural tensile strength, and thus high soil aggregate stability (Barral et al., 1998).

Previous studies have shown that pedogenic Fe with varying crystallinity may prefer to reside in different soil aggregate classes (Barral et al., 1998; Sollins et al., 2009; Lawrence et al., 2015; Huang et al., 2016; Jin et al., chapter 2), indicating that crystallinity and concentration of pedogenic Fe in soil may strongly influence physically stabilized SOC (Jin et al., chapter 2). Furthermore, amount of SOC stabilized by pedogenic Fe varied with Fe oxide crystallinity, concentration, types, and their compositions in soils (Torn et al., 1997; Kaiser and Guggenberger, 2003; Eusterhues et al., 2005; Kleber et al., 2005; Wagai et al., 2007 and 2013; Berhe et al., 2012; Lalonde et al., 2012; Huang et al., 2016; Coward et al., 2017; Heckman et al., 2018; Porras et al., 2017; Hall et al., 2018; Jin et al., chapter 2). Strong positive correlations between pedogenic Fe and SOM were also documented in many soil systems in bulk soils or size fractions, especially in silt and clay fractions (Torn et al., 1997; Eusterhues et al., 2005; Kleber et al., 2005 and 2015; Chenu and Plante, 2006; Kogel-Knabner et al., 2008; Mikutta et al., 2009; Hall et al., 2018; Heckman et al., 2018; Jin et al., chapter 2). Hence, determining the role of pedogenic Fe on the amount and the nature of physically stabilized OC inside soil aggregates is critical for overall understanding of how soil minerals control organic matter dynamics in soil, and its implications for soil structural dynamics (Totsche et al., 2018).

Dissolved organic matter (DOM) in soil undergoes molecular fractionation due to the varying affinity or adhesion strength of DOM components to mineral surfaces (Kaiser and Guggenberger, 2000 and 2003; Chasse et al., 2015; Lv et al., 2016; Coward et al., 2018). Molecular components rich in hydrophobic, aromatic or carboxyl C, or lignin-derived C group were found to be more likely to be bound to pedogenic Fe oxides (Gu et al., 1995; Kaiser and Guggenberger, 2000 and 2003; Adhikari and Yang, 2015; Zhao et al., 2016; Huang et al., 2019). It was previously shown that C compounds with high molecular weight or that are rich in oxygen containing functional groups may be preferentially sorbed on Fe oxides, especially ferrihydrite (Lv et al., 2016). More recently, it was shown that the relative importance of microbe-derived SOM may increase as the crystallinity of Fe phases increases in dense fractions, whereas an opposite trend was observed with increase in poorly crystalline Fe phases as a result of an increase

in plant derived SOM in the fraction (Hall et al., 2018). In addition, aliphatic and amide C abundance in soil were found to have a strong positive correlation with ammonium oxalate-extractable Fe (mainly poorly crystalline Fe oxide) in the dense fraction in Hawaiian soils (Mikutta et al., 2009). Therefore, pedogenic Fe oxides may selectively preserve SOM, and further regulate the components of SOM stabilized and accumulated in natural systems since the preferences of SOC functional groups may strongly link to the SOM decomposition and control the organic material that will enter the soils (Coward et al., 2018; Hall et al., 2018).

Soil organic carbon (SOC) associated with pedogenic Fe typically has long residence times (over decades or centuries) and serves as a long-term soil C reservoir in the global C cycle (Gu et al., 1995; Torn et al., 1997; Kogel-Knabner et al., 2008; Kleber et al., 2015; Hall et al., 2018; Heckman et al., 2018). Moni et al. (2010) found that OC within Fe_{DCB}-cemented silt-size aggregate size fraction had longer $\Delta^{14}C$ based residence time compared with free clay particles. Masiello et al. (2004) reported that $\Delta^{14}C$ value had a significant negative relationship with sodium pyrophosphate extractable Fe (mainly organically associated Fe) in top meter of Finchfold series Mollisols in Northern California. Ammonium oxalate-extractable Fe and Al oxides (mainly poorly crystalline Fe and Al oxide) were found to slow the turnover of SOC in acidic soils or volcanic soils in Hawaii (Torn et al., 1997; Porras et al., 2017). However, no relationship between Fe_{DCB} and $\Delta^{14}C$ value was found in variety of forest soils (Kleber et al., 2005). Contradictory results were found by Hall et al. (2018), where an increase in oxalate-extractable Fe (mainly poorly crystalline Fe oxide) increased $\Delta^{14}C$ value (i.e. faster-cycling SOM) and an increase in Fe_{DC} decreased $\Delta^{14}C$ value (i.e. slower-cycling SOM) in dense fraction heavier than 1.6g cm^{-3} sodium polytungstate solution. In agreement with his findings, Zhao et al. (2016) found that the stable carbon isotope composition ($\delta^{13}C$) was enriched in Fe_{DCB} (sodium dithionite-citrate-bicarbonate-extractable Fe represents total pedogenic Fe) associated SOC compared to the non-pedogenic Fe associated SOC in soils, and the same trend was also found in variety of sediment samples (Lalonde et al., 2012). These findings indicate that pedogenic Fe with varying crystallinity may be associated to SOM with different chemical compositions and structures, and with different turnover rates (Hall et al., 2018).

In this study, we analyzed the importance of the extractant-based crystallinity of pedogenic Fe on the C functional groups or structure and stable C isotopic composition that is physically protected in soil aggregates with soil depths. Our objectives were: (i) to identify the chemical functional groups or structure of SOM as determined with Diffuse Reflectance Infrared Fourier Transform (DRIFT) Spectroscopy analysis), (ii) to determine the changes in stable C isotopic composition in Fe containing fractions, and (iii) to determine if particular types of C functional groups are correlated with aggregate size and/or Fe oxide crystallinity.

3.2. METHODS

3.2.1. Sample collection and particle size fractionation

Soil B horizon samples were collected in a forest soil (Musick site) at the western Sierra Nevada Mountain (located at 37.06073N, 119.37348W). Sierra Nevada represents the dominant mountain range in California (Graham and O'Green, 2010), where western Sierra Nevada forms a slope with an elevational transect from 198 m to 2865 m a.s.l., and temperature decreases as precipitation increases with higher altitude. Musick site is located in the medium-elevation zone (1390 m) with a mean annual temperature of 11.1 ^{O}C and precipitation of 91 cm, where the highest concentrations of C and Fe oxides developed in this site, compared to other elevation zones along the slope (Dahlgren et al., 1997). The site is dominated with ponderosa pine, incense cedar, and manzanita, and its soil is derived from Jurassic granodiorite and classified as Ultic Haploxeralf (Dahlgren et al., 1997). The phyllosilicate clay minerals in the soil are mainly kaolinite, mica, and vermiculite (Dahlgren et al., 1997).

Upon collection, soil was air-dried and sequentially passed through 2 mm, 250 μm, 53 μm, and 20 μm sieves to separate macroaggregate (2000-250 μm), microaggregate (250-53 μm), coarse silt fraction (53-20 μm), and fine silt and clay fraction (<20 μm). The soil was categorized into a sandy loam soil in 29-38 cm depths and transformed to sandy clay loam soil in 38-54 cm and 54-69 cm depths (Dahlgren et al., 1997). Detailed particle size distribution and C content in Musick soil were described earlier (Jin, Chapter 2). Briefly, the range of fractions of each aggregate size class along soil depths was 61.7-67.2% for macroaggregate, 27.2-32.6% for microaggregate, 4.3-5.5% for coarse silt fraction, and 1.2-1.4% for fine silt and clay fraction, respectively. Mass loss from physical size fractionation was less than 5% (data not shown). C content in each fraction is ranged from 0.25-0.63wt% for macroaggregate, 0.54-0.98wt% for microaggregate, 0.87-1.37wt% for coarse silt fraction, and 0.98-1.75wt% for fine silt and clay fraction. C content in bulk soil was ranged from 0.38wt% in 54-69 cm depth to 0.81wt% in 29-38 cm depth. Soil pH for bulk soils from each horizon was below 6.

3.2.2. Fe and C extraction

Pedogenic Fe was extracted via a sequential Fe phase dissolution extraction that is followed by Heckman et al. (2018). Briefly, 1 g of samples were extracted sequentially with 40 ml of 0.1 M sodium pyrophosphate (PP), 0.25 M hydroxylamine hydrochloride (HH), and 0.05 M sodium dithionite-hydrochloride (DH). The samples after each treatment were shaken for 16 h and centrifuged at 10000 rpm for 30 min, which were then passed through a 0.2 μm filter. Fe and C extracted from PP, HH, and DH solutions were measured with ICP-OES with detection limit of 0.022 ppm for Fe and total organic carbon (TOC) analyzer with detection limit of 0.5μg l^{-1} and were considered as pedogenic Fe ion/oxides and C in pedogenic Fe ion/oxide containing fraction. Aliquot of the samples was freeze-dried for DRIFT analyses (Kaiser et al., 1997; Ellerbrock et al., 1999; Ellerbrock et al., 2005 and 2018; Lv et al., 2016).

3.2.3. Diffuse reflectance infrared Fourier transform (DRIFT) spectroscopy

SOC composition in PP-, HH-, and DH-extractable fractions were determined with DRIFT spectroscopy using a Bruker IFS 66v/S spectrophotometer (Ettlingen, Germany) equipped with potassium bromide (KBr) beam splitter and liquid nitrogen-cooled mercury cadmium telluride (MCT) detector. Absorption spectra were collected by averaging 32 scans at $4cm^{-1}$ resolution in mid-infrared region between 4000 and $400cm^{-1}$ in a Praying Mantis chamber (Harrick Scientific Corporation, Ossining, NY) using KBr powder as a background reference. The obtained spectra were then baseline corrected using the rubber band correction method in OPUS operating system. Spectral region between 3000 to $1200cm^{-1}$ was focused for SOM characterization to minimize the mineral interference (Parikh et al., 2014; Hall et al., 2018).

Assignment of the infrared absorption bands to correspond with organic C functional groups was based on the previous works (Coates, 2006; Chatterjee et al., 2012; Ryals et al., 2014; Hall et al., 2018). The peaks in the spectra from 2976 to $2898cm^{-1}$ and from 2870 to $2839cm^{-1}$ were attributed to aliphatic C-H asymmetrical and symmetrical stretch, respectively (Chatterjee et al., 2012; Ryal et al., 2014; Hall et al., 2018), and their sum was assigned to aliphatic C-H stretch. Peaks spanning from 1710 to $1570cm^{-1}$ was interpreted as the carbonyl C=O of amides, quinones, and ketones (Artz et al., 2008; Ryal et al., 2014; Hall et al., 2018). Peak spanning from 1550 to $1500cm^{-1}$ corresponds to aromatic C=C stretch (Artz et al., 2008; Demyan et al., 2012; Hall et al., 2018), and range from 1480 and $1380cm^{-1}$ corresponds to C-O stretch in carboxyl (COOH) (Artz et al., 2008; Ryal et al., 2014; Hall et al., 2018). Peak area integration on baseline corrected spectra was calculated with "approxfun" and "integrate" functions in R program 3.5.3. (Hall et al., 2018). For quantitative analysis, relative peak areas were calculated by dividing individual peak area with total peak areas from all four C functional groups.

3.2.4. Stable carbon isotope composition analysis

Stable C isotopic composition in the residue samples after each extraction and original soil samples from different soil size classes and depths were analyzed with an isotope ratio mass spectrometer (IRMS) (DELTA V Plus Isotope Ratio Mass Spectrometer, Thermo Fisher Scientific, Inc., Waltham, MA, USA). Prior to the analysis, samples after/without extractions were oven-dried at $40^{O}C$ and ground. The isotopic ratio ($^{13}C/^{12}C$) was reported as:

$$\delta X = \left(\frac{R_{sample}}{R_{standard}} - 1\right) \times 1000$$

where, X is ^{13}C, and R is $^{13}C/^{12}C$. Standards used for C was Vienna Pee Dee Belemnite (VPDB).

Stable C isotopic compositions in pedogenic Fe extracted fraction (PP-, HH-, and DH-extractable fractions), organo-mineral associations (PP-extractable fraction), and Fe oxides (HH- and DH-extractable fractions) were calculated by fitting the $\delta^{13}C$ and total C values to a mixing model (Phillips, 2012; Zhao et al., 2016), and compared to that in original samples without extractions.

3.2.5. Data analysis

Fe and C data was analyzed with analysis of variance (ANOVA) and linear regression to test the significance in relationships between extracted Fe concentrations or Fe crystallinity and peak areas of C functional groups, ratios between peak areas of different functional groups, or $\delta^{13}C$ using R software 3.5.3 (R Foundation for Statistical Computing) and R studio (Rstudio Inc.).

3.3. RESULTS

3.3.1. DRIFT based characterization of C extracted with different pools of Fe in soil

We observed important differences in the spectral features of OM associated in pedogenic Fe-containing fractions, but, not for the same pool extracted from the different soil depths or soil aggregate classes (Figure 3-1). In general, FTIR spectra were characterized by: 1) two broad saturated aliphatic peaks between 3000 and 2800cm^{-1}, 2) a carbonyl C=O peak between 1710 and 1570cm^{-1}, 3) a broad but distinguishable aromatic peak between 1550 and 1500cm^{-1}, and 4) a very sharp carboxyl peak between 1480 and 1380cm^{-1} in DH-extractable fractions.

Spectra of extractable fractions showed some distinct spectral features among PP-, HH- and DH-extractable pools (Figure 3-1). In general, we observed two weak and/or broad aliphatic C-H peaks, and carbonyl C=O peak in PP-, HH-, and DH-extractable fractions. A strong and profound carboxyl C-O peak was found in the DH-extractable fraction, while no visible or a weak shoulder carboxyl C-O peak was detected in PP- and HH-extractable fractions. Spectral features that appeared at wavenumbers below 1000cm^{-1} or between 2000-1790cm^{-1} were assumed to be highly influenced by mineral matrix (Calderon et al., 2011a and 2011b) and excluded for data interpretation in this study.

3.3.2. Diverse C functional groups extracted with different pools of Fe in soil

Relative peak area of aliphatic C-H increased as soil size fraction decreased in PP- and DH-extractable fraction, while it tended to decrease with decreasing soil size in HH extractable fraction (Figure 3-2). Specifically, relative peak area of aliphatic C-H in PP extractable fraction increased from 0.17 in average in larger aggregate size fraction to 0.25 in average in smaller aggregate size fraction. Relative peak area of aliphatic C-H in DH-extractable fraction also increased from 0.26 in average in larger aggregate size fractions to 0.30 in average in smaller aggregate size fraction. On the other hand, relative peak area of aliphatic C-H in HH-extractable fraction decreased from around 0.40 in

average in larger aggregate size fraction to 0.38 in average in smaller aggregate size fraction.

Relative peak area of aromatic C=C decreased as soil size decreased in PP-extractable fractions, whereas that of aromatic C=C slightly increased with decreasing soil size in HH- and DH-extractable fraction (Figure 3-2). Specifically, relative peak area of aromatic C=C in PP-extractable fraction decreased from 0.13 in average in larger aggregate size fraction to 0.11 in average in smaller aggregate size fractions, whereas that of aromatic C=C in HH- and DH-extractable fractions increased from 0.13 in average and 0.07 in average in larger size aggregate fraction to 0.14 in average and 0.19 in average in smaller size fractions in HH- and DH-extractable fractions, respectively.

Similarly, relative peak area of carboxyl C-O decreased with decreasing soil size fraction in PP-extractable fractions, whereas relative peak area of carboxyl C-O increased as soil size fraction decreased in DH-extractable fractions (Figure 3-2). No consistent trend was found along soil size in HH-extractable fraction. Specifically, the relative peak area of carboxyl C-O decreased from 0.23 in average in larger aggregate size fraction to 0.18 in average in smaller aggregate size fraction in PP-extractable fraction, whereas it increased from 0.15 in average in larger aggregate size fraction to 0.19 in average in smaller aggregate size fraction in DH extractable fraction.

Relative peak area of carbonyl C=O decreased as soil size fraction decreased in PP and DH extractable fractions (Figure 3-2). No consistent trend was found along soil size in HH extractable fraction. Specifically, relative peak area of carbonyl C=O decreased from 0.46 in average in larger aggregate size fraction to 0.44 in average in smaller aggregate size fraction in PP extractable fraction, and it decreased from 0.51 in average in larger aggregate size fraction to 0.43 in average in smaller aggregate size fraction in DH-extractable fraction.

3.3.3. Relationship between extractable Fe and C

Relative peak area of aliphatic C-H was closely correlated to PP-extractable Fe concentration (Figure 3-3), where it increased with decreasing size fractions regardless of soil depths and sizes with R^2 value of 0.73 ($p<0.0001$). In contrast, relative peak areas of aromatic C=C, carbonyl C=O, and carboxyl C-O decreased with increasing PP-extractable Fe concentrations, with R^2 values of 0.78 ($p<0.0001$), 0.46 ($p=0.003$), and 0.69 ($p<0.0001$), respectively (Figure 3-3).

Relative peak area of aliphatic C-H in HH extractable Fe tended to decrease as HH-extractable Fe concentrations decreased, whereas that of aromatic C=C, carbonyl C=O, and carboxyl C-O increased tended to increase with increasing HH-extractable fraction (Figure 3-3). However, there was no significant relationships between relative peak area of C functional groups or structure and HH extractable Fe concentrations, except for aromatic C=C with R^2 value of 0.43 ($p=0.004$).

Relative peak area of aromatic C=C and carboxyl C-O significantly increased with increasing DH-extractable Fe concentrations with R^2 values of 0.41 ($p=0.006$) and 0.36 ($p=0.01$), whereas that of carbonyl C=O decreased as DH-extractable Fe concentration increased (Figure 3-3). No correlations between relative peak area of aliphatic C-H and DH extractable Fe concentration was found. In addition, relative peak area of aromatic C=C and carboxyl C-O significantly increased with increasing relative contribution of poorly crystalline Fe oxide to total Fe oxide in HH-extractable fraction, whereas opposite trend was found in DH-extractable fractions (Figure 3-4) (not for CH/CO ratio in DH-extractable fraction). Relative peak area of aromatic C=C tended to increase with increasing carboxyl C-O in HH- and DH-extractable fractions (Figure 3-5). Relative peak area of carbonyl C=O was also strongly correlated to carboxyl C-O in HH- and DH-extractable fractions (Figure 3-5).

Ratios between aliphatic C-H and O-containing C functional groups (carbonyl C=O or carboxyl C-O, index for the extent of OM decomposition) were significantly correlated to the concentrations of PP-extractable Fe (Figure 3-6). Specifically, ratios between aliphatic C-H and carbonyl C=O or carboxyl C-O were positively correlated with PP extractable Fe with $R^2=0.70$ ($p<0.0001$) and $R^2=0.71$ ($p<0.001$), respectively. On the other hand, ratios between aliphatic C-H and carbonyl C=O or carboxyl C-O tended to decrease with increasing HH-extractable Fe concentrations (Figure 3-6). Similarly, aliphatic C-H to carboxyl C-O ratio tended to decrease with increasing DH-extractable Fe concentrations. However, aliphatic to carbonyl C=O ratio increased as DH-extractable Fe concentration increased with R^2 value of 0.36 ($p=0.009$).

3.3.4. Stable isotopic composition of pedogenic Fe associated C

Stable C isotopic composition ($\delta^{13}C$) in the Musick B horizon soils ranged from -26.02‰ to -26.44‰, with an average of -26.30±0.04‰. The average values increased to -25.96±0.26‰ in Fe ion/oxide containing fractions (i.e. all PP-, HH-, and DH-extractable fractions). Fe oxide containing fractions (i.e. HH- and DH-extractable fractions) had enriched $\delta^{13}C$ value of -24.87±1.11‰ in average. The Fe- containing fraction (i.e. PP extractable fraction), however, had lower $\delta^{13}C$ value of, mean of -27.94±0.70‰ (Table 2).

3.4. DISCUSSION

3.4.1. Carbon functional group or structure and extractable iron

Relative abundance of aliphatic C-H was strongly positively correlated to the PP-extractable Fe in soil as was indicated by the strong correlations between PP-extractable Fe concentration and the relative peak area of aliphatic C-H that was extracted in the same pool regardless of soil size fractions and soil depths (Figure 3-3). However, the relative peak area of aliphatic C-H decreased with increasing HH-extractable Fe concentrations, or no significant relationship was found in DH-extractable fraction. The PP solution that was used in selective extraction procedures targets organic colloids in

soil and organic compounds that are associated with minerals, and releases Fe that is associated in these fractions, and may also dissolve a small amount of poorly crystalline Fe oxide (Masiello et al., 2004; Kaiser et al., 2011; Berhe et al., 2012; Lopez-Sangil and Rovira, 2013; Lawrence et al., 2015; Coward et al., 2017 and 2018; Hechman et al., 2018). On the other hand, HH solution extracts mainly poorly crystalline Fe oxides, and DH solution extracts crystalline Fe oxides, such as crystalline hematite and goethite (Lawrence et al., 2015) in our sequential procedure. Note that in the procedure we followed in this work, DH does not extract poorly crystalline Fe oxides as they were removed by PP and HH extractions in the previous steps of the sequential extraction scheme (Wagai and Mayer, 2007; Heckman et al., 2018; Jin et al., chapter 2). Previous study on the same Musick soils also found a strong positive relationship between extractable Fe and C in the PP-extractable fraction (Jin et al., chapter 2). Positive correlations between PP-extractable Fe and aliphatic C found in this study further suggests that aliphatic C-H may be one of the major C structures that are associated with Fe in organically associated fraction (i.e. PP-extractable fraction) in such medium to highly weathered soils. PP-extractable Fe also increased as soil aggregate size decreased as reported by previous study on same soils (Jin et al., chapter 2), which may indicate that more aliphatic C-H may be associated to organically associated Fe in PP-extractable fraction in smaller aggregate size fractions. FT-ICR-MS analyses of soils that used a parallel extraction procedure previously found that relative abundance of unsaturated aliphatic C was higher in PP-extractable fraction, compared to HH- and DH-extractable fraction in an Oxisol soil, and suggested that the unsaturated aliphatic C is likely derived from microbes and/or root exudates (Coward et al., 2018). Note that direct comparison of relative abundance between two studies is not possible because the two techniques used target different features of the organic compounds and as the extraction methods used were also slightly differently (parallel vs. sequential) despite of the same chemicals used in both studies. However, both studies found the close relationships between aliphatic C and organically associated Fe in the same pool, which may suggest that aliphatic C is likely a major pool of OM that is strongly associated to pedogenic Fe in soils, especially in PP-extractable fraction in smaller aggregate size fractions. We note here though that, because of the nature of the FTIR analyses we used, we are not able to further infer the specific types of aliphatic groups that may be associated with Fe oxides in soils in general.

The affinity of aromatic C=C on pedogenic Fe in different extraction pools varied as was shown by a strong negative correlation between PP-extractable Fe and the relative peak area of aromatic C=C, but significant positive correlations between HH- and DH-extractable Fe and the relative peak area of aromatic C=C (Figure 3-3). Similarly, aromatic compounds were found to be associated to parallelly extracted PP-, HH-, and DH-extractable fractions (as opposed to the sequential extraction procedure in this study), where their relative abundance increased in the extractable fractions in an order of PP<HH<DH relative to aliphatic and carbohydrate and unsaturated lignin-like compounds as detected by FT-ICR-MS (Coward et al., 2018). Again, direct comparison between the findings of the two studies is not possible (see above discussion). High affinity of aromatic C=C on Fe oxides were well documented in previous studies. Kaiser

and Guggenberger (1997, 2000) reported that C compound containing aromatic structure detected by ^{13}C-NMR was preferentially sorbed by synthesized Fe oxides, compared to alkyl group. Higher affinity of UV index (UV absorbance at 254nm as aromaticity index) based aromatic compound to synthesized hematite was also observed in a recent study, compared to aliphatic C (Adhiraki and Yang, 2015). Similarly, Gu et al. (1995) reported that Fe oxide may preferentially sorb SOM with high molecular size and with aromatic (phenolic group) structure through ligand exchange complexation, where they proposed that aromatic structure with carboxyl or hydroxyl group with high affinity to mineral surface may allow them to be sorbed on Fe oxide first and fast and consequently, adsorption of aliphatic C-H or other C compounds with low affinity may become slow as surface coverage changed (Gu et al., 1995). More recently, Huang et al., (2019) also observed that lignin-derived C preferentially associated with Fe oxides during an aerobic incubation. These results suggest that aromatic C=C groups are indeed mostly associated to Fe oxides in soil and less commonly found in organically associated fraction.

Relative peak area of aromatic C=C tended to increase as that of carboxyl C-O groups increased regardless of different Fe oxide extractions, soil aggregate size classes, or soil depths (Figure 3-5), indicating that aromatic C=C may be closely related to carboxyl C-O in Fe extractable fractions. Note that carboxyl C-O may be affected by the extractant remained in the sample after freeze drying processes. This finding is consistent with previous findings that also found that SOM rich in both aromatic structure and carboxyl functional groups, such as aromatic carboxyl acid, were preferentially associated with Fe oxide in soils mainly through surface complexation, such as ligand exchange complexations, where increasing carboxyl functionality may increase the surface complexation (Kaiser and Guggenberher, 1997; Boily et al., 2000; Chasse et al., 2015). Specifically, carboxyl functional groups attached to aromatic compounds may react with protonated -OH group on Fe oxide surface and mainly contribute to the ligand exchange complexation on Fe oxide surface (McNight et al., 1992; Kaiser and Guggenberger, 1997; Chasse et al., 2015). The resulting complexes may exhibit high adhesion forces on Fe oxide surfaces and form a stable bond when two carboxyl groups were involved in the complexation (Boily et al., 2000; Chasse et al., 2015). Outer-sphere complexes may also occur on Fe oxide surface considering the low pH (pH <6) in Musick soils (Chasse et al., 2015). To summarize, the findings suggest that SOM rich in aromatic structure with carboxyl functionalities may preferentially be associated to crystalline Fe oxides.

Relative peak area of carbonyl C=O was strongly correlated to that of carboxyl C-O (Figure 3-5). In previous studies, carbonyl C=O was usually interpreted together with carboxyl C-O as they were both considered to be common oxygen-containing functional groups occurring in SOM and their spectral regions were mostly overlapping (Parikh et al., 2014). Ellerbrock et al. (2009) have proposed that the aliphatic C-H/carbonyl C=O (CH/CO) ratio may indicate soil wettability and spatial orientation of SOM compounds in soil, where aliphatic C-H may indicate soil hydrophobicity and carbonyl C=O may indicate soil hydrophilicity (Ellerbrock and Gerke, 2013). In our soils, CH/CO increased as PP- and DH-extractable Fe concentration increased, whereas the ratio tended to decrease as HH-extractable Fe concentration increased (Figure 3-6). These findings may

indicate that soil hydrophobicity increased as PP- and DH-extractable Fe concentration increased, whereas soil hydrophilicity increased as HH extractable Fe concentration increased. PP extractable fraction in Musick soil with high amount of SOC and high soil hydrophobicity, highly likely to form onion-like structure on mineral surface, where multi-layered SOM may be associated on mineral surfaces (Kleber et al., 2007; Ellerbrock and Gerke, 2013), where Ca cation may regulate the amount of SOM attached to the mineral surface (Jin et al., chapter 2). On the other hand, DH-extractable fraction with lower amount of SOC, a dense SOM single layer structure may be formed on Fe oxide surfaces, compared to multi-layered structure with higher amount of SOC and Fe. HH- extractable Fe with lowest amount of Fe concentration and high soil hydrophilicity, mostly like to form sparse SOM monolayer on mineral surface (Ellerbrock et al., 2005; Ellerbrock and Gerke, 2013). The finding was also in agreement with previous findings on the same soils, that found much lower C:Fe ratio in HH- and DH-extractable fraction compared to that in PP extractable fraction, which may also indicate that sorption-like mechanism on Fe oxide surface may be the major C stabilization mechanism in these Musick soils (Wagai et al., 2013; Jin et al., chapter 2). On the other hand, it is also likely that onion-like structure (opposite to sorption) may be a major mechanism that regulate the size of the PP-extractable C in organically associated fraction.

On the other hand, extractable Al also had similar relationships with C functional groups or structure in corresponding extractable pools, compared to extractable Fe that was discussed above (Figure S3-1 and S3-2). Therefore, it should be noted that reactive minerals may in general contribute to the distribution of C stored in the same fraction.

3.4.2. Carbon functional group or structure and extractant-based iron oxide crystallinity

Relative abundance of HH-extractable Fe to HH- and DH-extractable Fe in this study was referred to Fe crystallinity index, where higher the ratio indicates lower Fe oxide crystallinity. Relative peak areas of aromatic C=C and carboxyl C-O in HH-extractable fractions increased as Fe crystallinity decreased, whereas those in DH extractable fractions tended to decrease as Fe crystallinity decreased (Figure 3-4). This finding indicates that relative peak areas of aromatic C=C and carboxyl C-O increased as HH-extractable poorly crystalline Fe oxide or DH-extractable crystalline Fe oxide increased. In line with these findings, $\delta^{13}C$ was found to be mostly enriched in HH- and DH-extractable Fe oxide fractions compared to PP-extractable fraction (Table 3-1). Aliphatic C-H relative to carbonyl C=O or carboxyl C-O increased with increasing PP-extractable Fe concentration, whereas the ratios tended to decrease with increasing HH- and DH-extractable Fe concentrations (Figure 3-6). Note that aromatic C-H to carbonyl C=O ratio in DH-extractable fraction acted differently may due to the overlapping peaks in carbonyl integration range (Figure 3-1). These results may indicate that C preserved in HH and DH extractable Fe containing fraction may undergo greater microbial decomposition, compared to PP-extractable fraction. In agreement with our findings, Lalonde et al (2012) and Zhao et al. (2016) also found that the DH-extractable C (in a parallel extraction scheme) in most sediment and US soil samples was enriched with $\delta^{13}C$ compared to non-Fe oxide-associated fractions. Moreover, Hall et al., (2018) reported that the relative

contribution of plant derived C functional groups (such as aliphatic C-H) decreased with increasing Fe crystallinity and amount of microbe derived C functional groups (such as carbonyl C=O and carboxyl C-O) increased with increasing Fe crystallinity. Coward et al. (2018) similarly observed that C derived from microbial biomass and root exudates was preferentially associated with more crystalline Fe oxides. Therefore, we conclude that aromatic and carboxyl C that were mainly microbe-derived C may preferentially reside in poorly crystalline and crystalline Fe oxides containing fractions, whereas aliphatic C that was mainly plant-derived C may preferentially reside in organically associated Fe containing fraction. The findings may indicate that as microbial decomposition and transformation of litter increases over time, the resultant microbially altered organic compounds may accumulate in soil and form strong associations with Fe oxides that tend to be more crystalline and stable (Coward et al., 2018).

3.5. CONCLUSION

C functional groups or structure of soil aggregate associated SOM in sequentially extracted pedogenic Fe containing fractions in an Alfisol were determined with DRIFT in order to identify the molecular fractionation of SOC involved in extractable Fe fractions. Stable C isotopic composition was also determined to evaluate the source of soil organic carbon and to trace the C flow in soils. Molecular fractionation of SOM was observed with changes in extractant-based Fe crystallinity and soil aggregate size classes, indicating that pedogenic Fe may control the SOM that may enter the soils and be stabilized thereafter. Aliphatic C-H that mainly derived from plant materials may tend to be enriched in organically associated (i.e. PP-extractable) Fe containing fraction, especially in smaller aggregate size fractions. On the other hand, aromatic C=C and carboxyl C-O that mainly derived from microbial produces may tend to be enriched in poorly crystalline and crystalline Fe oxide (i.e. HH- and DH-extractable) containing fractions. Microbial decomposition may be enhanced as extractant-based Fe oxide crystallinity increased, and therefore, pedogenic Fe may influence the organic material that will enter the soils.

ACKNOWLEDGEMENTS

The authors gratefully acknowledge lab assistance from Liying Zhao at the Environmental Analytical Lab and Justin Van De Velde at Stable Isotope Lab at UC Merced, and Samuel Negusse Araya and Randy Dahlgren for information about field sites and the Musick soil. The authors also acknowledge support of dissertation committee members Drs. Peggy O`Day, Samuel Traina, Steven Hall (and Peter Nico?) for comments on earlier versions of this manuscript. Funding for this work was provided from UC Merced and the National Science Foundation (CAREER EAR -1352627) award to A. A. Berhe.

REFERENCES

Adhikari, D. and Yang, Y. (2015). Selective stabilization of aliphatic organic carbon by iron oxide. Scientific reports, 5, 11214.

Artz, R. R., Chapman, S. J., Robertson, A. J., Potts, J. M., Laggoun-Défarge, F., Gogo, S., Comont, L., Disnar, J. and Francez, A. J. (2008). FTIR spectroscopy can be used as a screening tool for organic matter quality in regenerating cutover peatlands. Soil Biology and Biochemistry, 40(2), 515-527.

Barral, M. T., Arias, M. and Guerif, J. (1998). Effects of iron and organic matter on the porosity and structural stability of soil aggregates. Soil and Tillage Research, 46(3-4), 261-272.

Berhe, A. A., Harden, J. W., Torn, M. S., Kleber, M., Burton, S. D. and Harte, J. (2012). Persistence of soil organic matter in eroding versus depositional landform positions. Journal of Geophysical Research: Biogeosciences, 117(G2).

Boily, J. F., Persson, P. and Sjöberg, S. (2000). Benzenecarboxylate surface complexation at the goethite (α-FeOOH)/water interface: II. Linking IR spectroscopic observations to mechanistic surface complexation models for phthalate, trimellitate, and pyromellitate. Geochimica et Cosmochimica Acta, 64(20), 3453-3470.

Bronick, C. J. and Lal, R. (2005). Soil structure and management: a review. Geoderma, 124(1-2), 3-22.

Calderón, F. J., Mikha, M. M., Vigil, M. F., Nielsen, D. C., Benjamin, J. G. and Reeves III, J. B. (2011a). Diffuse-reflectance mid-infrared spectral properties of soils under alternative crop rotations in a semi-arid climate. Communications in soil science and plant analysis, 42(17), 2143-2159.

Calderón, F. J., Reeves, J. B., Collins, H. P. and Paul, E. A. (2011b). Chemical differences in soil organic matter fractions determined by diffuse-reflectance mid-infrared spectroscopy. Soil Science Society of America Journal, 75(2), 568-579.

Chassé, A. W., Ohno, T., Higgins, S. R., Amirbahman, A., Yildirim, N. and Parr, T. B. (2015). Chemical force spectroscopy evidence supporting the layer-by-layer model of organic matter binding to iron (oxy) hydroxide mineral surfaces. Environmental science & technology, 49(16), 9733-9741.

Chatterjee, S., Santos, F., Abiven, S., Itin, B., Stark, R. E. and Bird, J. A. (2012). Elucidating the chemical structure of pyrogenic organic matter by combining magnetic resonance, mid-infrared spectroscopy and mass spectrometry. Organic geochemistry, 51, 35-44.

Chenu, C. and Plante, A. F. (2006). Clay-sized organo-mineral complexes in a cultivation chronosequence: revisiting the concept of the 'primary organo-mineral complex'. European Journal of Soil Science, 57(4), 596-607.

Coates, J. (2006). Interpretation of infrared spectra, a practical approach. Encyclopedia of analytical chemistry: applications, theory and instrumentation.

Cornell, R. M. and Schwertmann, U. (2003). The iron oxides: structure, properties, reactions, occurrences and uses. John Wiley & Sons.

Coward, E. K., Thompson, A. T. and Plante, A. F. (2017). Iron-mediated mineralogical control of organic matter accumulation in tropical soils. Geoderma, 306, 206-216.

Coward, E. K., Thompson, A. and Plante, A. F. (2018). Contrasting Fe speciation in two humid forest soils: Insight into organomineral associations in redox-active environments. Geochimica et Cosmochimica Acta, 238, 68-84.

Coward, E. K., Ohno, T. and Plante, A. F. (2018). Adsorption and molecular fractionation of dissolved organic matter on iron-bearing mineral matrices of varying crystallinity. Environmental science & technology, 52(3), 1036-1044.

Dahlgren, R. A., Boettinger, J. L., Huntington, G. L. and Amundson, R. G. (1997). Soil development along an elevational transect in the western Sierra Nevada, California. Geoderma, 78(3-4), 207-236.

Demyan, M. S., Rasche, F., Schulz, E., Breulmann, M., Müller, T. and Cadisch, G. (2012). Use of specific peaks obtained by diffuse reflectance Fourier transform mid-infrared spectroscopy to study the composition of organic matter in a Haplic Chernozem. European Journal of Soil Science, 63(2), 189-199.

Ellerbrock, R. H., Höhn, A., & Gerke, H. H. (1999). Characterization of soil organic matter from a sandy soil in relation to management practice using FT-IR spectroscopy. Plant and Soil, 213(1-2), 55-61.

Ellerbrock, R. H. and Kaiser, M. (2005). Stability and composition of different soluble soil organic matter fractions–evidence from δ13C and FTIR signatures. Geoderma, 128(1-2), 28-37.

Ellerbrock, R. H., Gerke, H. H. and Böhm, C. (2009). In situ DRIFT characterization of organic matter composition on soil structural surfaces. Soil Science Society of America Journal, 73(2), 531-540.

Ellerbrock, R. H. and Gerke, H. H. (2013). Characterization of organic matter composition of soil and flow path surfaces based on physicochemical principles—A review. In Advances in agronomy (Vol. 121, pp. 117-177). Academic Press.

Eusterhues, K., Rumpel, C., Kleber, M. and Kögel-Knabner, I. (2003). Stabilisation of soil organic matter by interactions with minerals as revealed by mineral dissolution and oxidative degradation. Organic Geochemistry, 34(12), 1591-1600.

Eusterhues, K., Rumpel, C. and Kögel-Knabner, I. (2005). Organo-mineral associations in sandy acid forest soils: importance of specific surface area, iron oxides and micropores. European Journal of Soil Science, 56(6), 753-763.

Graham, R. C. and O'Geen, A. T. (2010). Soil mineralogy trends in California landscapes. Geoderma, 154(3-4), 418-437.

Gu, B., Schmitt, J., Chen, Z., Liang, L. and McCarthy, J. F. (1995). Adsorption and desorption of different organic matter fractions on iron oxide. Geochimica et Cosmochimica Acta, 59(2), 219-229.

Hall, S. J., Berhe, A. A. and Thompson, A. (2018). Order from disorder: do soil organic matter composition and turnover co-vary with iron phase crystallinity? Biogeochemistry, 140(1), 93-110.

Heckman, K., Lawrence, C. R. and Harden, J. W. (2018). A sequential selective dissolution method to quantify storage and stability of organic carbon associated with Al and Fe hydroxide phases. Geoderma, 312, 24-35.

Huang, X., Jiang, H., Li, Y., Ma, Y., Tang, H., Ran, W. and Shen, Q. (2016). The role of poorly crystalline iron oxides in the stability of soil aggregate-associated organic carbon in a rice–wheat cropping system. Geoderma, 279, 1-10.

Huang, W., Hammel, K., Hao, J., Thompson, A., Timokhin, V., & Hall, S. (2019). Enrichment of lignin-derived carbon in mineral-associated soil organic matter. Environmental science & technology.

Jin, L., O'Day, P. and Berhe, A.A. Role of iron oxides on physical protection of soil organic matter inside aggregates. In preparation.

Kaiser, K., Guggenberger, G., Haumaier, L. and Zech, W. (1997). Dissolved organic matter sorption on sub soils and minerals studied by 13C-NMR and DRIFT spectroscopy. European Journal of Soil Science, 48(2), 301-310.

Kaiser, K. and Guggenberger, G. (2000). The role of DOM sorption to mineral surfaces in the preservation of organic matter in soils. Organic geochemistry, 31(7-8), 711-725.

Kaiser, K. and Guggenberger, G. (2003). Mineral surfaces and soil organic matter. European Journal of Soil Science, 54(2), 219-236.

Kaiser, M., Walter, K., Ellerbrock, R. H. and Sommer, M. (2011). Effects of land use and mineral characteristics on the organic carbon content, and the amount and composition of Na-pyrophosphate-soluble organic matter, in subsurface soils. European Journal of Soil Science, 62(2), 226-236.

Kleber, M., Mikutta, R., Torn, M. S. and Jahn, R. (2005). Poorly crystalline mineral phases protect organic matter in acid subsoil horizons. European Journal of Soil Science, 56(6), 717-725.

Kleber, M., Sollins, P. and Sutton, R. (2007). A conceptual model of organo-mineral interactions in soils: self-assembly of organic molecular fragments into zonal structures on mineral surfaces. Biogeochemistry, 85(1), 9-24.

Kleber, M., Eusterhues, K., Keiluweit, M., Mikutta, C., Mikutta, R. and Nico, P. S. (2015). Mineral–organic associations: formation, properties, and relevance in soil environments. In Advances in agronomy (Vol. 130, pp. 1-140). Academic Press.

Kögel-Knabner, I., Guggenberger, G., Kleber, M., Kandeler, E., Kalbitz, K., Scheu, S., Eusterhues, K. and Leinweber, P. (2008). Organo-mineral associations in temperate soils: Integrating biology, mineralogy, and organic matter chemistry. Journal of Plant Nutrition and Soil Science, 171(1), 61-82.

Lalonde, K., Mucci, A., Ouellet, A. and Gélinas, Y. (2012). Preservation of organic matter in sediments promoted by iron. Nature, 483(7388), 198.

Lawrence, C. R., Harden, J. W., Xu, X., Schulz, M. S. and Trumbore, S. E. (2015). Long-term controls on soil organic carbon with depth and time: A case study from the Cowlitz River Chronosequence, WA USA. Geoderma, 247, 73-87.

Lopez-Sangil, L. and Rovira, P. (2013). Sequential chemical extractions of the mineral-associated soil organic matter: An integrated approach for the fractionation of organo-mineral complexes. Soil Biology and Biochemistry, 62, 57-67.

Lv, J., Zhang, S., Wang, S., Luo, L., Cao, D. and Christie, P. (2016). Molecular-scale investigation with ESI-FT-ICR-MS on fractionation of dissolved organic matter induced by adsorption on iron oxyhydroxides. Environmental Science & Technology, 50(5), 2328-2336.

Masiello, C. A., Chadwick, O. A., Southon, J., Torn, M. S. and Harden, J. W. (2004). Weathering controls on mechanisms of carbon storage in grassland soils. Global Biogeochemical Cycles, 18(4).

McKnight, D. M., Bencala, K. E., Zellweger, G. W., Aiken, G. R., Feder, G. L. and Thorn, K. A. (1992). Sorption of dissolved organic carbon by hydrous aluminum and iron

oxides occurring at the confluence of Deer Creek with the Snake River, Summit County, Colorado. Environmental science & technology, 26(7), 1388-1396.

Mikutta, R., Schaumann, G. E., Gildemeister, D., Bonneville, S., Kramer, M. G., Chorover, J., Chadwick, O.A. and Guggenberger, G. (2009). Biogeochemistry of mineral–organic associations across a long-term mineralogical soil gradient (0.3–4100 kyr), Hawaiian Islands. Geochimica et Cosmochimica Acta, 73(7), 2034-2060.

Parikh, S. J., Goyne, K. W., Margenot, A. J., Mukome, F. N. and Calderón, F. J. (2014). Soil chemical insights provided through vibrational spectroscopy. In Advances in agronomy (Vol. 126, pp. 1-148). Academic Press.

Phillips, D. L. (2012). Converting isotope values to diet composition: the use of mixing models. Journal of Mammalogy, 93(2), 342-352.

Porras, R. C., Pries, C. E. H., McFarlane, K. J., Hanson, P. J. andTorn, M. S. (2017). Association with pedogenic iron and aluminum: effects on soil organic carbon storage and stability in four temperate forest soils. Biogeochemistry, 133(3), 333-345.

Regelink, I. C., Stoof, C. R., Rousseva, S., Weng, L., Lair, G. J., Kram, P., Nikolaidis, N.P., Kercheva, M., Banwart, S. and Comans, R. N. (2015). Linkages between aggregate formation, porosity and soil chemical properties. Geoderma, 247, 24-37.

Ryals, R., Kaiser, M., Torn, M. S., Berhe, A. A. and Silver, W. L. (2014). Impacts of organic matter amendments on carbon and nitrogen dynamics in grassland soils. Soil Biology and Biochemistry, 68, 52-61.

Six, J., Bossuyt, H., Degryze, S. and Denef, K. (2004). A history of research on the link between (micro) aggregates, soil biota, and soil organic matter dynamics. Soil and Tillage Research, 79(1), 7-31.

Sollins, P., Kramer, M. G., Swanston, C., Lajtha, K., Filley, T., Aufdenkampe, A. K., Wagai, R. and Bowden, R. D. (2009). Sequential density fractionation across soils of contrasting mineralogy: evidence for both microbial-and mineral-controlled soil organic matter stabilization. Biogeochemistry, 96(1-3), 209-231.

Torn, M. S., Trumbore, S. E., Chadwick, O. A., Vitousek, P. M. and Hendricks, D. M. (1997). Mineral control of soil organic carbon storage and turnover. Nature, 389(6647), 170.

Totsche, K. U., Amelung, W., Gerzabek, M. H., Guggenberger, G., Klumpp, E., Knief, C., Lehndorff, E., Mikutta, R., Peth, S., Prechtel, A., Ray, N. and Kogel-Knabner, I. (2018). Microaggregates in soils. Journal of Plant Nutrition and Soil Science, 181(1), 104-136.

Wagai, R. and Mayer, L. M. (2007). Sorptive stabilization of organic matter in soils by hydrous iron oxides. Geochimica et Cosmochimica Acta, 71(1), 25-35.

Wagai, R., Mayer, L. M., Kitayama, K. and Shirato, Y. (2013). Association of organic matter with iron and aluminum across a range of soils determined via selective dissolution techniques coupled with dissolved nitrogen analysis. Biogeochemistry, 112(1-3), 95-109.

Yang, X. M., Drury, C. F., Reynolds, W. D. and Yang, J. Y. (2016). How do changes in bulk soil organic carbon content affect carbon concentrations in individual soil particle fractions? Scientific reports, 6, 27173.

Zhao, Q., Poulson, S. R., Obrist, D., Sumaila, S., Dynes, J. J., McBeth, J. M. and Yang, Y. (2016). Iron-bound organic carbon in forest soils: quantification and characterization.

TABLES

Table 3-1. Stable C (^{13}C) isotopic composition in pedogenic Fe ion/oxide containing fraction (PP+HH+DH), Fe ion containing fraction (PP), Fe oxide containing fraction (HH+DH), and non-Fe ion/oxide containing fraction (i.e. residue samples) in different size fractions along soil profile.

Soil depths	Size fractions (μm)	^{13}C in PP, HH, and DH extractable fractions calculated[a]	^{13}C in PP extractable fraction calculated[b]	^{13}C in HH and DH extractable fraction calculated[c]	^{13}C in original samples[d]
29-38 cm	2000-250	-24.44±0.68	-34.12±7.98	-27.88±0.08	-26.29±0.02
	250-53	-25.65±0.14	-27.10±0.30	-24.00±0.89	-26.37±0.01
	53-20	-26.36±0.01	-27.21±0.06	-24.70±0.09	-26.40±0.02
	<20	-26.77*	-26.66*	n/a	-26.18±0.02
	Bulk soil	-27.14±0.01	-27.87±0.31	-25.00±1.45	-26.44±0.06
38-54 cm	2000-250	-23.81±0.56	-23.28±1.39	-26.95±0.24	-25.74±0.03
	250-53	-26.21±0.12	-26.91±0.01	n/a	-26.43±0.02
	53-20	-26.11±0.01	-26.94±0.04	n/a	-26.37±0.01
	<20	-26.64*	n/a	-27.70*	-26.01±0.01
	Bulk soil	-26.21±0.08	-28.50±0.13	-24.75±0.07	-26.43±0.24
54-69 cm	2000-250	-25.64±0.18	-27.73±5.03	-25.69±1.00	-25.88±0.02
	250-53	-25.55±1.01	-32.62±6.43	-16.71	-26.19±0.01
	53-20	-26.40±0.07	-28.07±0.06	-18.22±1.45	-26.37±0.01
	<20	-26.84±0.17	-26.76	-27.01	-26.27±0.01
	Bulk soil	-26.75*	-28.44±0.17	-29.81±0.62	-26.07±0.05

[a] $\delta^{13}C$ values in extractable fractions (PP+HH+DH extractions) were calculated by fitting the data with following mixing model: $\delta^{13}C_{\text{original soils}} = f_{\text{residue after DH extraction}} \times \delta^{13}C_{\text{residue after DH extraction}} + f_{\text{extracted in PP, HH, and DH extractions}} \times \delta^{13}C_{\text{extracted in PP, HH, and DH extractions}}$.

[b] $\delta^{13}C$ values in PP extractable fractions were calculated by fitting the data with following mixing model: $\delta^{13}C_{\text{original soils}} = f_{\text{residue after PP extraction}} \times \delta^{13}C_{\text{residue after PP extraction}} + f_{\text{extracted in PP extraction}} \times \delta^{13}C_{\text{extracted in PP extraction}}$.

[c] $\delta^{13}C$ values in HH and DH extractable fractions were calculated by fitting the data with following mixing model: $\delta^{13}C\ f_{\text{residue after PP extraction}} = f_{\text{residue after DH extraction}} \times \delta^{13}C_{\text{residue after DH extraction}} + f_{\text{extracted in HH and DH extractionS}} \times \delta^{13}C_{\text{extracted in HH and DH extractions}}$.

[d] Experimental data obtained using an isotope ratio mass spectrometer (IRMS).

[*] No replicates due to the small amount of samples.

FIGURES

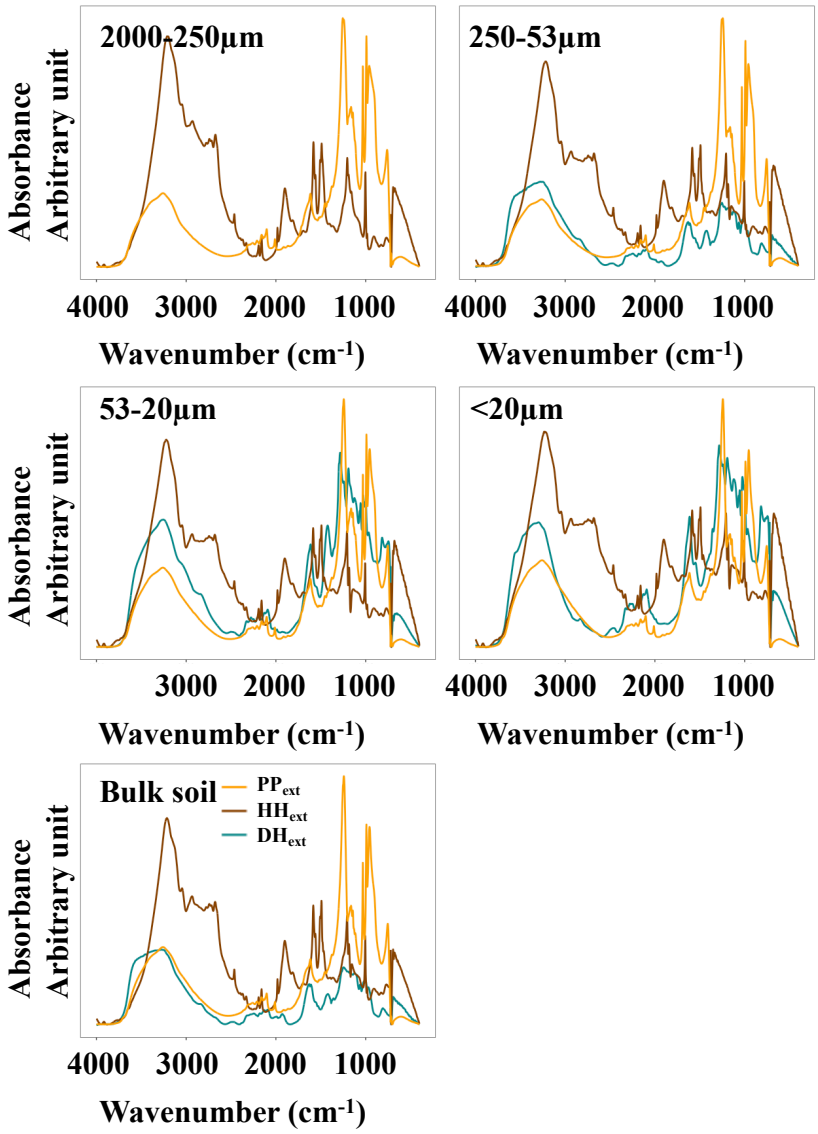

Figure 3-1. Typical DRIFT-FTIR spectra for PP-, HH-, and DH-extracted samples or original soils. The figure is showing the example spectra for all size fractions in B horizon (38-54 cm). PP_{ext}, HH_{ext}, and DH_{ext} represent PP, HH, and DH extractable fractions. Original soil samples (untreated) are denoted as UN.

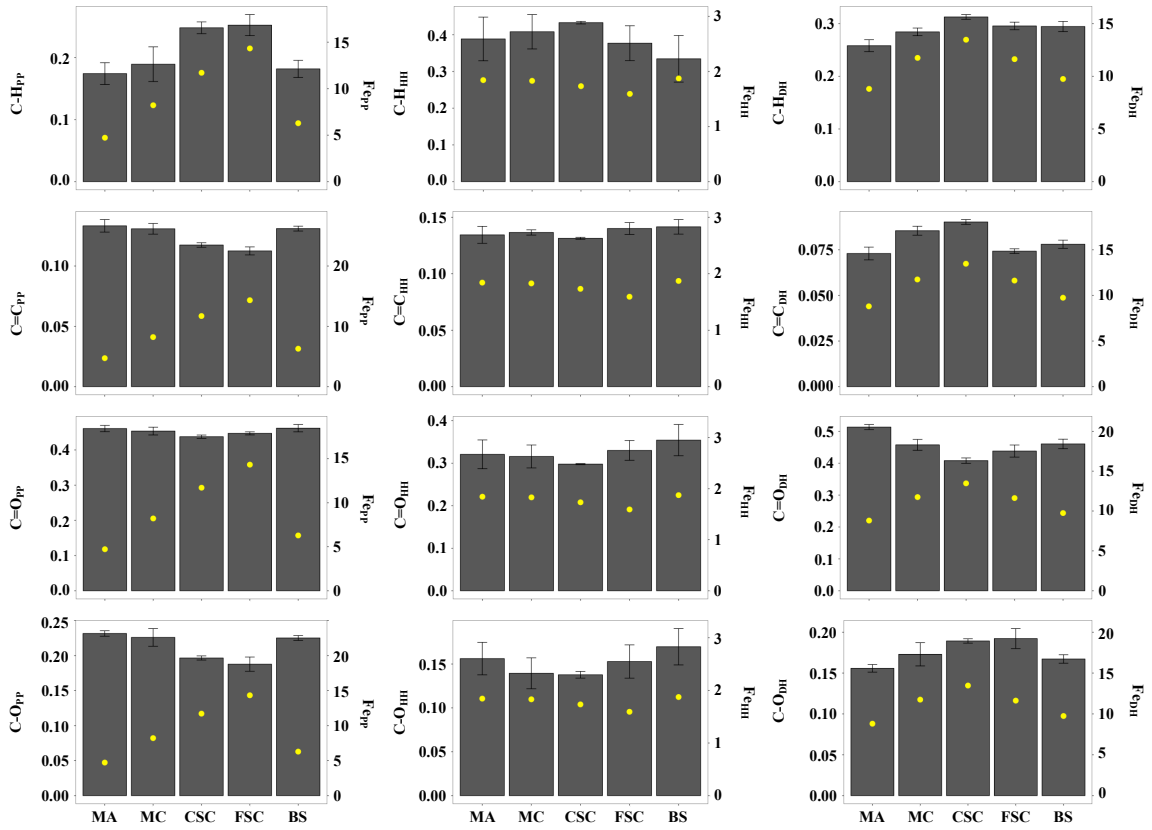

Figure 3-2. Relative peak areas in bars of aliphatic C-H, aromatic C=C, carbonyl C=O, and carboxyl C-O groups and pedogenic Fe concentrations in yellow dots in PP- (left panel), HH- (middle panel), and DH- (right panel) extractable fractions in different size fractions in B horizons.

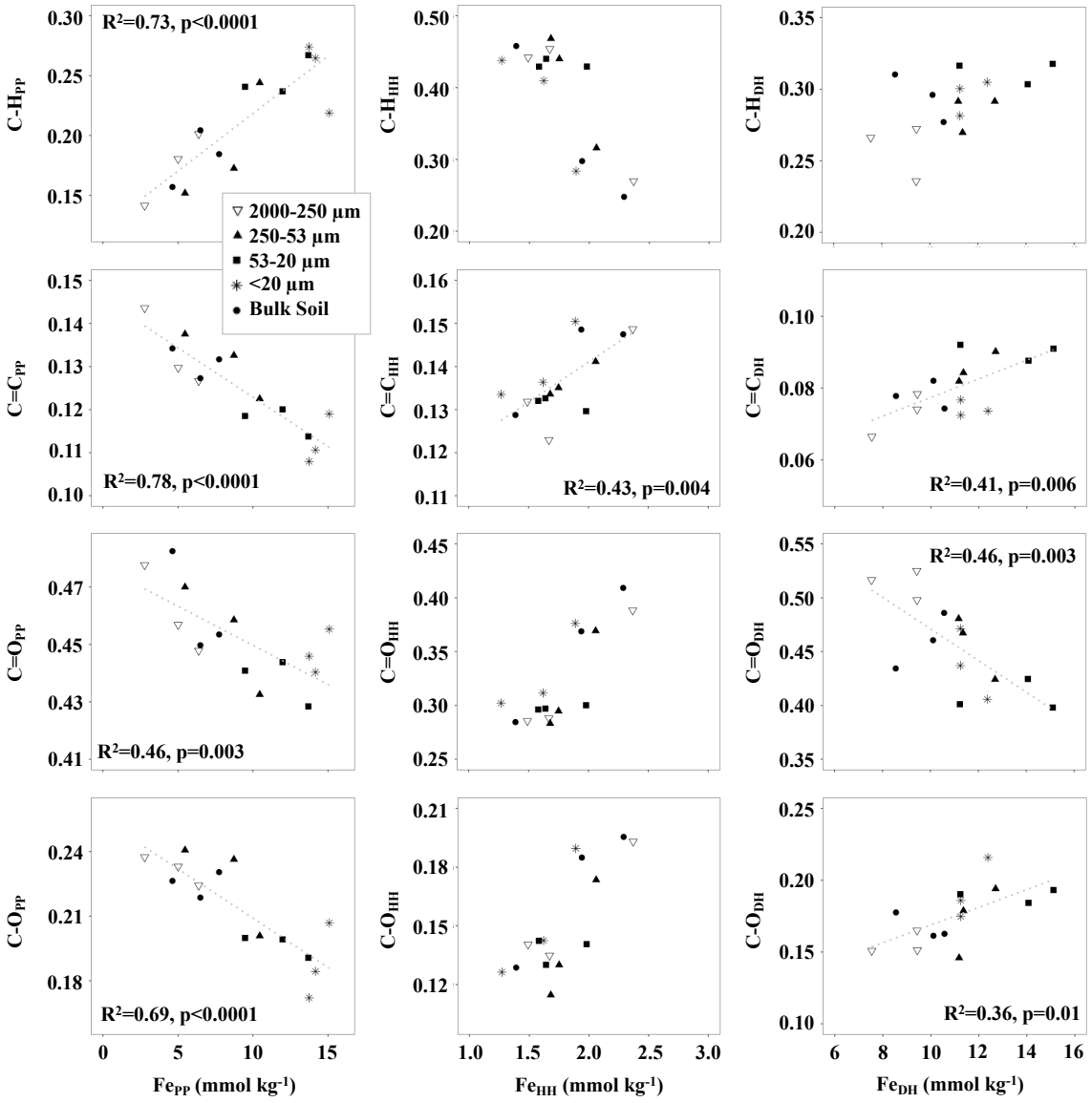

Figure 3-3. Correlations between relative peak areas of aliphatic C-H, aromatic C=C, carbonyl C=O, and carboxyl C-O groups and pedogenic Fe in PP- (left panel), HH- (middle panel), and DH- (right panel) extractable fractions regardless of soil size fractions and soil depths.

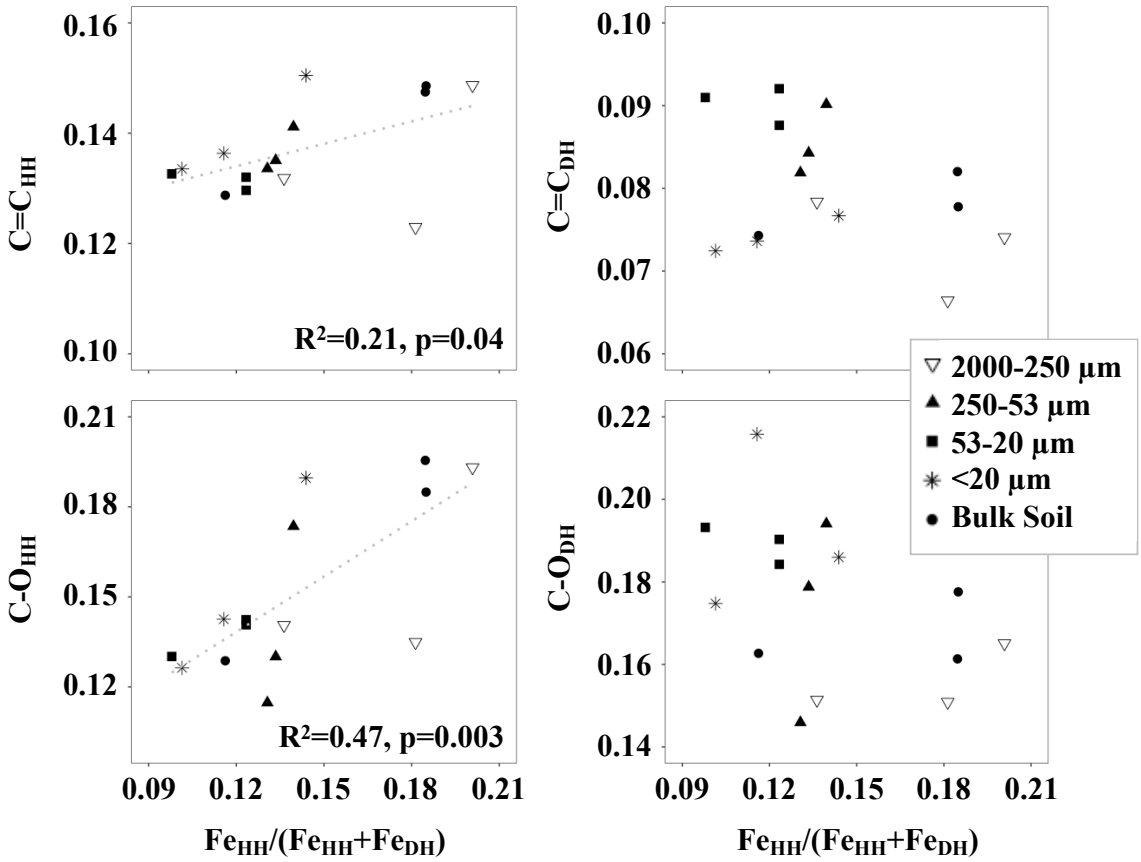

Figure 3-4. Correlations between peak areas of aromatic C=C and carboxyl C-O and molar ratio of HH-extractable Fe and HH- and DH-extractable Fe in different size fractions in Musick soils. The adjusted R^2 and P values were given for the correlations with statistical significances.

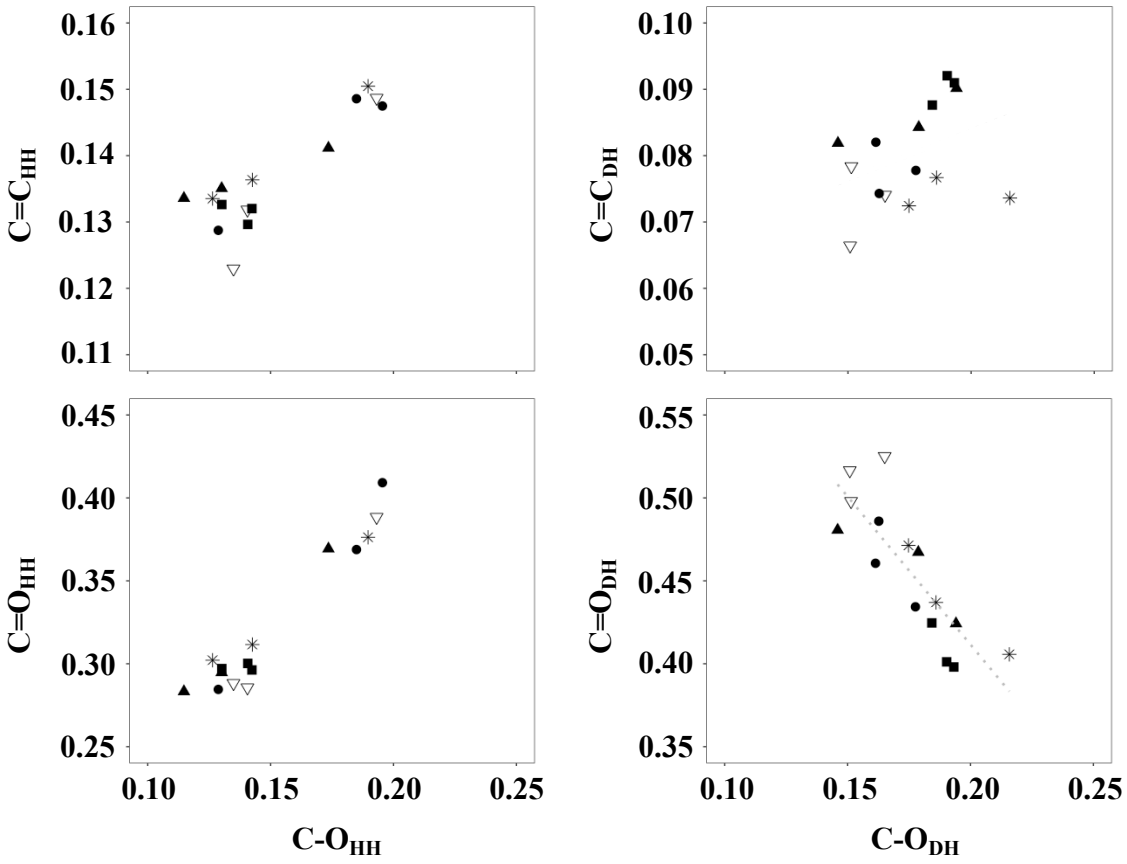

Figure 3-5. Correlations between relative peak areas of aromatic C=C or carbonyl C=O and carboxyl C-O in HH- and DH-extractable fractions. The adjusted R^2 and P values for linear regression between relative peak area of carbonyl C=O and carboxyl C-O in DH-extractable fraction was 0.68 and <0.0001.

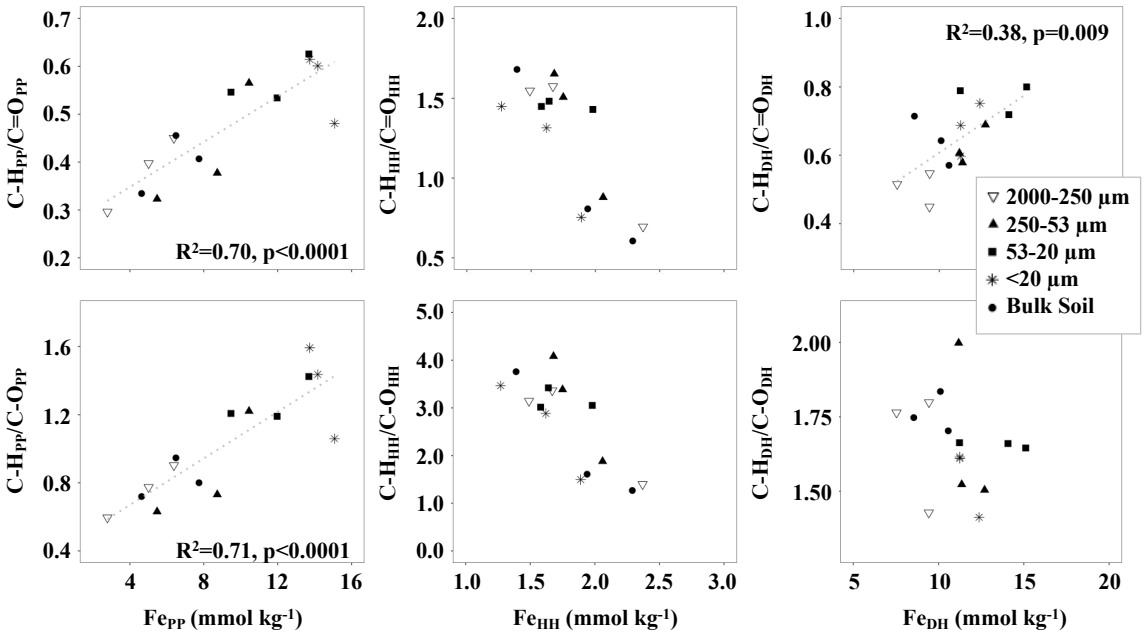

Figure 3-6. Ratios of aliphatic C-H to carbonyl C=O or carboxyl C-O as a function of pedogenic Fe concentrations in PP- (left panel), HH- (middle panel), and DH- (right panel) extractable fractions in B horizons.

CHAPTER 4. SORPTION AND DESORPTION OF SOIL ORGANIC MATTER FROM MINERAL SOILS WITH VARYING IRON OXIDE CONCENTRATIONS

ABSTRACT

Binding of soil organic matter (SOM) to pedogenic Fe oxides contributes to its long-term stabilization. In this study, adsorption and desorption ((de)sorption) capacity and the selective stabilization of specific organic matter (OM) functional groups were determined in artificial mixtures and natural soils with different Fe oxide concentrations to evaluate the effects of Fe oxides on stabilization (sorption) and destabilization (desorption) of SOM in western Sierra Nevada soils. Ultrasonication energy was applied during desorption in order to evaluate its efficiency on Fe oxides to promote physical stabilization of OM that is occluded inside soil aggregates. Results showed that once sorbed to Fe oxides, SOM was highly kinetically irreversible and less than 10% of the sorbed SOM was released during desorption phase in our time frame. C sorption capacity was higher in artificial soils with Fe oxides, and similar or higher in H_2O_2-treated natural soils with higher Fe oxide concentrations. Relative peak area of carboxylic C-O and aromatic C=C compounds increased with increasing Fe oxide concentrations. The inability of ultrasonication to liberate OM stabilized by Fe oxides (and other reactive minerals) in our study system suggests that the contribution of Fe oxides to physical stabilization of SOM in macro- and micro-aggregates is limited. Our findings show preferential stabilization of carboxyl and aromatic compounds by Fe oxides and/or other minerals.

4.1. INTRODUCTION

Pedogenic Fe oxides promote soil organic matter (SOM) storage and stabilization against microbial degradation by forming strong associations with SOM, likely through strong chemical bonds or due to the physical inaccessibility caused by physical occlusion within soil pores or aggregates (Kaiser and Guggenberger, 2000 and 2003; Mikutta et al., 2007; Moni et al., 2010; Eusterhues et al., 2010; Oren and Chefetz, 2012; Saidy et al., 2013; Zhao et al., 2016; Coward et al., 2018; Hall et al., 2018; Jin et al., chapter2 and 3). Sorptive association of SOM with Fe oxides and their associated bonding mechanisms have been extensively studied previously and several important mechanisms have been identified (McNight et al., 1992; Gu et al., 1994 and 1995; Kaiser et al., 1997; Boily et al., 2000; Mikutta et al., 2007; Chasse et al., 2015; Rowley et al., 2018). Recently, as the importance of physical inaccessibility of SOM to microbes, and the associated limitations for diffusion of oxygen and enzymes are being recognized in their role on SOM stabilization, different methods have been developed to isolate and analyze physically protected SOM (Barral et al., 1998; Schmidt et al., 1999; Kaiser and Guggenberger, 2000 and 2003; Rumpel et al., 2004; McCarthy et al., 2008; Moni et al., 2010; Kaiser and Berhe, 2014).

Sorption of SOM on the surfaces of pedogenic Fe oxides is one of the major mechanisms that controls stability of SOM (Gu et al., 1994 and 1995; Kaiser et al., 1997; Kaiser, 2003; Saidy et al., 2013; Adhikari and Yang, 2015; Chasse et al., 2015; Zhao et al., 2016; Coward et al., 2018; Hall et al., 2018). Ligand exchange mechanism has long been recognized as a major bonding mechanism that results in a direct and strong adsorption of SOM (McNight et al., 1992; Gu et al., 1994; Kaiser and Guggenberger, 1997; Boily et al., 2000; Mikutta et al., 2007; Chasse et al., 2015; Rowley et al., 2018). Cation bridging, especially as mediated by Calcium (Ca), was also previously found to allow the interactions between two negatively charged surfaces, and thus, promote the formation of soil aggregates and their stability (Kleber et al., 2007; Rowley et al., 2018; Jin et al., chapter 2). Coprecipitation of ferrihydrite and SOM allows for SOM-Fe association (Eusterhues et al., 2010; Kleber et al., 2015). Recently, Mikutta et al. (2007) found that goethite was predominantly associated with SOM from O horizon of Haplic Podzol via ligand exchange, whereas clay minerals were bound to SOM through cation bridging and van der Waals force. Therefore, SOM sorbed to pedogenic Fe oxides may be highly stable and may not readily desorb from Fe oxide surface, where the nature of SOM and mineral surface properties may regulate the process (Gu et al., 1995; Kaiser and Guggenberger, 2000; Kalbitz et al., 2005; Mikutta et al., 2007; Oren and Chefetz et al., 2012; Saidy et al., 2013; Eusterhues et al., 2014; Adhikari and Yang, 2015). However, microbial access to organo-mineral associations may weaken the strong relationships between mineral and C (Keiluweit et al., 2015), anerobic environment induced Fe reduction may also enhance the dissolution of SOM protected by minerals (Hall and Huang, 2017). However, most of the studies used Fe oxides in over one or few concentrations and were conducted on natural soils or pure Fe oxide compounds in suspensions. Neither of the sorbents were ideal to evaluate the effects of Fe oxide (solely)

on soils since natural soils are highly heterogenous and pure Fe oxide compounds are extremely simple compared to the real soil system. Therefore, we introduced artificial soil mixtures with or without Fe oxide to better mimic the real soil systems. We further used natural soils after removing their SOM using hydrogen peroxide to enable determination of the effects of Fe oxides with varying concentrations in soils on SOM stabilization.

Though the sorption process is important to evaluate the amount of SOM that is sorbed to Fe oxides, doing so does not allow us to determine how stable the C sorbed to Fe oxides will be. Determining the reversibility of sorption process is important in order to determine the stability of SOM-Fe assocaitions (Kaiser and Guggenberger, 2000). However, so far, desorption process hasn't received the same level of extensive attention in literature that sorption has (Gu et al., 1995). Previous studies have shown that sorption of SOM by Fe oxides was largely kinetically irreversible (Gu et al., 1995; Kaiser and Guggernberger, 2000; Mikutta et al., 2007; Saidy et al., 2013), and suggest that the fate of SOM associated with Fe oxides is largely dependent on to what extent and under what conditions, it would be possible to desorb the organic compounds associated with Fe oxides. Most of the previous studies used water or background electrolyte for shaking during desorption process, which may only desorb C that is loosely attached to the Fe oxide. However, such processes are unlikely to enable the release of physically occluded C that is associated with Fe oxides, for example, through the ability of Fe oxides to enable the formation and the stabilization of aggregates, and/or aggregates formed from mixtures of organic and inorganic compounds that include SOM that is chemically bound to Fe oxides.

Especially, with unique heterogenous structure of soils, a large proportion of organo-Fe oxide complexes may be entrapped in the soil aggregates or soil pores (Barral et al., 1998; Kaiser and Guggenberger, 2000; Chenu and Plante, 2006; Moni et al., 2010; Barre et al., 2014; Totsche et al., 2018; Jin et al., chapter 2). Fe oxide coating within clay sized aggregates (<2 μm size fraction), but not free Fe oxides, was observed from forest and cultured soils using transmission electron microscope (TEM) with energy dispersive X-ray spectroscopy (EDS) (Chenu and Plante, 2006). Moni et al (2010) also found that OC within Fe cemented silt size aggregates had longer radiocarbon-based residence time compared to the free clay particles in a Plinthic Cambisol soil, where around 40% of total C was located in the silt-size aggregates. Lower total soil porosity and higher soil aggregate stability was also observed in soils with high Fe oxides and SOM (Barral et al., 1998). In addition, poorly crystalline Fe oxides were found to be preferentially reside in larger soil aggregates (Huang et al., 2016; Jin et al., chapter 2). These results demonstrate that Fe oxides promote soil aggregation (Totsche et al., 2018), and a significant proportion of Fe oxides and their associated C may reside in the soil aggregates. In order to evaluate the Fe oxides associated C that is protected in soil aggregates, ultrasonication as one of the aggregate disintegration technique, is often used (Schmidt et al., 1999; Rumpel et al., 2004; Moni et al., 2010; Kaiser and Berhe, 2014) since ultrasonication energy can physically disperse soil aggregates without or with minimum interruptions on isolated components in soils (Kaiser et al., 2014). However, the efficiency of

ultrasonication energy on releasing Fe oxides associated C in soil aggregates is still unknown.

Therefore, in this study, we evaluated the (de)sorption behavior of SOM that is associated to Fe oxides in artificial soil mixture with or without Fe oxide, and H_2O_2-treated natural soils in a batch (de)sorption experiment. We aimed to test the following main questions: (1) Do higher Fe oxide concentrations will lead to a greater total amount of sorption? (2) Do Fe oxides preferentially accumulate the carboxyl and aromatic C functional groups? and (3) Does sonication energy will release physically occluded SOM that is sorbed by Fe oxides?

4.2. METHODS

4.2.1. Soil site description

Soils were sampled from Sirretta (37.16189 N, 119.20198 W, 2195 m a.s.l) and Musick (37.06073 N, 119.37348 W, 1390 m a.s.l) sites at western slope of Sierra Nevada mountain. Soils along this elevational transect were largely affected by climate, mainly temperature and precipitation, which resulted in different vegetation zones in two sites. With mean annual air temperate of 7.2 ^{O}C and precipitation of 108 cm, Sirretta site developed a mixed-conifer forest with dominant vegetation of *Pinus jeffreyi*, *Abies magnifica*, and *Abies concolor*. On the other hand, Musick site with mean annual air temperate of 11.1^{O}C and precipitation of 91cm, developed an oak/mixed-conifer forest with *Pinus ponderosa*, *Calocedrus decurrens*, *Quercus kelloggii*, and *Chamaebatia foliolosa* as dominant vegetation (Dahlgren et al., 1997). Musick soil was intensely weathered with high clay content (11-27%) and sodium dithionite extracted pedogenic Fe concentration of 136.09 mmol kg^{-1} in A horizon (0-29 cm), and 212.49 mmol kg^{-1} in B horizon (29-56 cm) and was classified as Ultic Haploxeralf Alfisol. Compared to Musick soils, Sirretta soil was moderately weathered with lower clay content (3-7%) and sodium dithionite extracted pedogenic Fe concentration of 86.55 mmol kg^{-1} in A horizon (0-29 cm), and 95.50 mmol kg-1 in B horizon (29-102 cm), and was classified as Dystric Xerorthent Entisol (Dahlgren et al., 1997). Musick soil is dominated by kaolin mineral, which may be weathered to gibbsite that became dominant in Sirretta soil under intense leaching environment. Ferrihydrite may be a major Fe oxide in surface soils and crystallized to more crystalline hematite in deeper soils in Musick soils (Jin et al., chapter 2). Mica and hydroxy-Al interlayered vermiculite were also found in Musick soil, while mica may mostly be weathered to hydroxy-Al interlayered vermiculite and became dominant in Sirretta soil that experiences high leaching intensity (Dahlgren et al., 1997; Araya et al. 2016, 2017).

4.2.2. Water extractable soil organic matter

Soil from O horizons of Sirretta and Musick sites was used to extract water extractable organic matter (WEOM). The O-horizon samples collected from the field were cut into small pieces and ground to a uniform, fine powder using a ball mill prior to the extraction

of WEOM with ultrapure water in a ratio of 1:10 (SOM mass/water volume) (Kaiser et al., 1997; Kaiser et al., 2001; Dilling and Kaiser, 2002; Oren and Chefetz, 2012; Coward et al., 2018). The mixture was shaken for 15 min and allowed to sit for 18 h before it was vacuum filtered through a 0.45 μm filter twice prior to further procedures (Kaiser et al., 2001). Concentration of WEOM (<0.2μm) was determined with TOC analyzer (Shimadzu TOC-Vcsh Total Organic Carbon Analyzer with the detection limit of 0.5 μg l^{-1}). The original WEOM concentration of Musick soil was 159.25 mmol l^{-1}, and that of Sirretta soil was 24.17 mmol l^{-1}. Subsample of original WEOM was freeze-dried and its chemical composition was determined using FTIR on a Bruker IFS 66v/S spectrophotometer (Ettlingen, Germany) as described below.

4.2.3. Artificial soil mixtures

Artificial soil mixtures were prepared with the components and the proportions of sand, silt and clay sized particles following methods of Kaiser et al. (2014), see Table 4-1. Clay-sized minerals used in the artificial mixture were bentonite, kaolinite, Al oxide and Fe oxide, which largely resembled composition of Musick soils (Dahlgren et al., 1997; Jin et al., chapter 2). Basic properties of individual minerals are given in Table S4-1. Artificial soils with 1% Fe oxides were prepared by adjusting the proportions of sand size fractions (while leaving the proportions of other components the same) with an assumption made that sand is not a major contributor to soil C storage. That is, the proportions of each component in non-Fe soil mixtures (AS_{NA}) were 65% of sand size fraction, 20% of silt size fraction, and 15% of clay minerals and Al oxide, whereas those with 1% Fe oxide mixed in the soil mixtures ($AS_{1\%}$) were 64% of sand size fraction, 20% for silt size fraction, 15% of clay minerals and Al oxide, and 1% of Fe oxides (Table 4-1). Artificial soil mixtures were stored under the room temperature in dark until (de)sorption experiments. Individual mineral in the artificial mixtures were identified with XRD (PANalytical X'Pert PRO Theta/Theta Powder X-ray Diffraction system with revolutionary X'Celerator detector) (Figure S4-1 and S4-2).

4.2.4. H_2O_2 treatment on natural soils

Musick and Sirretta soils from A and B horizons were treated with 30% hydrogen peroxide to remove SOM. Specifically, 2 g of soils were treated with 20 ml 30% hydrogen peroxide until all the liquid was dried at 40 ^{O}C (Oren and Chefetz, 2012; Wissing et al., 2014). H_2O_2-treated samples were then ground and analyzed for C content with an isotope ratio mass spectrometer (IRMS) (DELTA V Plus Isotope Ratio Mass Spectrometer, Thermo Fisher Scientific, Inc., Waltham, MA, USA), and the results showed that more than 80% of the SOM was removed after hydrogen peroxide treatment (data not shown). Soil minerals in H_2O_2-treated soils were identified with XRD and compared with original A and B horizon soils, and no significant changes were found (Figure S4-3). Field replicates of the soil samples were combined prior to the (de)sorption experiment.

4.2.5. (De)sorption experiments

In order to compare the effectiveness of Fe-facilitated physical vs. chemical stabilization of C in soil, we performed two parallel experiments (Figure 4-1). Each WEOM had four combinations with soils: WEOM from Musick soils mixed with artificial soil mixtures (with or without Fe oxides) and H_2O_2-treated natural soils from Musick A and B horizons, whereas WEOM from Sirretta soils was mixed with artificial soil mixtures (with or without Fe oxides) and H_2O_2-treated natural soils from Sirretta A and B horizons (Figure 4-1). Musick and Sirretta WEOM was applied to their own surface and subsoils in order to mimic the real sitation that would happen in each site. At the end of the sorption experiments, we applied ultrasonic energy to one set of the samples to break down aggregates and liberate physically protected C, while the other set was not exposed to such treatment. We applied ultrasonication energy at 440 J ml^{-1} to liberate the soil C that is associated with soil macro- and micro-aggregates (Kaiser et al., 2012; Kaiser and Berhe, 2014).

Adsorption experiments were performed by mixing original WEOM solutions with artificial soils or H_2O_2-treated natural soils from Musick and Sirretta sites. Specifically, 20 ml of SOM solutions in buffer of 0.01 M $CaCl_2$ solutions were mixed with 2 g of either artificial soil mixtures with or without Fe oxide or H_2O_2-treated natural soils, and the mixtures were shaken for 4 days until the sorption equilibrium was established as was determined in preliminary kinetic experiments. The suspensions were then centrifuged at 7000rpm, and syringe filtered through a 0.2 μm filter for C concentration measurements. To conduct the desorption experiments, 20 ml of WEOM-free 0.01M $CaCl_2$ solutions was added to the residue samples from the adsorption experiments for a period of 4 days. At the end of the desorption period, ultrasonication energy at 440 J ml^{-1} was applied for one set of samples, while the other set of samples was directly centrifuged, and syringe filtered through a 0.2 μm filter for C concentration measurements. The results of C mass balance showed that >95% of C was recovered after experiments (data not shown).

4.2.6. Diffuse reflectance infrared Fourier transform (DRIFT) spectroscopy

C functional groups or structure of residue samples after sorption and desorption periods were determined with DRIFT spectroscopy using a Bruker IFS 66v/s spectrophotometer (Ettinger, Germany). Measurements were performed in mid-infrared region between 4000 and 400cm^{-1}, and the resolution was optimized at 4 cm^{-1} by averaging 32 scans. The spectra were then baseline corrected in the OPUS operating systems prior to the peak area calculation. Peaks between 2976 to 2898cm^{-1} and between 2870 and 2839cm^{-1} were derived from aliphatic C-H asymmetrical and symmetrical stretch, respectively, and were grouped as aliphatic C-H stretch (e.g. Coates, 2006; Chatterjee et al., 2012; Ryal et al., 2014; Hall et al., 2018). A profound peak between 1710 and 1570cm^{-1} was corresponding to carbonyl C=O of amides, quinones, and ketones (e.g. Artz et al., 2008; Ryal et al., 2014; Hall et al., 2018). A visible peak between 1550 and 1500cm^{-1} was assigned to aromatic C=C stretch (e.g. Artz et al., 2008; Demyan et al., 2012; Hall et al., 2018). A shoulder peak between 1480 and 1380cm^{-1} was interpreted as carboxyl C-O stretch (e.g.

Artz et al., 2008; Ryal et al., 2014; Hall et al., 2018). Spectra of original A and B horizon soils in Musick and Sirretta soils were also measured to compare the differences between original soils and residue samples after (de)sorption processes. Peak area of individual C functional group was calculated using "integration" function and was divided by total peak area of total C functional group to obtain relative peak area for each C functional group.

4.2.7. Data analysis

Relationships between Fe concentrations and the peak areas of C functional groups or the fractions of C desorption were tested with normality and analysis of variance (ANOVA), and the significance of the relationships was evaluated with linear regression model on R 3.5.3.

4.3. RESULTS

4.3.1. WEOM (de)sorption to soils

In general, the quantity of C sorbed during (de)sorption were greater in artificial soils with Fe oxides ($AS_{1\%}$) than without Fe oxides (AS_{NA}) (Table 4-2). More specifically, the amount of Musick WEOC sorbed to $AS_{1\%}$ soils during sorption were 756.74±6.66 mmol kg^{-1} and that of Sirretta WEOC sorbed to $AS_{1\%}$ soils during sorption were 143.82±0.88 mmol kg^{-1}, respectively. On the other hand, the amount of Musick WEOC sorbed to AS_{NA} soils were 729.60±11.99 mmol kg^{-1}, and that of Sirretta WEOC sorbed to AS_{NA} soils were 131.79±4.38 mmol kg^{-1}, respectively. Compared to the original C concentrations from O horizons, 47.56% and 45.85% of Musick WEOC were sorbed to $AS_{1\%}$ and AS_{NA} soils during sorption, whereas 59.56% and 54.58% of Sirretta WEOC were sorbed to $AS_{1\%}$ and AS_{NA} soils during sorption, respectively.

Majority of C sorbed on minerals, however, was not detached during desorption in our time frame in general. For example, only 2.32% and 5.93 % of Musick and Sirretta WEOC sorbed during sorption were released during desorption without ultrasonication treatment in $AS_{1\%}$ soils, respectively. On the other hand, additional 0.05% and 2.18% of Musick and Sirretta WEOC were attached to the mineral surface during desorption with ultrasonication treatment in $AS_{1\%}$ soils, respectively. In contrast, 7.86% and 7.09% of Musick and Sirretta WEOC sorbed during sorption were released during desorption without ultrasonication in AS_{NA} soils, and 4.11% and 1.48% of Musick and Sirretta WEOC were detached from the AS_{NA} soils during desorption with ultrasonication. The C detached from mineral surface during desorption was nearly doubled or tripled in AS_{NA} than in $AS_{1\%}$ soils.

Amount and the fraction of C sorbed to H_2O_2-treated natural soils during (de)sorption were generally higher than those sorbed to artificial soils (Table 4-2). Specifically, the amount of Musick WEOC sorbed to H_2O_2-treated Musick A horizon soils during sorption were 1056.28±73.03 mmol kg^{-1} and that of Musick WEOC sorbed to H_2O_2-treated

Musick B horizon soils were 957.72±35.50 mmol kg^{-1}, which accounted for 60.23% and 59.39% of original Musick WEOC concentrations, respectively. Similarly, the amount and the fraction of Sirretta WEOC sorbed to H_2O_2-treated Sirretta A horizon soils during sorption were 196.48±10.66 mmol kg^{-1} and that of Sirretta WEOC sorbed to H_2O_2-treated Sirretta B horizon soils were 216.48±0.34 mmol kg^{-1}, which accounted for 80.43% and 87.86% of original Sirretta WEOC concentrations, respectively.

Similar to artificial soils, majority of C sorbed in natural soils during sorption were kinetically irreversible and less than 10% of the sorbed C was released during desorption with or without sonication treatment. For example, 1.07% and 4.31% of Musick WEOC sorbed to H_2O_2-treated Musick A and B horizon soils during sorption were released after desorption without sonication treatment. On the other hand, 4.98% of C was additionally sorbed onto the minerals in Musick A horizon soils with ultrasonication treatment. Similarly, 2.14% and 1.14% of Sirretta WEOC sorbed to H_2O_2-treated Sirretta A and B horizon soils during sorption was released after desorption without sonication treatment. On the other hand, 1.10% of additional C was sorbed to mineral with ultrasonication treatment in A horizon, whereas 1.80% of the C sorbed during sorption was released with ultrasonication treatment in B horizon soils.

In this study, we further assessed the general relationship between Fe oxide and the C (de)sorbed by normalizing Fe concentration in different soil types/sites in the same unit scales. To do that, Fe concentrations of natural soils were adopted from previous work (Dahlgren et al., 1997, sodium dithionite-extracted Fe concentration unit was converted from g kg^{-1} to mmol kg^{-1}) and those of artificial soils were calculated (Fe oxide unit was converted from mass% to mmol kg^{-1}), and the general relationship between Fe concentration and the fraction of C (de)sorbed regardless of soil sites or soil types were evaluated. Based on calculation, Fe concentrations in Musick soils were 0, 125.24, 136.09, and 212.49 mmol kg^{-1} for AS_{NA}, $AS_{1\%}$, NS_A, and NS_B. Fe concentrations in Sirretta soils were 0, 86.55, 95.50, and 125.24 mmol kg^{-1} for AS_{NA}, NS_A, NS_B, and $AS_{1\%}$. Results showed that the fraction of sorbed C tended to increase with increasing Fe concentrations, whereas the fraction of desorbed C decreased as Fe concentrations increased (Figure 4-2).

4.3.2. DRIFT based C functional groups in soils

Spectra of residue samples after (de)sorption phases were similar to the original spectra of WEOM or soil samples (Figure 4-3). However, the intensity of absorbance of C functional groups after (de)sorption phases was generally higher in $AS_{1\%}$ soils than AS_{NA} soils and was also higher during sorption compared to the desorption phases with or without ultrasonication treatment. In agreement with what we observed by visual inspection of the spectra, relative peak area of C sorbed to $AS_{1\%}$ soils were higher than that of C sorbed to AS_{NA} soils after both sorption and desorption periods (Figure 4-4, Table S4-2 and S4-3). In addition, we found that the relative peak areas of aromatic C=C and carboxyl C-O tended to increase with increasing Fe concentrations with R^2 values of 0.26 ($p=0.10$) and 0.30 ($p=0.09$), whereas relative peak area of aliphatic C-H tended to

decrease as Fe concentration increased with R^2 value of 0.29 (p=0.09) (Figure 4-4). Regardless of different types of WEOM or soils used, or which stages of the experiment were at (i.e. (de)sorption), peak area of aromatic C=C was strongly positively correlated to the peak areas of carboxyl C-O (Figure 4-5).

4.4. DISCUSSION

4.4.1. (De)sorption of SOM associated with Fe oxides

The greater sorption of WEOM in soils with higher Fe oxide concentrations in this study, as indicated by the higher C sorption capacity in soils with higher amount of Fe oxides in artificial and natural soils (Table 4-2), is in agreement with previous studies. Kaiser and Guggenberger (2000) found that Fe oxide coating on a spodic B horizon soils increased the C sorption capacity. Similarly, Saidy et al. (2013) reported that the C sorption capacity on kaolinite increased with goethite coating, and that of illite increased with ferrihydrite coating. Tombacz et al. (2004) reported that hematite and magnetite sorbed more humic acid than kaolinite and montmorillionite. Mikutta et al. (2007) also found that the sorption of SOM on goethite was highest compared to that on pyrophyllite and vermiculite. In addition, SOM mostly sorbed on goethite via ligand exchange mechanism was highly stable against microbial degradation, when compared to that sorbed on pyrophyllite and vermiculite, which were mostly associated via cation bridging and van der Waals force (Mikutta et al., 2007). Higher sorption capacity of SOM in natural soils than artificial soils is likely due to the other sorbents that presents in natural soils. These findings support the previous findings that Fe oxides in our concentration range in general may enhance the C sorption capacity of soils.

Desorption released a small portion of C (less than 10% of the total C added) that was sorbed during sorption phase of our experiments (Table 4-2), and less sorbed C was liberated with increasing Fe oxide concentrations. Saidy et al (2013) previously reported similar findings, where 5.69%, and 11.58% of C sorbed during sorption period were released with goethite coating on kaolinite and illite, whereas 9.13% and 11.69% of C sorbed during sorption period were released without any Fe oxide coating on the same clay minerals. In addition, 11.89% of sorbed C was released during desorption period with hematite coating on illite, whereas 11.69% of sorbed C was released during desorption period from illite without any Fe oxide coating (Saidy et al., 2013). Kaiser and Guggenberger (2000) found that less than 3% of the sorbed DOC was released from goethite after 24h of desorption period. Similarly, Kaiser and Guggenberger (2007) found that C desorbed barely from goethite with deionized water, but the efficiency increased with sodium containing salts. Furthermore, Mikutta et al. (2007) reported that less than 6% of the sorbed C was released from goethite during desorption period. In addition, Gu et al. (1994, 1995) suggested that the strong inner-sphere interaction such as ligand exchange mechanisms may be a primary sorption mechanism. Ligand exchange mechanism was also found to be dominant between SOM and goethite by Mikutta et al (2007). Therefore, in general, C sorbed to Fe oxide may be strongly associated with Fe

oxide via strong chemical bond and highly kinetically irreversible and stable against microbial degradation (Kaiser and Guggenberger, 2000; Kalbitz et al., 2005).

On the other hand, ultrasonication treatment during desorption phase of our experiments did not release a lot more C (Table 4-2), likely because in our soils, the interaction between Fe oxides and C is mostly through sorption-like mechanism. Moni et al. (2010) found that OC recovered after ultrasonication applied at 320 J ml^{-1} in <50 μm size fraction exceeded for 0.2-17% compared to initial amount of OC, where clay size fraction increased at most 7 times compared to the moderate dispersion without ultrasonication energy applied. In addition, Fe oxides were found to be preferentially reside in the larger soil aggregates (Huang et al., 2016; Jin et al., chapter 2). Therefore, we propose that ultrasonication energy at 440 J ml^{-1}, which is often used to break soil macro- and microaggregates (Kaiser and Berhe, 2014), may relocate previously physically occluded Fe oxides and their associated C to smaller aggregate size fractions through flocculation (Moni et al., 2010) or precipitation process. It is also highly possible that the desorption time period in this study may be too short to allow the SOM to diffuse into the aggregate. However, the exact mechanisms will warrant further studies. Other clay-sized minerals in soils may also contribute to the strong bonding in soils considering that we have considerable amount of Al in our artificial soils. These results suggest that the use of ultrasonication to release physically occluded C in soil macro- and micro-aggregates may not be efficient in our time frame.

4.4.2. Soil organic matter fractionation during (de)sorption

We observed relative peak area of aliphatic C-H decreased with increasing Fe concentrations in soils (Figure 4-4), compared to other C functional groups during the timescale and concentration range in this study, likely suggesting limited role in chemical association of these functional groups with reactive soil minerals. In agreement with our result, McKnight et al. (1992) previously reported that aliphatic C-H groups were primarily remained in the solution, whereas carboxyl group bound to aromatic structure of stream dissolved organic matter were preferentially sorbed by Al and Fe oxides on the streambed as indicated by ^{13}C liquid phase NMR spectra. Similarly, Gu et al. (1994) found that SOM sorbed to Fe oxides were low in aliphatic methylene, alcoholic, and carbohydrate C as indicated by ^{13}C solid state NMR spectra. Kaiser and Guggenberger (2000) also found that aliphatic C-H was mostly remained in solution, while carbonyl and aromatic C were depleted in solution after the sorption of hydrophobic acidic fraction of SOM on goethite. In contrast, the high absorbance of aliphatic C-H in AS_{NA} soil in this study may due to the selective sorption of aliphatic C-H by clay minerals, such as kaolinite and montmorilionite as reported by Wang and Xing (2005). These results suggest that aliphatic C-H may be selectively remained in the solution during sorption. However, the preference for aliphatic C-H to Fe oxide surface may differ with Fe crystallinity since aliphatic C-H may become favorable as Fe oxide crystallinity increases (Jin et al., chapter 3), which may due to the inner-sphere bonding to Fe oxides (Adhikari and Yang, 2015).

On the other hand, strong positive relationships between relative peak areas of aromatic C=C or carboxyl C-O and Fe oxide concentrations were observed, suggesting strong selective sorption of aromatic C=C and carboxyl C-O functional groups on Fe oxides in soils. Previously, strong positive correlations between peak areas of aromatic C=C or carboxyl C-O and the concentrations of hydroxylamine hydrochloride-extracted poorly crystalline Fe oxides and sodium dithionite hydrochloride-extracted well crystalline Fe oxides regardless of soil size fractions and soil depths in Musick soils using a sequential Fe extraction procedures were also reported (Jin et al., chapter 3). The strong relationships between aromatic C=C and/or carboxyl C-O, and Fe oxide were also found in varying systems. Mcknight et al. (1992) reported that stream SOM with aromatic moieties and carboxyl acid groups may preferentially sorb to Fe oxides. Similarly, Gu et al. (1994) also found that carboxyl functional groups of SOM from a wetland pond was selectively sorbed by pure Fe oxides. Kaiser et al. (1997) found that preferential removal of carboxyl and aromatic C of SOM collected from O horizon Entic Haplorthod Spodosol from solutions to pure Fe oxide minerals. With high adhesion strength of SOM rich in carboxyl C-O and aromatic C=C (Chasse et al., 2015; Lv et al., 2016), inner-sphere ligand exchange mechanism may be responsible for the strong bond between carboxyl C-O, aromatic C=C and Fe oxide (Mcknight et al., 1992; Gu et al., 1994; Kaiser et al., 1997; Boily et al., 2000; Chasse et al., 2015). The close relationship between aromatic and carboxyl C was also supported by our finding, where a strong positive correlation between the peak areas of carboxyl C-O and aromatic C=C was found regardless of varying conditions in this study (Figure 4-5) and was also found by Jin et al. (chapter 3) previously. The similar relationships found in variety of soil conditions and minerals (batch sorption experiments) may indicate that the close relationship between Fe oxides and carboxyl C-O and aromatic C=C may commonly exist in variety of soil and aquatic systems.

Carbonyl C=O may not be affected by Fe oxide since no relationship between carbonyl C=O and Fe oxide concentrations was found (Figure 4-4). No significant correlations between carbonyl C=O and well crystalline Fe concentrations were also found in Musick soils previously, but the peak area of carbonyl C=O significantly decreased as Fe oxide crystallinity decreased in the same soil (Jin et al., chapter 3). These results show no preference of carbonyl C=O on Fe oxide concentrations, but Fe crystallinity may affect the preference of carbonyl C=O to Fe oxide in soils.

In addition, we didn't observe any correlations between peak areas of C functional groups during desorption and Fe concentrations, which may partly due to the limited amount of C desorbed in this study. However, Oren and Chefetz (2012) found that the carboxyl and phenolic structures of SOM were irreversibly associated to mineral soils. Further investigations may be needed to better understand the selective destabilization of C functional groups by Fe oxides in Sierra soils.

4.5. CONCLUSION

(De)sorption of SOM by Fe oxides with varying concentrations in artificial soils with or without Fe oxide and H_2O_2-treated natural A and B horizon soils were evaluated to understand the C sorption capacity of Fe oxides in soils. We also further converted Fe concentrations from two soil sites and soil types in same unit scales, in order to evaluate the general relationship between Fe oxide concentrations and the sorption capacity, and the relative peak areas of C functional groups. Functional groups of Fe oxide sorbed C were also assessed to understand the selective stabilization of C functional groups by Fe oxide. Sonication treatment was applied to evaluate if physically occluded C that is associated with Fe oxides will be released. Our results showed that the C sorption capacity tended to increase as Fe concentrations increased (Q1). C functional groups or structure were selectively sorbed to Fe oxides, where Fe oxides preferentially stabilized carboxyl C-O and aromatic C=C (Q2). Though sonication energy at 440 J ml^{-1} may not be efficient in soils (Q3).

ACKNOWLEGEMENTS

The authors gratefully acknowledge lab assistance from Liying Zhao at the Environmental Analytical Lab, field sampling from Wenjun Ge at Oak Ridge National Lab, and Samuel Negusse Araya and Randy Dahlgren for information about field sites and the Musick soil. The authors also acknowledge support of dissertation committee member, Dr. Steven Hall for comments on earlier versions of this manuscript. Funding for this work was provided from UC Merced and the National Science Foundation (CAREER EAR -1352627) award to A. A. Berhe.

REFERENCES

Adhikari, D. and Yang, Y. (2015). Selective stabilization of aliphatic organic carbon by iron oxide. Scientific reports, 5, 11214.

Araya, S. N., Meding, M. and Berhe, A. A. (2016). Thermal alteration of soil physico-chemical properties: a systematic study to infer response of Sierra Nevada climosequence soils to forest fires. Soil, 2(3), 351-366.

Araya, S. N., Fogel, M. L. and Berhe, A. A. (2017). Thermal alteration of soil organic matter properties: a systematic study to infer response of Sierra Nevada climosequence soils to forest fires. Soil, 3(1), 31-44.

Artz, R. R., Chapman, S. J., Robertson, A. J., Potts, J. M., Laggoun-Défarge, F., Gogo, S., Comont, L., Disnar, J. and Francez, A. J. (2008). FTIR spectroscopy can be used as a screening tool for organic matter quality in regenerating cutover peatlands. Soil Biology and Biochemistry, 40(2), 515-527.

Barral, M. T., Arias, M. and Guerif, J. (1998). Effects of iron and organic matter on the porosity and structural stability of soil aggregates. Soil and Tillage Research, 46(3-4), 261-272.

Barré, P., Fernandez-Ugalde, O., Virto, I., Velde, B. and Chenu, C. (2014). Impact of phyllosilicate mineralogy on organic carbon stabilization in soils: incomplete knowledge and exciting prospects. Geoderma, 235, 382-395.

Boily, J. F., Persson, P. and Sjöberg, S. (2000). Benzenecarboxylate surface complexation at the goethite (α-FeOOH)/water interface: II. Linking IR spectroscopic observations to mechanistic surface complexation models for phthalate, trimellitate, and pyromellitate. Geochimica et Cosmochimica Acta, 64(20), 3453-3470.

Chassé, A. W., Ohno, T., Higgins, S. R., Amirbahman, A., Yildirim, N. and Parr, T. B. (2015). Chemical force spectroscopy evidence supporting the layer-by-layer model of organic matter binding to iron (oxy) hydroxide mineral surfaces. Environmental science & technology, 49(16), 9733-9741.

Chatterjee, S., Santos, F., Abiven, S., Itin, B., Stark, R. E. and Bird, J. A. (2012). Elucidating the chemical structure of pyrogenic organic matter by combining magnetic resonance, mid-infrared spectroscopy and mass spectrometry. Organic geochemistry, 51, 35-44.

Chenu, C. and Plante, A. F. (2006). Clay-sized organo-mineral complexes in a cultivation chronosequence: revisiting the concept of the ‘primary organo-mineral complex’. European Journal of Soil Science, 57(4), 596-607.

Coates, J. (2006). Interpretation of infrared spectra, a practical approach. Encyclopedia of analytical chemistry: applications, theory and instrumentation.

Coward, E. K., Ohno, T. and Plante, A. F. (2018). Adsorption and molecular fractionation of dissolved organic matter on iron-bearing mineral matrices of varying crystallinity. Environmental science & technology, 52(3), 1036-1044.

Dahlgren, R. A., Boettinger, J. L., Huntington, G. L. and Amundson, R. G. (1997). Soil development along an elevational transect in the western Sierra Nevada, California. Geoderma, 78(3-4), 207-236.

Demyan, M. S., Rasche, F., Schulz, E., Breulmann, M., Müller, T. and Cadisch, G. (2012). Use of specific peaks obtained by diffuse reflectance Fourier transform mid-infrared spectroscopy to study the composition of organic matter in a Haplic Chernozem. European Journal of Soil Science, 63(2), 189-199.

Dilling, J. and Kaiser, K. (2002). Estimation of the hydrophobic fraction of dissolved organic matter in water samples using UV photometry. Water Research, 36(20), 5037-5044.

Eusterhues, K., Neidhardt, J., Hädrich, A., Küsel, K. and Totsche, K. U. (2014). Biodegradation of ferrihydrite-associated organic matter. Biogeochemistry, 119(1-3), 45-50.

Eusterhues, K., Rennert, T., Knicker, H., Kögel-Knabner, I., Totsche, K. U. and Schwertmann, U. (2010). Fractionation of organic matter due to reaction with ferrihydrite: coprecipitation versus adsorption. Environmental Science & Technology, 45(2), 527-533.

Gu, B., Schmitt, J., Chen, Z., Liang, L. and McCarthy, J. F. (1994). Adsorption and desorption of natural organic matter on iron oxide: mechanisms and models. Environmental Science & Technology, 28(1), 38-46.

Gu, B., Schmitt, J., Chen, Z., Liang, L. and McCarthy, J. F. (1995). Adsorption and desorption of different organic matter fractions on iron oxide. Geochimica et Cosmochimica Acta, 59(2), 219-229.

Hall, S. J., Berhe, A. A. and Thompson, A. (2018). Order from disorder: do soil organic matter composition and turnover co-vary with iron phase crystallinity? Biogeochemistry, 140(1), 93-110.

Hall, S. J., & Huang, W. (2017). Iron reduction: a mechanism for dynamic cycling of occluded cations in tropical forest soils?. Biogeochemistry, 136(1), 91-102.

Huang, X., Jiang, H., Li, Y., Ma, Y., Tang, H., Ran, W. and Shen, Q. (2016). The role of poorly crystalline iron oxides in the stability of soil aggregate-associated organic carbon in a rice–wheat cropping system. Geoderma, 279, 1-10.

Jin, L., O'Day, P. and Berhe, A. A. Role of iron oxides on physical protection of soil organic matter inside aggregates. In preparation.

Jin, L. and Berhe, A. A. Characterization of organic matter in pedogenic iron-containing mineral fractions: effect of iron phase crystallinity. In preparation.

Kaiser, K. (2003). Sorption of natural organic matter fractions to goethite (α-FeOOH): effect of chemical composition as revealed by liquid-state ^{13}C NMR and wet-chemical analysis. Organic Geochemistry, 34(11), 1569-1579.

Kaiser, K., Guggenberger, G., Haumaier, L. and Zech, W. (1997). Dissolved organic matter sorption on sub soils and minerals studied by ^{13}C-NMR and DRIFT spectroscopy. European Journal of Soil Science, 48(2), 301-310.

Kaiser, K. and Guggenberger, G. (2000). The role of DOM sorption to mineral surfaces in the preservation of organic matter in soils. Organic geochemistry, 31(7-8), 711-725.

Kaiser, K., Guggenberger, G. and Zech, W. (2001). Isotopic fractionation of dissolved organic carbon in shallow forest soils as affected by sorption. European Journal of Soil Science, 52(4), 585-597.

Kaiser, K. and Guggenberger, G. (2003). Mineral surfaces and soil organic matter. European Journal of Soil Science, 54(2), 219-236.

Kaiser, M. and Asefaw Berhe, A. (2014). How does sonication affect the mineral and organic constituents of soil aggregates? —A review. Journal of Plant Nutrition and Soil Science, 177(4), 479-495.

Kaiser, M., Berhe, A. A., Sommer, M. and Kleber, M. (2012). Application of ultrasound to disperse soil aggregates of high mechanical stability. Journal of Plant Nutrition and Soil Science, 175(4), 521-526.

Kaiser, M., Ghezzehei, T. A., Kleber, M., Myrold, D. D. and Berhe, A. A. (2014). Influence of calcium carbonate and charcoal applications on organic matter storage in silt-sized aggregates formed during a microcosm experiment. Soil Science Society of America Journal, 78(5), 1624-1631.

Kalbitz, K., Schwesig, D., Rethemeyer, J. and Matzner, E. (2005). Stabilization of dissolved organic matter by sorption to the mineral soil. Soil Biology and Biochemistry, 37(7), 1319-1331.

Keiluweit, M., Bougoure, J. J., Nico, P. S., Pett-Ridge, J., Weber, P. K., & Kleber, M. (2015). Mineral protection of soil carbon counteracted by root exudates. Nature Climate Change, 5(6), 588.

Kleber, M., Sollins, P. and Sutton, R. (2007). A conceptual model of organo-mineral interactions in soils: self-assembly of organic molecular fragments into zonal structures on mineral surfaces. Biogeochemistry, 85(1), 9-24.

Kleber, M., Eusterhues, K., Keiluweit, M., Mikutta, C., Mikutta, R. and Nico, P. S. (2015). Mineral–organic associations: formation, properties, and relevance in soil environments. In Advances in agronomy (Vol. 130, pp. 1-140). Academic Press.

McCarthy, J. F., Ilavsky, J., Jastrow, J. D., Mayer, L. M., Perfect, E. and Zhuang, J. (2008). Protection of organic carbon in soil microaggregates via restructuring of aggregate porosity and filling of pores with accumulating organic matter. Geochimica et Cosmochimica Acta, 72(19), 4725-4744.

McKnight, D. M., Bencala, K. E., Zellweger, G. W., Aiken, G. R., Feder, G. L. and Thorn, K. A. (1992). Sorption of dissolved organic carbon by hydrous aluminum and iron oxides occurring at the confluence of Deer Creek with the Snake River, Summit County, Colorado. Environmental science & technology, 26(7), 1388-1396.

Mikutta, R., Mikutta, C., Kalbitz, K., Scheel, T., Kaiser, K. and Jahn, R. (2007). Biodegradation of forest floor organic matter bound to minerals via different binding mechanisms. Geochimica et Cosmochimica Acta, 71(10), 2569-2590.

Moni, C., Rumpel, C., Virto, I., Chabbi, A. and Chenu, C. (2010). Relative importance of sorption versus aggregation for organic matter storage in subsoil horizons of two contrasting soils. European Journal of Soil Science, 61(6), 958-969.

Oren, A. and Chefetz, B. (2012). Sorptive and desorptive fractionation of dissolved organic matter by mineral soil matrices. Journal of Environmental Quality, 41(2), 526-533.

Rowley, M. C., Grand, S. and Verrecchia, É. P. (2018). Calcium-mediated stabilisation of soil organic carbon. Biogeochemistry, 137(1-2), 27-49.

Rumpel, C., Eusterhues, K. and Kögel-Knabner, I. (2004). Location and chemical composition of stabilized organic carbon in topsoil and subsoil horizons of two acid forest soils. Soil Biology and Biochemistry, 36(1), 177-190.

Ryals, R., Kaiser, M., Torn, M. S., Berhe, A. A. and Silver, W. L. (2014). Impacts of organic matter amendments on carbon and nitrogen dynamics in grassland soils. Soil Biology and Biochemistry, 68, 52-61.

Saidy, A. R., Smernik, R. J., Baldock, J. A., Kaiser, K. and Sanderman, J. (2013). The sorption of organic carbon onto differing clay minerals in the presence and absence of hydrous iron oxide. Geoderma, 209, 15-21.

Schmidt, M. W. I., Rumpel, C. and Kögel-Knabner, I. (1999). Evaluation of an ultrasonic dispersion procedure to isolate primary organomineral complexes from soils. European Journal of Soil Science, 50(1), 87-94.

Tombacz, E., Libor, Z., Illes, E., Majzik, A. and Klumpp, E. (2004). The role of reactive surface sites and complexation by humic acids in the interaction of clay mineral and iron oxide particles. Organic Geochemistry, 35(3), 257-267.

Totsche, K. U., Amelung, W., Gerzabek, M. H., Guggenberger, G., Klumpp, E., Knief, C., Lehndorff, E., Mikutta, R., Peth, S., Prechtel, A., Ray, N. and Kogel-Knabner, I. (2018). Microaggregates in soils. Journal of Plant Nutrition and Soil Science, 181(1), 104-136.

Wang, K. and Xing, B. (2005). Structural and sorption characteristics of adsorbed humic acid on clay minerals. Journal of Environmental Quality, 34(1), 342-349.

Wissing, L., Kölbl, A., Schad, P., Bräuer, T., Cao, Z. H. and Kögel-Knabner, I. (2014). Organic carbon accumulation on soil mineral surfaces in paddy soils derived from tidal wetlands. Geoderma, 228, 90-103.

Zhao, Q., Poulson, S. R., Obrist, D., Sumaila, S., Dynes, J. J., McBeth, J. M. and Yang, Y. (2016). Iron-bound organic carbon in forest soils: quantification and characterization.

TABLES

Table 4-1. Type and percentage of sand-, silt-, and clay-sized components used to create artificial soils. Proportions were adapted from Kaiser et al. (2014).

Soil compartment		$AS_{1\%}$	AS_{NA}
Sand-sized (wt%)		**64/total soil**	**65/total soil**
	course > 500um	35/total sand	35/total sand
	medium >250um	55/total sand	55/total sand
	fine <250 and >53um	10/total sand	10/total sand
Silt-sized (wt%)		**20/total soil**	**20/total soil**
	Silt-sized sand	100/total silt	100/total silt
Clay-sized (wt%)		**15/total soil**	**15/total soil**
	Al-oxides	3.2/total clay	3.2/total clay
	Kaolinite	60/total clay	60/total clay
	Montmorillionite	36.8/total clay	36.8/total clay
Fe oxide (wt%)		**1/total soil**	**0/total soil**
	Fe oxides	100/total Fe	0/total Fe

Table 4-2. Amount and percent of C sorbed after (de)sorption period in artificial and SOM-free natural soils applied with Musick and Sirretta water extractable organic matter (WEOM).

Treatment	C sorbed at equilibrium after sorption[a]	% C sorbed after sorption	C sorbed at equilibrium after desorption without sonication[a]	% C sorbed after desorption without sonication	C sorbed at equilibrium after sorption with sonication[a]	% C sorbed after desorption with sonication
Musick						
$AS_{1\%}$	756.74±6.66	47.56	739.15±0.20	97.68	757.12±0.25	100.05
AS_{NA}	729.60±11.99	45.85	672.27±0.03	92.14	699.60±28.35	95.89
NS_A	1056.28±73.03	60.23	1044.94±0.20	98.93	1108.86±0.56	104.98
NS_B	957.72±35.50	59.39	916.49±0.36	95.69	n/a	n/a
Sirretta						
$AS_{1\%}$	143.82±0.88	59.56	135.30±0.30	94.07	146.96±0.28	102.18
AS_{NA}	131.79±4.38	54.58	122.45±0.01	92.91	129.85±0.10	98.52
NS_A	196.48±10.66	80.43	192.23±0.15	97.86	198.64±0.04	101.10
NS_B	216.48±0.34	87.86	214.02±0.02	98.86	212.59±0.10	98.20

FIGURES

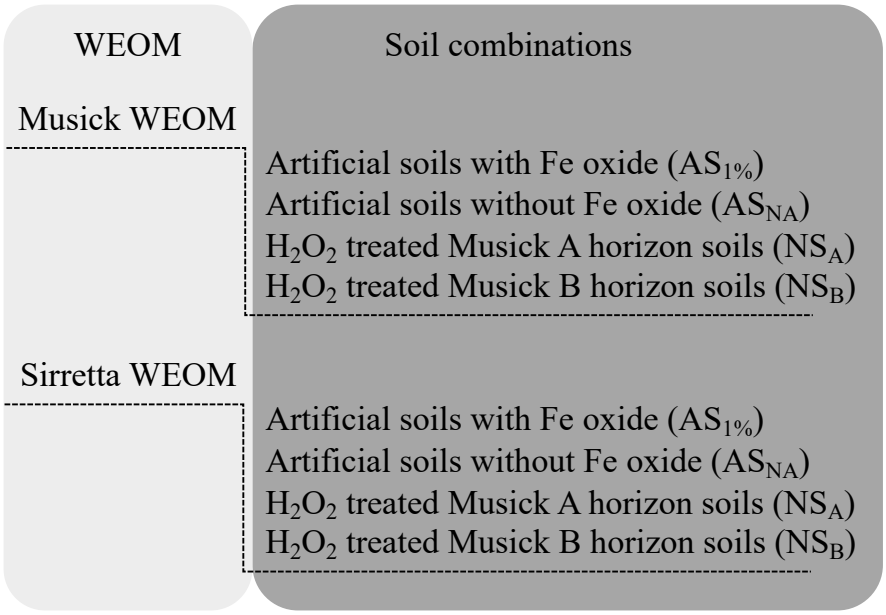

Figure 4-1. Experimental design showing Musick or Sirretta WEOM (light grey) applied to soils with four combinations (dark grey) in this study.

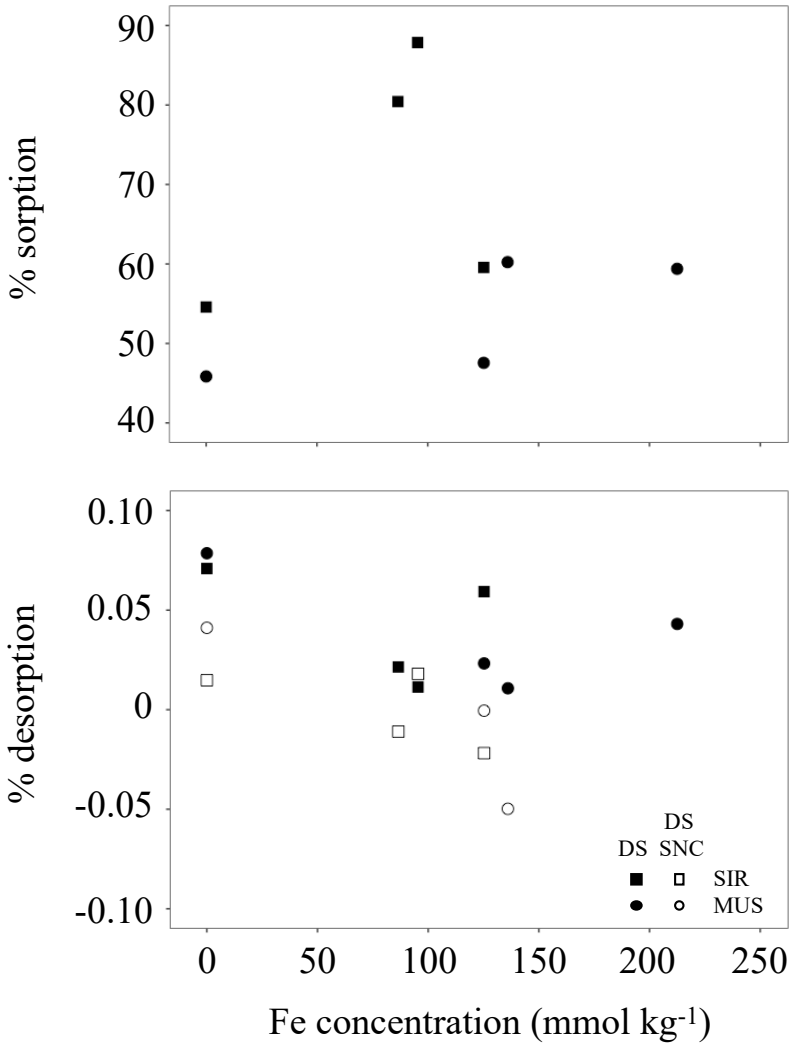

Figure 4-2. Comparisons of percent of sorbed C (top) and desorbed C (bottom) with Fe concentration. Circles indicate soil samples applied with Musick WEOM, while squares indicate soil samples applied with Sirretta WEOM. Open circles/squares in the bottom plot indicates the soil samples with sonication treatment, while closed circles/square indicates the soil samples without sonication treatment.

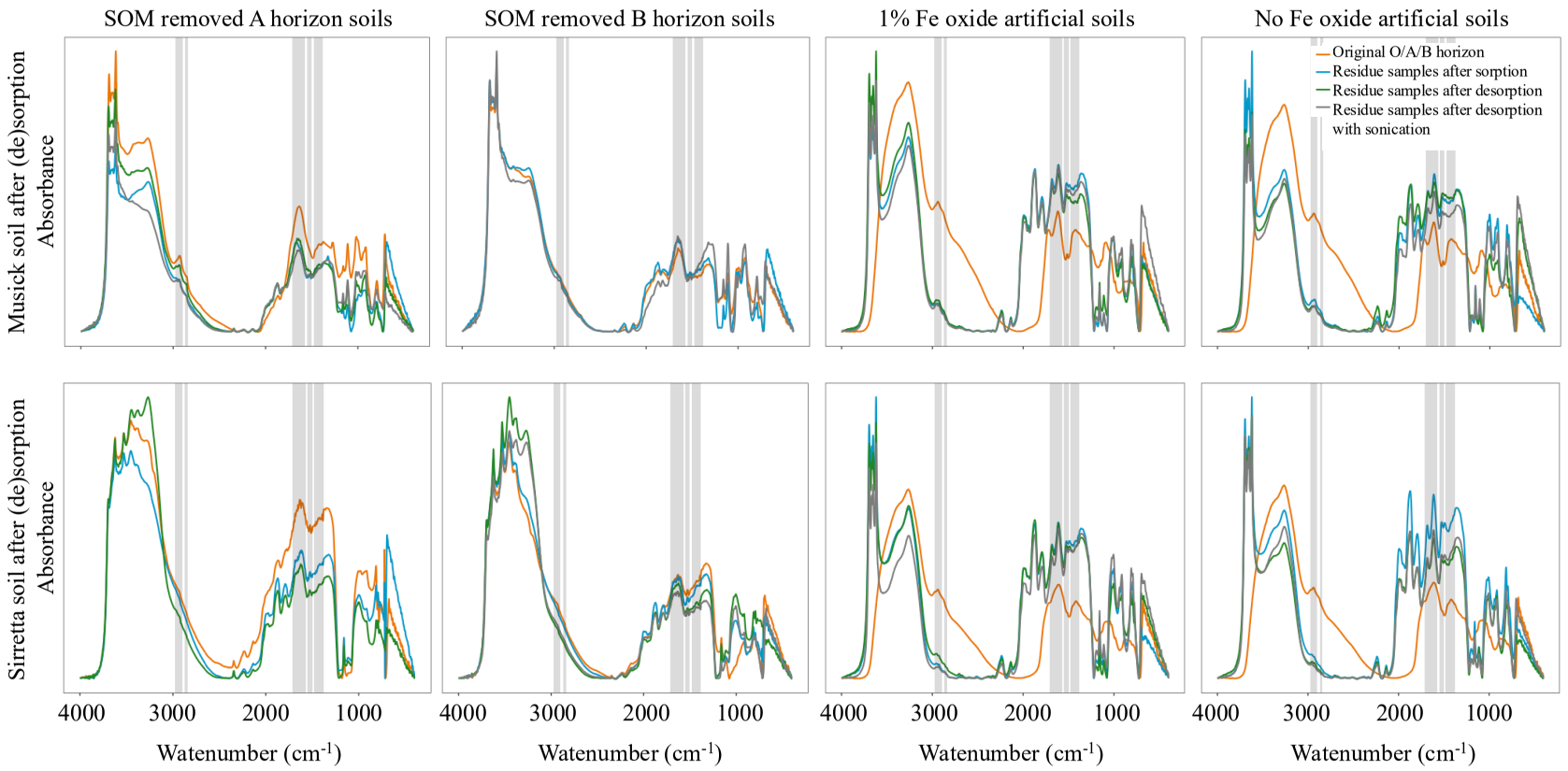

Figure 4-3. FTIR spectra of artificial and SOM-free natural soils applied with Musick (top) and Sirretta (bottom) WEOM.

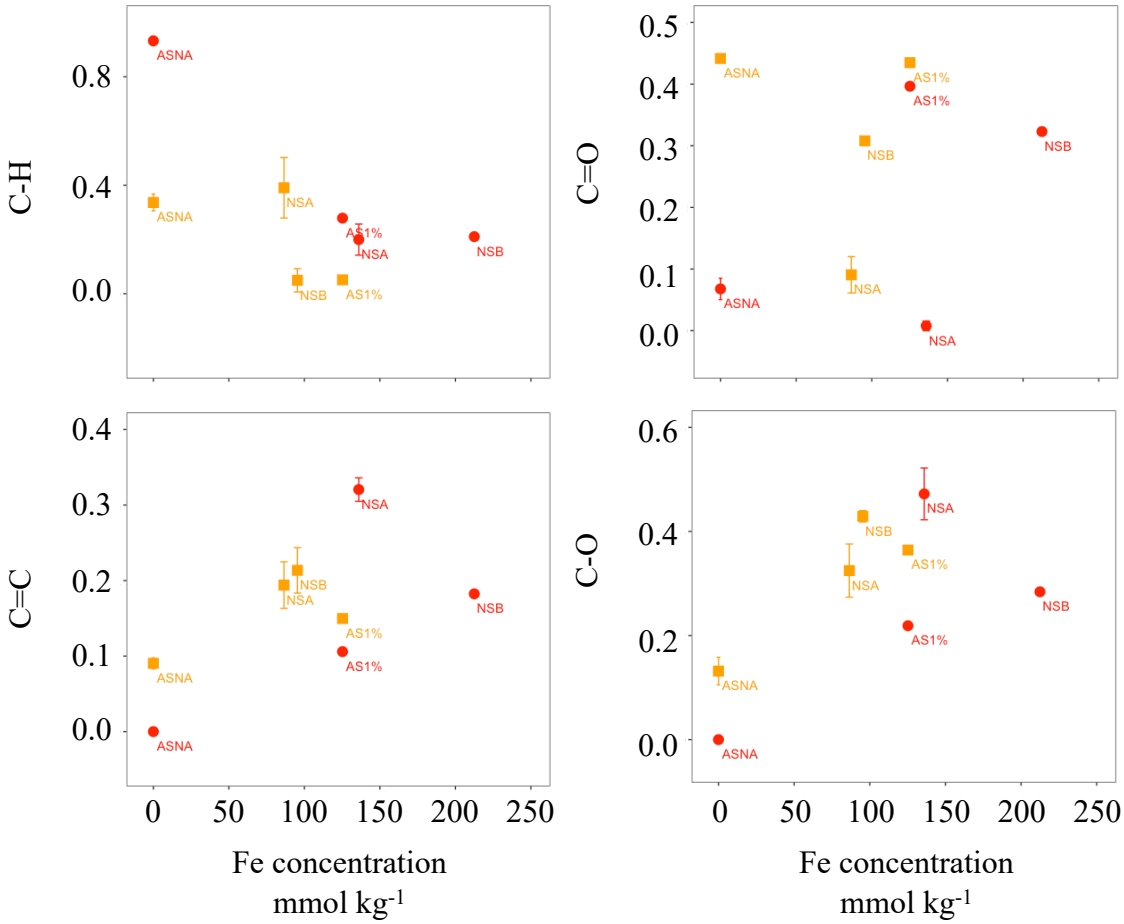

Figure 4-4. Correlations between relative peak areas of C functional groups and Fe concentrations in artificial soils with or without Fe oxides ($AS_{1\%}$ and AS_{NA}) and H_2O_2 treated natural soils (NS_A and NS_B).

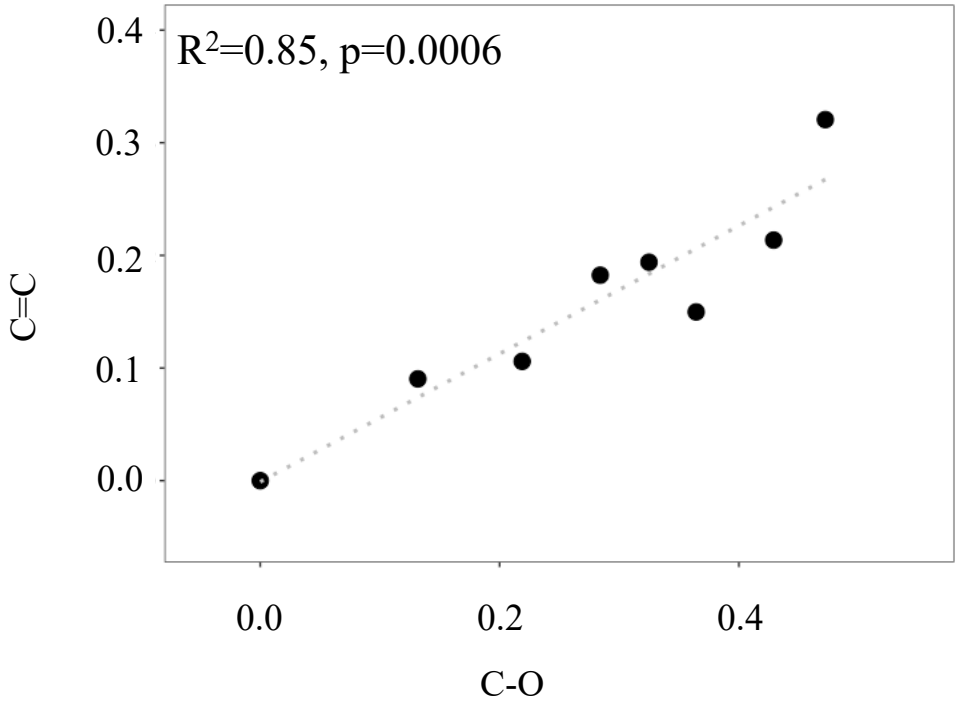

Figure 4-5. Correlations between peak areas of aromatic C=C and carboxyl C-O regardless of soil types and WEOM source during (de)sorption.

CHAPTER 5. CONCLUSION

Strong relationships between pedogenic Fe oxides and soil C storage are often found in different natural soil systems (Dahlgren et al., 1997; Kaiser et al., 1997; Torn et al., 1997; Eusterhues et al., 2003; Lilienfein et al., 2003; Wagai and Mayer, 2007; Mikutta et al., 2006 and 2009; Moni et al., 2010; Sollins et al., 2009; Berhe et al., 2012; Lalonde et al., 2012; Wagai et al., 2013; Feng et al., 2014; Zhao et al., 2016; Coward et al., 2018a and 2018b; Hall et al., 2018; Heckman et al., 2018; Jin et al., chapter 2). However, questions remain as to what extend the relationship between pedogenic Fe oxides and soil C storage can be generalized in global scale, or how Fe oxide distribution in the soil profile responds to long-term processes of soil development and/or short-term exposure to changes in environmental conditions. Thus, in my dissertation Chapter 1, I gathered data from related works conducted in the last 20 years to reveal the general relationships between pedogenic Fe oxides and soil development, and implications for soil C storage in variety of environments globally. My results show that measured total pedogenic Fe concentration ranged from 4 g kg^{-1} in least weathered soils to 155 g kg^{-1} in most weathered soils. Poorly crystalline Fe oxides relative to total pedogenic Fe decreased from 0.65 in least weathered soils to 0.08 in most weathered soils. A strong correlation between Fe oxide crystallinity and total pedogenic Fe concentrations suggests that Fe oxide concentration and its crystallinity reflect soil weathering intensity and affect soil development, where Fe oxide crystallinity increased with soil development. Poorly crystalline Fe oxide concentrations increased with increasing soil C content in soils, which may suggest that poorly crystalline Fe oxides may play an important role in soil C storage in soil systems (Figure 5-1).

While pedogenic Fe oxides play very important roles in persistence of SOM (Torn et al., 1997; Kalbitz et al., 2000; Eusterhues et al., 2005; Wagai and Mayer, et al., 2007; Moni et al., 2010; Eglinton, 2012; Lalonde et al., 2012; Wissing et al., 2014; Porras et al., 2017; Heckman et al., 2018), typically physical (aggregation, occlusion) vs. chemical (sorptive interactions) mechanisms of SOM storage and stability tend to be analyzed in isolation. Most available studies don't consider how SOM storage and stability are highly influenced by soil structures, i.e. extent, size, and stability of soil aggregates, and how pedogenic Fe oxides may regulate the formation and stability of soil aggregates (Cornell and Schwertmann, 2003; Kleber et al., 2015). Here I present data to show that concentration of pedogenic Fe oxides and amount of physically occluded SOM (aggregate protected SOM) are closely related.

Recent studies have shown that crystallinity of Fe oxides influences soil C storage and their relative abundance may regulate SOM sequestration and stabilization (Coward et al., 2017 and 2018; Hall et al., 2018; Heckman et al., 2018). However, there has been no extensive studies so far on how the relative contribution of different Fe pools (i.e. organically associated, poorly crystalline, and crystalline Fe) is related to C distribution and sequestration in soil aggregates. Therefore, we determined the association of Fe in different extractable pools of soil with C in distinct aggregate size classes along depth profiles in an Alfisol from the Sierra Nevada in California (Musick

soil series) using a sequential Fe dissolution extraction approach in Chapter 2. Results showed that Fe oxides with varying crystallinity may have different capacity to preserve SOM. Poorly crystalline Fe oxides preferentially reside in larger aggregate size fractions, whereas organically associated Fe may prefer smaller aggregate size fractions. Concentrations of crystalline Fe oxides and organically associated Fe were closely correlated to C in corresponding pools. Organically associated Fe concentration increased as soil C content increased, whereas well crystalline Fe oxide concentration decreased with increasing soil C content (Figure 5-1). These findings suggest that Fe oxides crystallinity plays important role in soil C storage in soils.

To further understand the selective stabilization of soil C functional groups on Fe oxides with varying crystallinity, we determined the relationship of pedogenic Fe oxide crystallinity on the chemical compositions and the stability of SOC that is physically protected in soil aggregates in Chapter 3. The findings suggest that organically associated Fe may contribute to the abundance of aliphatic C in organically associated mineral fraction, whereas poorly crystalline and crystalline Fe oxides may contribute to the abundance of aromatic and carboxyl C in the Fe oxide containing fractions. The extent of processing C was higher as relative Fe oxide crystallinity increased. Our findings suggest that preferential association of different organic functional groups with pedogenic Fe-containing mineral fractions may play an important role in composition of OM preserved in soils.

Finally, we evaluated the effects of Fe oxides on stabilization (sorption) and destabilization (desorption) of SOM to understand how Fe oxides affect the C (de)sorption capacity and selective stabilization of C functional groups in general in western Sierra Nevada soils in Chapter 4. Our results showed that C sorption capacity was higher with increasing Fe oxide concentrations. Fe oxide selectively stabilized carboxyl C-O and aromatic C=C, whereas aliphatic C-H was selectively remained in solutions (Figure 5-1). Only small proportion of the OM associated with Fe-oxide mixtures was released by breaking soil macro and microaggregates with ultrasonication energy suggesting that the SOM may be chemically sorbed to reactive mineral surfaces in associations that are not likely to be broken by application of ultrasonic energy.

Therefore, in my dissertation, I have shown the important role of Fe oxides on soil C storage, distribution, and composition, and found that Fe oxide crystallinity may strongly affect soil C storage with selective stabilization of carboxyl and aromatic C with increasing Fe oxide concentration. My results contribute to the growing body of literature that is highlighting the role of Fe oxides soil C storage and stabilization in systems at varying stages of soil development (weathering environments) globally.

REFERENCES

Berhe, A. A., Harden, J. W., Torn, M. S., Kleber, M., Burton, S. D. and Harte, J. (2012). Persistence of soil organic matter in eroding versus depositional landform positions. Journal of Geophysical Research: Biogeosciences, 117(G2).

Cornell, R. M. and Schwertmann, U. (2003). The iron oxides: structure, properties, reactions, occurrences and uses. John Wiley & Sons.

Coward, E. K., Thompson, A. T. and Plante, A. F. (2017). Iron-mediated mineralogical control of organic matter accumulation in tropical soils. Geoderma, 306, 206-216.

Coward, E. K., Ohno, T. and Plante, A. F. (2018). Adsorption and molecular fractionation of dissolved organic matter on iron-bearing mineral matrices of varying crystallinity. Environmental science & technology, 52(3), 1036-1044.

Coward, E. K., Thompson, A. and Plante, A. F. (2018). Contrasting Fe speciation in two humid forest soils: Insight into organomineral associations in redox-active environments. Geochimica et Cosmochimica Acta, 238, 68-84.

Dahlgren, R. A., Boettinger, J. L., Huntington, G. L. and Amundson, R. G. (1997). Soil development along an elevational transect in the western Sierra Nevada, California. Geoderma, 78(3-4), 207-236.

Eglinton, T. I. (2012). Geochemistry: A rusty carbon sink. Nature, 483(7388), 165.

Eusterhues, K., Rumpel, C., Kleber, M. and Kögel-Knabner, I. (2003). Stabilisation of soil organic matter by interactions with minerals as revealed by mineral dissolution and oxidative degradation. Organic Geochemistry, 34(12), 1591-1600.

Eusterhues, K., Rumpel, C. and Kögel-Knabner, I. (2005). Organo-mineral associations in sandy acid forest soils: importance of specific surface area, iron oxides and micropores. European Journal of Soil Science, 56(6), 753-763.

Feng, W., Plante, A. F., Aufdenkampe, A. K. and Six, J. (2014). Soil organic matter stability in organo-mineral complexes as a function of increasing C loading. Soil Biology and Biochemistry, 69, 398-405.

Hall, S. J., Berhe, A. A. and Thompson, A. (2018). Order from disorder: do soil organic matter composition and turnover co-vary with iron phase crystallinity? Biogeochemistry, 140(1), 93-110.

Heckman, K., Lawrence, C. R. and Harden, J. W. (2018). A sequential selective dissolution method to quantify storage and stability of organic carbon associated with Al and Fe hydroxide phases. Geoderma, 312, 24-35.

Jin, L., O'Day, P. and Berhe, A.A. Role of iron oxides on physical protection of soil organic matter inside aggregates. In preparation.

Kaiser, K., Guggenberger, G., Haumaier, L. and Zech, W. (1997). Dissolved organic matter sorption on sub soils and minerals studied by 13C-NMR and DRIFT spectroscopy. European Journal of Soil Science, 48(2), 301-310.

Kalbitz, K., Solinger, S., Park, J. H., Michalzik, B. and Matzner, E. (2000). Controls on the dynamics of dissolved organic matter in soils: a review. Soil science, 165(4), 277-304.

Kleber, M., Eusterhues, K., Keiluweit, M., Mikutta, C., Mikutta, R. and Nico, P. S. (2015). Mineral–organic associations: formation, properties, and relevance in soil environments. In Advances in agronomy (Vol. 130, pp. 1-140). Academic Press.

Lalonde, K., Mucci, A., Ouellet, A. and Gélinas, Y. (2012). Preservation of organic matter in sediments promoted by iron. Nature, 483(7388), 198.

Lilienfein, J., Qualls, R. G., Uselman, S. M. and Bridgham, S. D. (2003). Soil formation and organic matter accretion in a young andesitic chronosequence at Mt. Shasta, California. Geoderma, 116(3-4), 249-264.

Mikutta, R., Kleber, M., Torn, M. S. and Jahn, R. (2006). Stabilization of soil organic matter: association with minerals or chemical recalcitrance?. Biogeochemistry, 77(1), 25-56.

Mikutta, R., Schaumann, G. E., Gildemeister, D., Bonneville, S., Kramer, M. G., Chorover, J., Chadwick, O.A. and Guggenberger, G. (2009). Biogeochemistry of mineral–organic associations across a long-term mineralogical soil gradient (0.3–4100 kyr), Hawaiian Islands. Geochimica et Cosmochimica Acta, 73(7), 2034-2060.

Moni, C., Rumpel, C., Virto, I., Chabbi, A. and Chenu, C. (2010). Relative importance of sorption versus aggregation for organic matter storage in subsoil horizons of two contrasting soils. European Journal of Soil Science, 61(6), 958-969.

Porras, R. C., Pries, C. E. H., McFarlane, K. J., Hanson, P. J. and Torn, M. S. (2017). Association with pedogenic iron and aluminum: effects on soil organic carbon storage and stability in four temperate forest soils. Biogeochemistry, 133(3), 333-345.

Sollins, P., Kramer, M. G., Swanston, C., Lajtha, K., Filley, T., Aufdenkampe, A. K., Wagai, R. and Bowden, R. D. (2009). Sequential density fractionation across soils of contrasting mineralogy: evidence for both microbial-and mineral-controlled soil organic matter stabilization. Biogeochemistry, 96(1-3), 209-231.

Torn, M. S., Trumbore, S. E., Chadwick, O. A., Vitousek, P. M. and Hendricks, D. M. (1997). Mineral control of soil organic carbon storage and turnover. Nature, 389(6647), 170.

Wagai, R. and Mayer, L. M. (2007). Sorptive stabilization of organic matter in soils by hydrous iron oxides. Geochimica et Cosmochimica Acta, 71(1), 25-35.

Wagai, R., Kishimoto-Mo, A. W., Yonemura, S., Shirato, Y., Hiradate, S. and Yagasaki, Y. (2013). Linking temperature sensitivity of soil organic matter decomposition to its molecular structure, accessibility, and microbial physiology. Global Change Biology, 19(4), 1114-1125.

Wissing, L., Kölbl, A., Schad, P., Bräuer, T., Cao, Z. H. and Kögel-Knabner, I. (2014). Organic carbon accumulation on soil mineral surfaces in paddy soils derived from tidal wetlands. Geoderma, 228, 90-103.

Zhao, Q., Poulson, S. R., Obrist, D., Sumaila, S., Dynes, J. J., McBeth, J. M. and Yang, Y. (2016). Iron-bound organic carbon in forest soils: quantification and characterization.

FIGURE

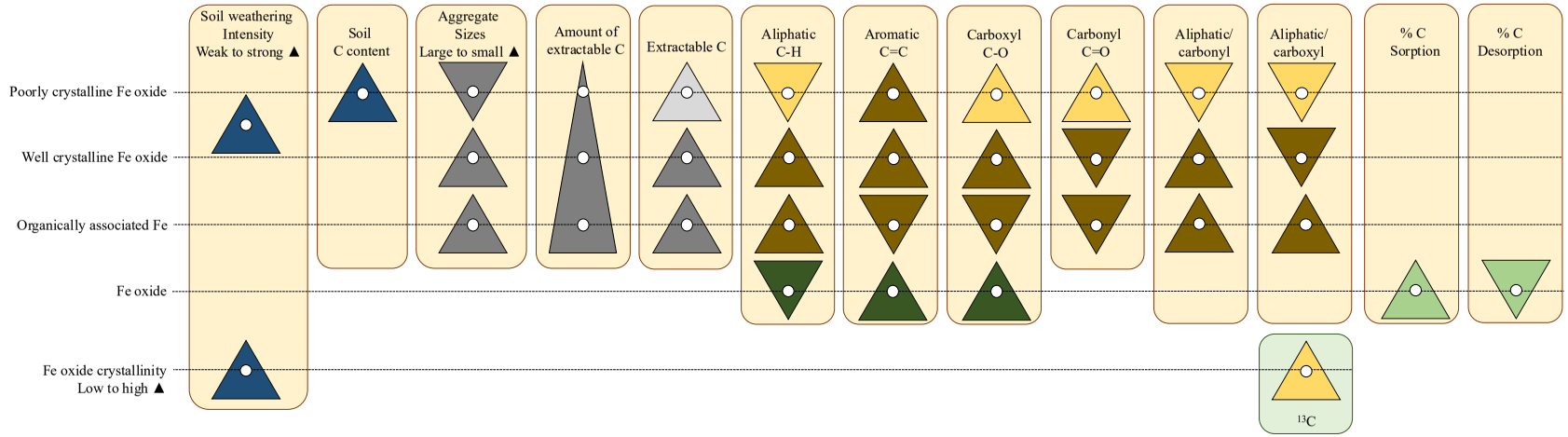

Figure 5-1. Summary of major relationships found in this thesis. Blue colored triangles indicate the findings from Chapter 1, Grey colored triangles indicate the findings from Chapter 2, Brown colored triangles indicate the findings from Chapter 3, and Green colored triangles indicate the findings from Chapter 4. Lighter grey, lighter brown, or lighter green (corresponding to the relationship between Fe oxide crystallinity and %C desorption) indicate the statistically insignificant relationships.

APPENDICES

TABLES

Table S1-1. Fe oxide data collected from previous studies that were used to analysis in this review.

Soil type	Detailed soil description	Soil horizon	Soil horizon unifed	Fed concentration in g kg^{-1}	Feo concentration in g kg^{-1}	C concentration in g kg^{-1}	Reference
Mollisol/Alfisol	Haplic Luvisol	L	A	6.34	3.20	16.10	Moni et al., 2010
Mollisol/Alfisol	Haplic Luvisol	E1g	E	6.29	2.51	6.40	Moni et al., 2010
Mollisol/Alfisol	Haplic Luvisol	E2g	E	6.11	2.11	3.90	Moni et al., 2010
Mollisol/Alfisol	Haplic Luvisol	EB	B	6.67	1.75	3.40	Moni et al., 2010
Mollisol/Alfisol	Haplic Luvisol	Bt	B	10.20	3.35	1.80	Moni et al., 2010
Mollisol/Alfisol	Plinthic Cambisol	L	A	23.12	2.59	9.40	Moni et al., 2010
Mollisol/Alfisol	Plinthic Cambisol	S	B	32.18	2.71	4.00	Moni et al., 2010
Mollisol/Alfisol	Plinthic Cambisol	S2	B	56.79	1.71	2.70	Moni et al., 2010
Mollisol/Alfisol	Plinthic Cambisol	C1	C	58.43	1.60	2.30	Moni et al., 2010
Mollisol/Alfisol	Plinthic Cambisol	C2	C	71.77	1.82	1.50	Moni et al., 2010
Inceptisol	Entic Cryumbrept	A1	A	2.30	2.00	30.40	Dahlgren et al., 1997
Inceptisol	Entic Cryumbrept	A2	A	2.70	2.00	30.40	Dahlgren et al., 1997
Inceptisol	Entic Cryumbrept	A3	A	2.90	1.80	n.a.	Dahlgren et al., 1997
Inceptisol	Entic Cryumbrept	A4	A	2.90	2.10	n.a.	Dahlgren et al., 1997
Inceptisol	Entic Cryumbrept	Bw	B	2.30	1.80	n.a.	Dahlgren et al., 1997
Inceptisol	Entic Cryumbrept	BC	B	2.20	1.40	n.a.	Dahlgren et al., 1997
Entisol	Dystric Xerothent	A1	A	4.60	3.90	32.40	Dahlgren et al., 1997
Entisol	Dystric Xerothent	A2	A	4.90	3.90	32.40	Dahlgren et al., 1997
Entisol	Dystric Xerothent	A3	A	5.00	4.20	n.a.	Dahlgren et al., 1997
Entisol	Dystric Xerothent	Bw1	B	4.10	3.30	n.a.	Dahlgren et al., 1997
Entisol	Dystric Xerothent	Bw2	B	4.40	2.70	n.a.	Dahlgren et al., 1997

Entisol	Dystric Xerothent	Bw3	B	7.50	1.50	n.a.	Dahlgren et al., 1997
Entisol	Dystric Xerothent	CB	C	5.40	1.20	n.a.	Dahlgren et al., 1997
Entisol	Dystric Xerothent	Cr	C	2.20	0.90	n.a.	Dahlgren et al., 1997
Entisol	Pachic Xerumbrept	A1	A	4.20	2.70	29.40	Dahlgren et al., 1997
Entisol	Pachic Xerumbrept	A2	A	4.40	2.80	29.40	Dahlgren et al., 1997
Entisol	Pachic Xerumbrept	A3	A	4.30	2.60	n.a.	Dahlgren et al., 1997
Entisol	Pachic Xerumbrept	A4	A	4.60	2.60	n.a.	Dahlgren et al., 1997
Entisol	Pachic Xerumbrept	Bw1	B	4.30	2.60	n.a.	Dahlgren et al., 1997
Entisol	Pachic Xerumbrept	Bw2	B	3.60	1.80	n.a.	Dahlgren et al., 1997
Entisol	Pachic Xerumbrept	Cr	C	3.70	1.40	n.a.	Dahlgren et al., 1997
Alfisol	Ultic Hapioxeralf	AE	A	7.60	1.00	31.50	Dahlgren et al., 1997
Alfisol	Ultic Hapioxeralf	EBt	B	9.30	0.80	8.13	Dahlgren et al., 1997
Alfisol	Ultic Hapioxeralf	Bt1	B	14.40	0.80	5.17	Dahlgren et al., 1997
Alfisol	Ultic Hapioxeralf	Bt2	B	11.90	0.80	3.75	Dahlgren et al., 1997
Alfisol	Ultic Hapioxeralf	BCt1	C	10.30	0.90	n.a.	Dahlgren et al., 1997
Alfisol	Ultic Hapioxeralf	BCt2	C	7.00	0.60	n.a.	Dahlgren et al., 1997
Alfisol	Ultic Hapioxeralf	A1	A	6.50	0.80	10.10	Dahlgren et al., 1997
Alfisol	Ultic Hapioxeralf	A2	A	8.40	0.70	10.10	Dahlgren et al., 1997
Alfisol	Ultic Hapioxeralf	BAt	B	8.50	0.60	n.a.	Dahlgren et al., 1997

Alfisol	Ultic Hapioxeralf	Bt1	B	5.20	0.60	n.a.	Dahlgren et al., 1997
Alfisol	Ultic Hapioxeralf	Bt2	B	4.20	0.50	n.a.	Dahlgren et al., 1997
Alfisol	Ultic Hapioxeralf	BC	C	3.90	0.60	n.a.	Dahlgren et al., 1997
Alfisol	Ultic Hapioxeralf	A1	A	5.60	0.70	11.80	Dahlgren et al., 1997
Alfisol	Ultic Hapioxeralf	A2	A	6.40	0.70	11.80	Dahlgren et al., 1997
Alfisol	Ultic Hapioxeralf	BAt	B	5.90	0.60	n.a.	Dahlgren et al., 1997
Alfisol	Ultic Hapioxeralf	Bt	B	5.20	0.50	n.a.	Dahlgren et al., 1997
Alfisol	Ultic Hapioxeralf	Cr	C	3.90	0.60	n.a.	Dahlgren et al., 1997
Inceptisol	Typic Xerochrept	A	A	4.30	0.60	17.80	Dahlgren et al., 1997
Inceptisol	Typic Xerochrept	Bw1	B	4.60	0.70	17.80	Dahlgren et al., 1997
Inceptisol	Typic Xerochrept	Bw2	B	5.30	0.70	n.a.	Dahlgren et al., 1997
Inceptisol	Typic Xerochrept	Bt	B	5.20	0.60	n.a.	Dahlgren et al., 1997
Oxisol	ridge	na	A	51.80	8.80	49.00	Hall et al., 2018
Oxisol	ridge	na	A	55.80	7.90	30.00	Hall et al., 2018
Oxisol	slope	na	A	46.60	9.50	33.00	Hall et al., 2018
Oxisol	slope	na	A	53.50	8.00	22.00	Hall et al., 2018
Oxisol	valley	na	A	35.60	9.20	34.00	Hall et al., 2018
Oxisol	valley	na	A	39.40	9.50	27.00	Hall et al., 2018
Ultisol	Edgemont	na	B	23.80	n.a.	n.a.	Feng et al., 2014
Mollisol	Drummer	na	B	45.00	n.a.	n.a.	Feng et al., 2014
Alfisol	San Ysidro	na	B	11.40	n.a.	n.a.	Feng et al., 2014
Ultisol	Towaliga	na	A	21.90	n.a.	n.a.	Feng et al., 2014
Spodosol	GS	na	A	0.08	n.a.	12.00	Zhao et al., 2016
Ultisol	OR	na	A	1.60	n.a.	23.10	Zhao et al., 2016
Alfisol	AL	na	A	4.87	n.a.	35.50	Zhao et al., 2016
Entisol	LVF	na	A	2.11	n.a.	13.60	Zhao et al., 2016

Entisol	LV	na	A	0.99	n.a.	10.70	Zhao et al., 2016
Mollisol	MS	na	A	19.31	n.a.	30.10	Zhao et al., 2016
Alfisol	TKF	na	A	1.85	n.a.	27.60	Zhao et al., 2016
Alfisol	TK	na	A	2.28	n.a.	54.00	Zhao et al., 2016
Alfisol	NR	na	A	1.27	n.a.	28.30	Zhao et al., 2016
Spodosol	HT	na	A	2.69	n.a.	30.00	Zhao et al., 2016
Spodosol	BL	na	A	4.13	n.a.	28.30	Zhao et al., 2016
Spodosol	HL	na	A	5.24	n.a.	33.40	Zhao et al., 2016
Inceptisol	TSI	na	A	6.20	n.a.	43.00	Zhao et al., 2016
Inceptisol	TSII	na	A	6.87	n.a.	60.50	Zhao et al., 2016
Oxisol		na	A	33.50	n.a.	n.a.	Coward et al., 2018_EST
Oxisol		na	A	45.10	n.a.	n.a.	Coward et al., 2018_GCA
Inceptisol		na	A	9.50	n.a.	n.a.	Coward et al., 2018_GCA
Inceptisol	Oxyaquic Eutrochrept	2Bw	B	29.20	12.90	7.00	Kaiser et al., 1997
Inceptisol	Typic Dystrochrept	Bw	B	35.10	16.80	22.00	Kaiser et al., 1997
A/M/S	dystric cambisol	A	A	1.40	1.30	82.60	Eusterhues et al., 2003
A/M/S	dystric cambisol	Bw1	B	2.70	1.60	9.80	Eusterhues et al., 2003
A/M/S	dystric cambisol	Bw2	B	1.50	0.50	3.00	Eusterhues et al., 2003

A/M/S	dystric cambisol	Bw3	B	1.10	0.60	1.40	Eusterhues et al., 2003
A/M/S	dystric cambisol	3C	C	0.70	0.30	1.10	Eusterhues et al., 2003
A/M/S	dystric cambisol	4C1	C	0.40	0.10	0.50	Eusterhues et al., 2003
A/M/S	haplic podzol	EA	A	1.70	0.60	38.10	Eusterhues et al., 2003
A/M/S	haplic podzol	Bh	B	24.50	3.30	92.80	Eusterhues et al., 2003
A/M/S	haplic podzol	Bs	B	16.40	10.10	52.00	Eusterhues et al., 2003
A/M/S	haplic podzol	Bw	B	6.40	1.60	7.70	Eusterhues et al., 2003
A/M/S	haplic podzol	C1	C	3.70	0.60	1.70	Eusterhues et al., 2003
A/M/S	haplic podzol	C2	C	4.50	0.60	1.90	Eusterhues et al., 2003
Spodosol		A	A	0.50	n.a.	20.50	Heckman et al., 2018
Spodosol		E	E	0.40	n.a.	2.60	Heckman et al., 2018
Spodosol		Bhs	B	1.50	0.60	10.71	Heckman et al., 2018
Spodosol		Bhs	B	0.80	0.50	10.47	Heckman et al., 2018
Forested Mollisol		A	A	20.80	4.00	49.37	Heckman et al., 2018
Forested Mollisol		Bt1	B	23.10	3.50	13.13	Heckman et al., 2018

Forested Mollisol		Bt2	B	25.90	4.30	10.31	Heckman et al., 2018
Forested Mollisol		Bt3	B	26.20	3.70	7.24	Heckman et al., 2018
Grassland Mollisol		A	A	7.10	1.50	24.17	Heckman et al., 2018
Grassland Mollisol		A	A	5.40	1.20	17.70	Heckman et al., 2018
Grassland Mollisol		A	A	5.90	1.00	8.89	Heckman et al., 2018
Grassland Mollisol		AB	B	7.50	0.80	5.36	Heckman et al., 2018
Andisol		Bw1	B	203.10	10.50	109.49	Heckman et al., 2018
Andisol		Bw2	B	200.70	11.80	114.79	Heckman et al., 2018
Andisol		Bw3	B	215.50	15.60	92.05	Heckman et al., 2018
A/M/S	dystric cambisol	Bw	B	23.00	2.20	10.80	Mikutta et al., 2006
A/M/S	haplic luvisol	E	E	12.60	1.00	11.50	Mikutta et al., 2006
A/M/S	haplic luvisol	Bt	B	22.70	1.00	4.90	Mikutta et al., 2006
	humic ferralsol	Bw	B	94.80	1.80	10.00	Mikutta et al., 2006
A/M/S	chromic cambisol	Bw	B	50.30	3.00	19.70	Mikutta et al., 2006
	vitric phaeozem	AB	B	63.90	9.50	38.20	Mikutta et al., 2006
A/M/S	chromic cambisol	Bw	B	52.60	18.70	36.00	Mikutta et al., 2006
A/M/S	haplic podzol	Bhs	B	22.70	9.30	13.80	Mikutta et al., 2006
A/M/S	andic luvisol	Bt	B	46.80	12.50	30.70	Mikutta et al., 2006
A/M/S	andic luvisol	2Bw	B	49.50	9.60	15.70	Mikutta et al., 2006
	umbric andosol	Bw	B	33.50	4.90	27.70	Mikutta et al., 2006

A/M/S	dystric cambisol	Bs	B	38.30	15.70	23.20	Mikutta et al., 2006
Inceptisol	andrew	na	A	12.50	9.30	49.00	Sollins et al., 2009
Oxisols	susua	na	A	204.00	9.80	59.00	Sollins et al., 2009
Alfisol	kellogg	na	A	4.90	3.90	15.00	Sollins et al., 2009
Inceptisol	kinabalu	na	A	7.30	4.70	42.00	Sollins et al., 2009
Ultisol	ult4	A	A	25.00	5.30	27.60	Wagai et al.,2013
Oxisols	ox4	Ac	A	185.00	2.40	29.90	Wagai et al.,2013
Oxisols	ox2	A	A	195.00	9.10	64.70	Wagai et al.,2013
Inceptisol	paddy	A	A	0.00	3.60	17.90	Wagai et al.,2013
Inceptisol	inc6	A	A	9.70	2.90	22.40	Wagai et al.,2013
Alfisol	alf4	A	A	32.00	4.60	43.10	Wagai et al.,2013
Inceptisol	inc5	A	A	25.00	12.00	93.90	Wagai et al.,2013
Inceptisol	inc7	A	A	1.20	0.70	126.00	Wagai et al.,2013
Spodosols	spd2b1	B1	B	23.00	13.00	60.90	Wagai et al.,2013
Spodosols	spd3B1	B1	B	32.00	25.00	86.80	Wagai et al.,2013
Andisol	ando	A	A	142.00	46.00	151.00	Wagai et al.,2013
Inceptisol	inc4	A	A	40.00	16.00	105.00	Wagai et al.,2013
Andisol	andkwt	A	A	0.00	9.50	98.50	Wagai et al.,2013
Andisol	andtkb	Ap	A	0.00	19.00	51.40	Wagai et al.,2013
Andisol	andmyk	2A	A	0.00	18.00	130.00	Wagai et al.,2013
Andisol	andos1	A1	A	0.00	14.00	150.00	Wagai et al.,2013
Andisol	andos2	A2	A	0.00	17.00	121.00	Wagai et al.,2013
Entisol	Hawaii island	A	A	n.a.	n.a.	165.00	Wagai and Mayer, 2007
Inceptisol	Massachusetts	E	E	8.50	n.a.	29.50	Wagai and Mayer, 2007

Inceptisol	Massachusetts	Bw	B	48.00	n.a.	30.30	Wagai and Mayer, 2007
Inceptisol	Massachusetts	Ap	A	n.a.	n.a.	28.90	Wagai and Mayer, 2007
Inceptisol	Washington	A	A	n.a.	n.a.	45.70	Wagai and Mayer, 2007
Inceptisol	Oregon	A	A	n.a.	n.a.	105.00	Wagai and Mayer, 2007
Inceptisol	Kinabalu, Malaysia	A	A	n.a.	n.a.	93.90	Wagai and Mayer, 2007
Inceptisol/Alfisol	Kinabalu, Malaysia	A	A	n.a.	n.a.	22.40	Wagai and Mayer, 2007
Inceptisol	Kinabalu, Malaysia	A	A	n.a.	n.a.	126.00	Wagai and Mayer, 2007
Alfisol	New Jersey	A	A	n.a.	n.a.	79.70	Wagai and Mayer, 2007
Alfisol	New Jersey	Ap	A	n.a.	n.a.	10.10	Wagai and Mayer, 2007
Alfisol	Mississippi	Ap	A	n.a.	n.a.	14.10	Wagai and Mayer, 2007
Alfisol	Kinabalu, Malaysia	A	A	n.a.	n.a.	43.10	Wagai and Mayer, 2007
Mollisol	North Dakota	A	A	n.a.	n.a.	23.80	Wagai and Mayer, 2007
Mollisol	Indiana	Ap	A	n.a.	n.a.	26.30	Wagai and Mayer, 2007

Ultisol	Virginia	Ap	A	n.a.	n.a.	44.80	Wagai and Mayer, 2007
Ultisol	Maryland	Ap	A	n.a.	n.a.	41.60	Wagai and Mayer, 2007
Ultisol	Virginia	Ap	A	n.a.	n.a.	60.90	Wagai and Mayer, 2007
Ultisol	Kinabalu, Malaysia	A	A	25.00	n.a.	27.60	Wagai and Mayer, 2007
Ultisol	Kinabalu, Malaysia	B	B	26.00	n.a.	n.a.	Wagai and Mayer, 2007
Ultisol	Kinabalu, Malaysia	B	B	29.00	n.a.	n.a.	Wagai and Mayer, 2007
Oxisol	Puerto Rico	A	A	176.00	n.a.	66.20	Wagai and Mayer, 2007
Oxisol	Puerto Rico	A	A	176.00	n.a.	64.70	Wagai and Mayer, 2007
Oxisol	Parana, Brazil	A	A	n.a.	n.a.	38.50	Wagai and Mayer, 2007
Oxisol	Kinabalu, Malaysia	Ac	A	185.00	n.a.	29.90	Wagai and Mayer, 2007
Oxisol	Kinabalu, Malaysia		B	212.00	n.a.	n.a.	Wagai and Mayer, 2007
Oxisol	Kinabalu, Malaysia		B	257.00	n.a.	n.a.	Wagai and Mayer, 2007
Spodosol	Massachusetts	E	E	1.50	n.a.	15.70	Wagai and Mayer, 2007

Spodosol	Massachusetts	Bhs	B	23.00	n.a.	72.60	Wagai and Mayer, 2007
Spodosol	Maine	B1	B	23.00	n.a.	60.90	Wagai and Mayer, 2007
Spodosol	Maine	B2	B	21.00	n.a.	39.30	Wagai and Mayer, 2007
Spodosol	Maine	B1	B	32.00	n.a.	86.80	Wagai and Mayer, 2007
Spodosol	Maine	B2	B	20.00	n.a.	92.10	Wagai and Mayer, 2007
Inceptisol	Thurston	A	A	5.00	4.30	18.70	Mikutta et al., 2009
Andisol	Laupahoehoe	A	A	153.60	84.20	177.50	Mikutta et al., 2009
Andisol	Kohala	A	A	46.90	37.40	187.60	Mikutta et al., 2009
	Pololu	A	A	43.70	40.00	290.40	Mikutta et al., 2009
Ultisol	Kolekole	A	A	40.10	15.40	131.10	Mikutta et al., 2009
Oxisols	Kokee	A	A	241.30	4.40	40.00	Mikutta et al., 2009
Inceptisol	Thurston	B	B	11.50	10.70	23.20	Mikutta et al., 2009
Andisol	Laupahoehoe	B	B	100.80	77.90	113.60	Mikutta et al., 2009
Andisol	Kohala	B	B	15.40	16.90	120.60	Mikutta et al., 2009
	Pololu	B	B	124.10	56.60	81.30	Mikutta et al., 2009
Ultisol	Kolekole	B	B	53.30	14.40	19.90	Mikutta et al., 2009
Oxisols	Kokee	B	B	143.90	2.30	12.10	Mikutta et al., 2009

Table S2-1. Summary of iron reference compounds for XAS analysis.

Compound	Source[a]	Data collection mode	Type	Beam line	Crystal	Collection temperature
Hematite (Si-doped)	Syn	Transmission	EXAFS			
Ferrihydrite	Syn	Fluorescence	EXAFS	4-3	Si(220)	Room temp.
Illite (IMt_1)	Nat	Ge	EXAFS	4-1	Si(220)	Liquid nitrogen
		Fluorescence	XANES	4-1	Si(220)	Room temp.
Smectite (SAz_1)	--	Fluorescence	EXAFS	2-3	Si(111)	Room temp.
		Fluorescence	XANES	4-1	Si(220)	Room temp.

[a]Syn: synthetic; Nat: natural

Table S2-2. Concentrations (in mmol kg^{-1}) of selectively extractable (i.e. PP, HH, DH sequential extractions) C calculated from supernatant solutions, C content (in wt%) in untreated soil samples, and C fraction recovered after extraction.

Soil depths	Size fractions	PP extractable C[a]	HH extractable C[a]	DH extractable C[a]	Residual C[b]	Total C[c]	Fraction C recovered[d]
0-29 cm	2000-250 μm	784.86±53.23	86.57±2.28	133.87±2.74	3179.51±29.15	2260.01±39.32	1.02±0.02
	250-53 μm	1354.81±89.25	120.77±3.57	183.06±5.41	3224.68±8.37	3441.32±38.71	0.86±0.02
	53-20 μm	1610.85±98.69	113.25±2.49	181.77±12.33	3183.19±11.96	3864.67±3.66	0.75±0.01
	<20 μm	2061.85±127.71	108.03±2.57	176.10±10.02	2225.58±7.24	4364.35±12.11	0.56±0.01
	Bulk soil	1170.93±81.35	92.01±2.15	145.65±7.64	2245.97±27.70	2622.54±10.99	0.80±0.01
29-38 cm	2000-250 μm	337.46±62.59	35.19±0.68	87.83±2.27	624.75±13.13	522.28±22.95	1.05±0.05
	250-53 μm	479.29±67.65	42.03±2.59	93.50±4.87	609.94±19.72	816.84±14.38	0.78±0.02
	53-20 μm	626.12±101.69	44.47±2.07	102.51±7.38	664.79±0.30	1143.16±3.39	0.63±0.01
	<20 μm	717.43±99.56	46.91±2.14	101.11±3.26	675.68±2.96	1458.95±69.44	0.46±0.02
	Bulk soil	391.27±62.87	35.00±1.08	93.16±4.33	502.48±5.76	677.13±67.57	0.70±0.07
38-54 cm	2000-250 μm	295.43±43.76	24.87±1.12	83.05±1.72	238.53±3.04	375.13±33.60	0.65±0.06
	250-53 μm	398.96±51.97	39.87±2.34	100.25±0.91	464.49±3.08	656.59±17.12	0.69±0.02
	53-20 μm	531.59±71.27	47.90±1.49	108.58±5.82	585.72±0.79	897.83±0.45	0.63±0.01
	<20 μm	648.44±89.45	45.66±0.62	126.75±6.52	562.91±0.30	820.08±0.31	0.70±0.05
	Bulk soil	380.67±49.72	34.19±4.21	86.97±4.95	335.22±0.99	430.53±6.03	0.83±0.02
54-69 cm	2000-250 μm	296.10±60.82	24.91±0.75	77.01±2.46	243.90±0.61	205.05±0.03	1.18±0.02
	250-53 μm	389.32±64.54	34.07±1.60	84.92±3.57	397.92±14.43	453.49±0.98	0.83±0.02
	53-20 μm	462.97±73.53	39.41±0.98	94.14±4.10	497.15±2.14	725.83±0.73	0.67±0.01
	<20 μm	591.75±77.02	47.38±1.66	104.34±3.43	553.62±3.22	947.15±0.14	0.65±0.01
	Bulk soil	364.08±67.50	27.77±0.18	86.75±2.22	320.44±1.15	312.54±8.35	0.96±0.05

[a]C concentrations in mmol kg^{-1} in PP, HH, and DH extractable fractions obtained from TOC analysis in this study.

[b]C concentration in mmol kg^{-1} in residues after DH extraction, and

[c]C concentration in mmol kg^{-1} in un-extracted soil fractions or bulk soil obtained from EA combustion analysis in this study. The original unit from EA analysis (i.e. wt%) was converted to mmol kg^{-1} for easier comparison among different pools.

[d]Fraction C was calculated as:

$$Fraction\ C\ recovered = \left(\frac{Cpp \times Mpp + Chh \times Mhh + Cdh \times Mdh + Cdhr \times Mdhr + Cppr \times 0.2 + Chhr \times 0.2}{Csoil \times Msoil}\right)$$

where, 1) Cpp, Chh, and Cdh were C concentrations in mg g^{-1};

2) Mpp, Mhh, and Mdh were the mass in PP, HH, and DH extractable fractions in g by calculating the differences between original mass and residue mass after each extraction;

3) Mdhr was the mass of residue samples after DH extractions in g;

4) 0.2g was the subsample mass that was taken out after PP and HH extractions for residue C or Fe analysis;

5) Cppr, Chhr, Cdhr and Csoil were the C concentration in residue sample after PP, HH, and DH extractions and in bulk soil without extraction by converting wt% to mg g^{-1};
and 6) Msoil was the soil mass started the extraction procedure with, which is 1g in this study. Note that more than 97% of the soil mass was recovered in this study (data not shown).

Table S2-3. Mass fraction of selectively extractable (i.e. PP, HH, DH sequential extractions) C calculated from supernatant solutions. Note that the mass fraction is normalized to extracted C.

Soil depths	Size fractions	PP extractable C	HH extractable C	DH extractable C
0-29 cm	2000-250 μm	0.88±0.02	0.04±0.01	0.08±0.01
	250-53 μm	0.89±0.02	0.03±0.01	0.08±0.02
	53-20 μm	0.91±0.01	0.03±0.00	0.06±0.01
	<20 μm	0.95±0.00	0.02±0.00	0.03±0.00
	Bulk soil	0.81±0.03	0.05±0.01	0.14±0.02
29-38 cm	2000-250 μm	0.80±0.04	0.04±0.01	0.16±0.03
	250-53 μm	0.72±0.03	0.05±0.01	0.23±0.04
	53-20 μm	0.54±0.03	0.07±0.02	0.39±0.02
	<20 μm	0.71±0.02	0.10±0.01	0.19±0.01
	Bulk soil	0.60±0.04	0.07±0.01	0.33±0.03
38-54 cm	2000-250 μm	0.74±0.05	0.04±0.01	0.22±0.04
	250-53 μm	0.83±0.02	0.03±0.01	0.14±0.02
	53-20 μm	0.68±0.04	0.10±0.02	0.22±0.02
	<20 μm	0.86±0.03	0.05±0.01	0.10±0.02
	Bulk soil	0.74±0.06	0.06±0.02	0.19±0.05
54-69 cm	2000-250 μm	0.79±0.03	0.03±0.01	0.18±0.03
	250-53 μm	0.68±0.04	0.07±0.01	0.26±0.03
	53-20 μm	0.52±0.02	0.09±0.03	0.39±0.04
	<20 μm	0.61±0.05	0.10±0.02	0.29±0.04
	Bulk soil	0.75±0.03	0.04±0.01	0.21±0.03

Table S2-4. Concentrations (in mmol kg^{-1}) of selectively extractable (i.e. PP, HH, DH sequential extractions) Fe calculated from supernatant solutions.

Soil depths	Size fractions	PP extractable Fe[a]	HH extractable Fe[a]	DH extractable Fe[a]	Residual Fe[b]	Total Fe[c]	Fraction Fe recovered[d]
0-29 cm	2000-250 μm	11.77±0.74	2.74±0.11	12.45±0.44	355.76±33.15	454.19±20.26	0.73±0.08
	250-53 μm	32.00±0.99	2.97±0.11	15.77±0.71	n/a	615.92±24.40	n/a
	53-20 μm	38.80±0.97	2.31±0.13	19.15±0.65	n/a	728.79±29.20	n/a
	<20 μm	50.11±3.86	1.98±0.10	16.92±1.24	n/a	766.48±28.86	n/a
	Bulk soil	24.37±0.24	2.49±0.04	15.43±0.72	607.79±19.56	565.61±34.40	1.02±0.07
29-38 cm	2000-250 μm	6.38±0.22	2.37±0.11	9.43±0.30	454.85±9.68	455.33±6.95	0.96±0.03
	250-53 μm	10.45±0.94	2.06±0.12	12.70±0.27	576.44±13.58	753.91±13.72	0.75±0.02
	53-20 μm	13.69±0.68	1.98±0.09	14.07±1.64	446.13	552.04±36.05	0.78±0.05
	<20 μm	15.08±0.49	1.89±0.04	11.25±1.04	712.36±14.86	655.62±10.10	1.04±0.03
	Bulk soil	7.74±0.29	2.29±0.06	10.11±0.47	626.47±38.89	544.77±23.38	1.11±0.08
38-54 cm	2000-250 μm	5.01±0.26	1.67±0.17	7.54±0.60	384.83±16.54	414.04±26.65	0.88±0.07
	250-53 μm	8.73±0.25	1.68±0.08	11.18±0.46	n/a	629.41±24.99	n/a
	53-20 μm	11.97±0.38	1.64±0.05	15.11±0.48	n/a	701.56±5.89	n/a
	<20 μm	14.17±0.74	1.62±0.11	12.38±1.40	622.07±35.83	917.38±28.40	0.59±0.06
	Bulk soil	6.49±0.46	1.94±0.34	8.55±1.31	267.01±8.42	425.83±6.34	0.59±0.03
54-69 cm	2000-250 μm	2.78±0.36	1.49±0.19	9.44±0.72	n/a	299.95±14.77	n/a
	250-53 μm	5.47±0.92	1.75±0.12	11.36±0.49	n/a	283.56±13.38	n/a
	53-20 μm	9.47±1.09	1.58±0.14	11.23±0.88	503.44±6.16	889.05±47.06	0.55±0.03
	<20 μm	13.74±1.17	1.27±0.07	11.25±1.11	800.27±32.07	889.98±27.99	0.87±0.05
	Bulk soil	4.63±0.66	1.39±0.12	10.57±0.47	561.60±25.22	808.91±42.14	0.69±0.05

[a]Fe concentrations in mmol kg^{-1} in PP, HH, and DH extractable fractions obtained from ICP-OES analysis in this study.

[b]Fe concentration in mmol kg^{-1} in residues after DH extraction

[c]Fe concentration of un-extracted soil fractions or bulk soil in mmol kg^{-1} obtained from digestion and analysis

[d]Fraction Fe was calculated as:

$$Fraction\ Fe\ recovered = \left(\frac{Fepp \times Mpp + Fehh \times Mhh + Fedh \times Mdh + Fedhr \times (Mdhr + 0.4)}{Fesoil \times Msoil}\right)$$

where, 1) Fepp, Fehh, and Fedh were Fe concentrations in mg g^{-1};
2) Mpp, Mhh, and Mdh were the mass in PP, HH, and DH extractable fractions in g by calculating the differences between original mass and residue mass after each extraction;
3) Mdhr was the mass of residue samples after DH extractions in g. Note that 0.4g was added to this part of the calculation because PP and HH residue samples were not able to perform soil digestion analysis due to the limited amount of samples. Therefore, we assumed the subsamples of 0.2g taken from PP and HH residues had same concentrations

as Fedhr. This may introduce a slightly under- or over-estimation of recovery of Fe fraction.

4) Fedhr and Fesoil were the Fe concentration in residue sample after DH extractions and in bulk soil without extraction by converting mol kg^{-1} to mg g^{-1};

and 6) Msoil was the soil mass started the extraction procedure with, which is 1g in this study.

Table S2-5. Mass fraction of selectively extractable (i.e. PP, HH, DH sequential extractions) Fe calculated from supernatant solutions. Note that the mass fraction is normalized to extracted Fe.

Soil depths	Size fractions	PP extractable Fe	HH extractable Fe	DH extractable Fe
0-29 cm	2000-250 μm	0.62±0.05	0.05±0.01	0.33±0.04
	250-53 μm	0.75±0.03	0.03±0.01	0.22±0.03
	53-20 μm	0.76±0.02	0.02±0.00	0.22±0.02
	<20 μm	0.88±0.01	0.01±0.00	0.11±0.01
	Bulk soil	0.53±0.05	0.04±0.01	0.43±0.05
29-38 cm	2000-250 μm	0.48±0.03	0.07±0.01	0.45±0.03
	250-53 μm	0.34±0.02	0.07±0.02	0.59±0.04
	53-20 μm	0.19±0.02	0.05±0.02	0.75±0.03
	<20 μm	0.40±0.04	0.10±0.01	0.50±0.04
	Bulk soil	0.26±0.04	0.09±0.01	0.65±0.04
38-54 cm	2000-250 μm	0.40±0.02	0.09±0.02	0.51±0.02
	250-53 μm	0.56±0.02	0.04±0.01	0.40±0.02
	53-20 μm	0.34±0.05	0.06±0.01	0.59±0.04
	<20 μm	0.66±0.04	0.05±0.01	0.28±0.03
	Bulk soil	0.43±0.06	0.10±0.02	0.48±0.07
54-69 cm	2000-250 μm	0.29±0.06	0.07±0.03	0.64±0.05
	250-53 μm	0.21±0.02	0.07±0.02	0.72±0.03
	53-20 μm	0.19±0.01	0.08±0.02	0.74±0.02
	<20 μm	0.32±0.03	0.06±0.01	0.62±0.03
	Bulk soil	0.28±0.03	0.06±0.01	0.66±0.02

Table S2-6. Concentrations (in mmol kg^{-1}) of selectively extractable (i.e. PP, HH, DH sequential extractions) Ca calculated from supernatant solutions.

Soil depths	Size fractions	PP extractable Ca
0-29 cm	2000-250 μm	31.23±2.92
	250-53 μm	72.57±3.00
	53-20 μm	82.98±4.26
	<20 μm	99.09±3.64
	Bulk soil	55.93±2.01
29-38 cm	2000-250 μm	10.12±0.91
	250-53 μm	17.53±2.09
	53-20 μm	22.43±2.45
	<20 μm	25.25±2.52
	Bulk soil	11.72±1.11
38-54 cm	2000-250 μm	6.95±0.15
	250-53 μm	13.05±0.61
	53-20 μm	17.67±0.78
	<20 μm	20.32±1.44
	Bulk soil	9.45±0.21
54-69 cm	2000-250 μm	6.34±0.18
	250-53 μm	11.48±0.90
	53-20 μm	14.12±1.43
	<20 μm	18.39±2.29
	Bulk soil	8.22±0.55

Table S4-1. Properties of minerals provided by manufacturers.

Mineral name	Formula	Purity	Specific surface area (m^2 g^{-1})	Particle size (nm)	Manufacturer
Fe oxide	α-Fe_2O_3	99%	40-60	20-40	Skyspring nanomaterials.Inc
Al oxide	α-Al_2O_3	99.99%	6-9	300-800	Skyspring nanomaterials.Inc
Kaolinite	$Al_2O_3 \cdot 2SiO_2 \cdot 2H_2O$	n/a	8.3[a]	200nm-2000μm[a,b]	Sigma-aldrich (product number: 03584)
Bentonite	n/a	n/a	n/a	n/a	Laguna clay company
Sand in different sizes[c]	SiO_2	n/a	n/a	n/a	Laguna clay company

[a] Values from Brennan et al., 2014, published at Science of the Total Environment journal.
[b] Size distribution of kaolinite is 9% of 20-2000μm, 80% of 2-20μm, and 11% of 0.2-2μm, according to Brennan et al., 2014.
[c] Kaiser et al., 2014.

APPENDICES

FIGURES

FIGURES

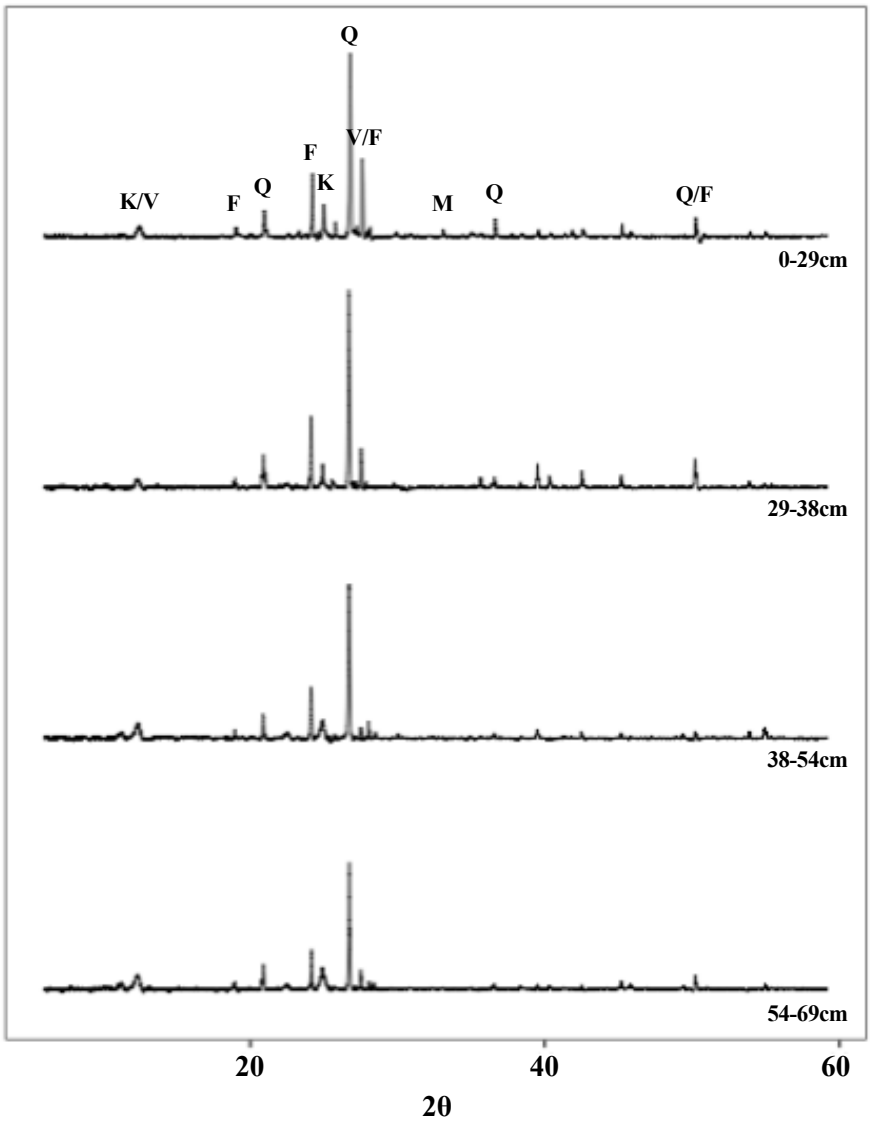

Figure S2-1. X-ray diffractograms of Musick soils along soil depths from XRD analysis (Q: quartz, M: mica, F: feldspar, K: kaolinite, V: vermiculite).

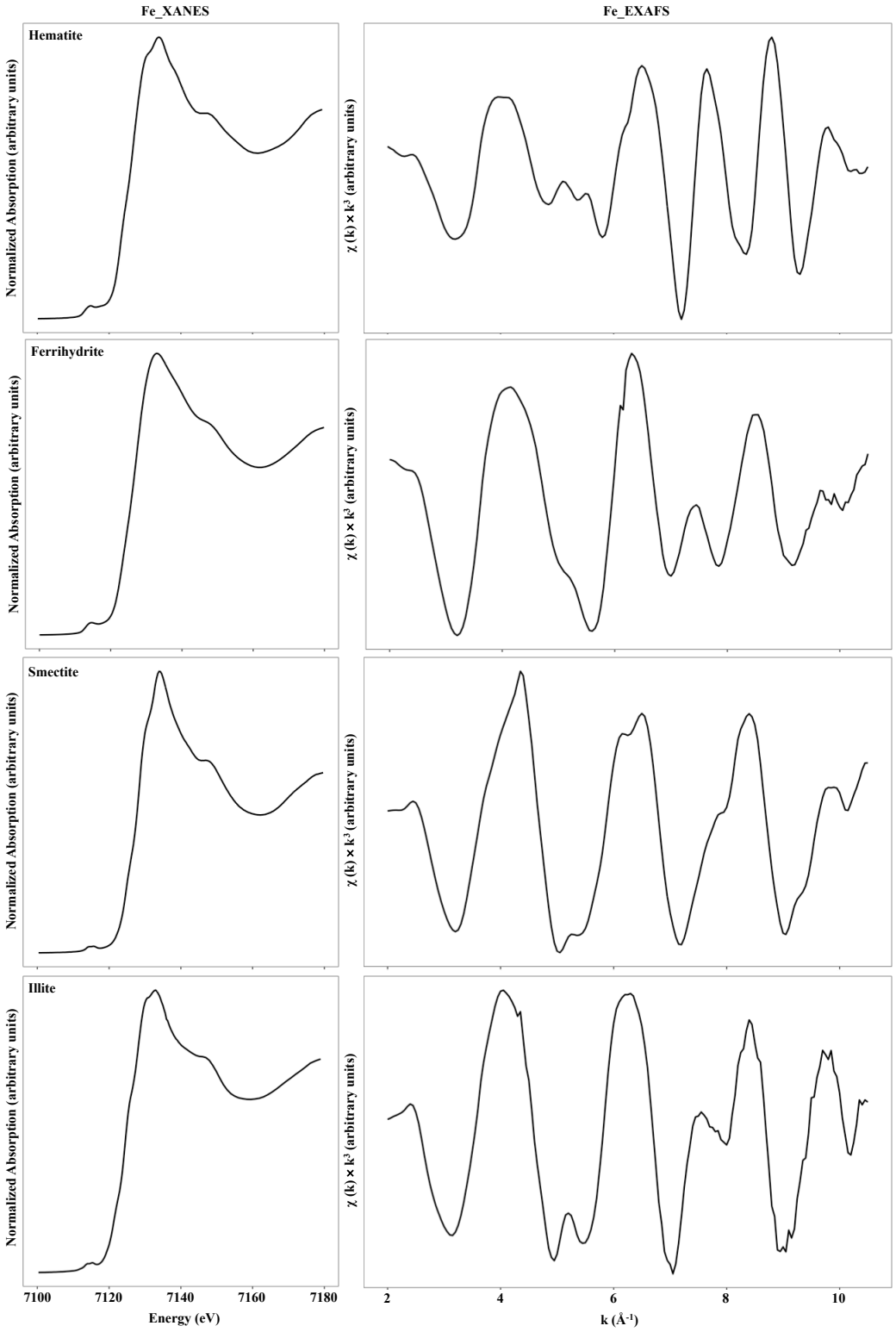

Figure S2-2. Iron reference compounds for XAS analysis.

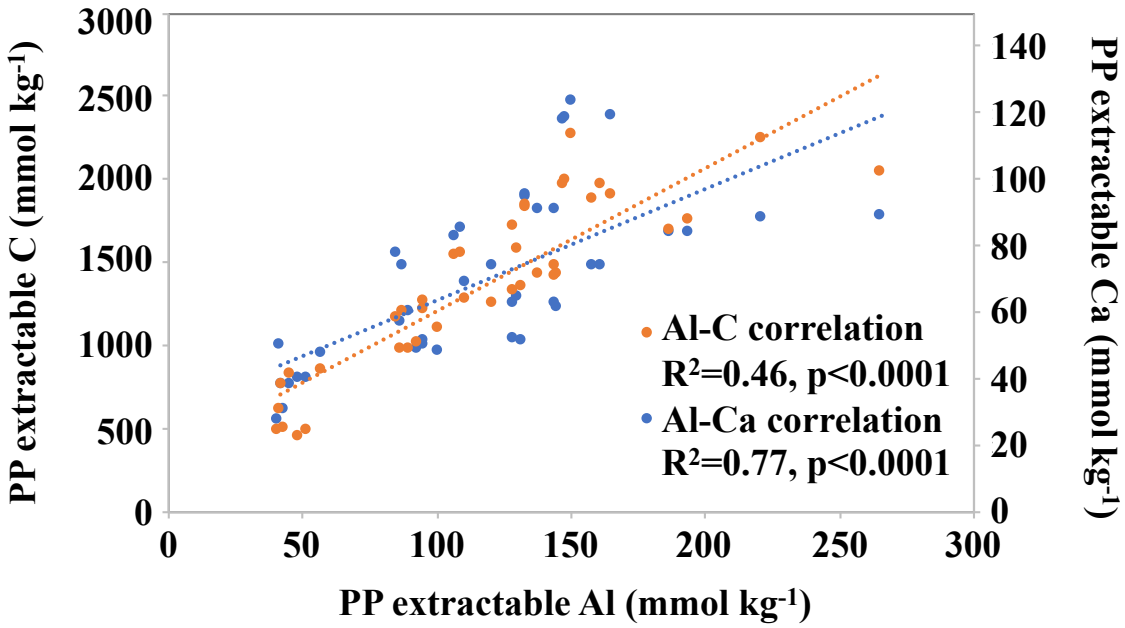

Figure S2-3. Correlations between concentrations of PP-extractable Al and Ca (data in blue) or C (data in orange) in A horizon. Given regression lines are significant at $p<0.0001$.

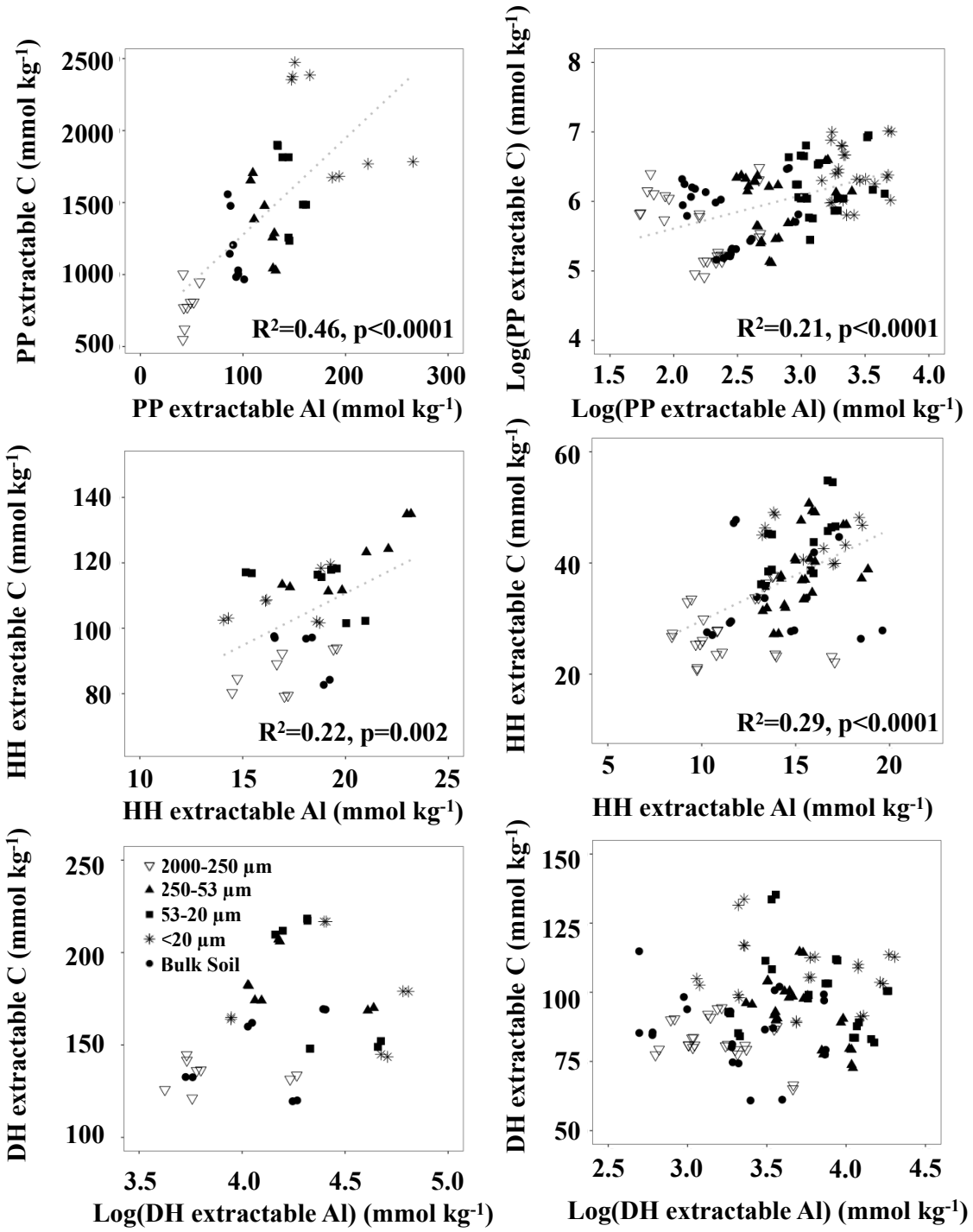

Figure S2-4. Correlations between concentrations of PP-, HH-, and DH-extractable Al and extractable C in different size aggregates in A (left) and B horizon (right).

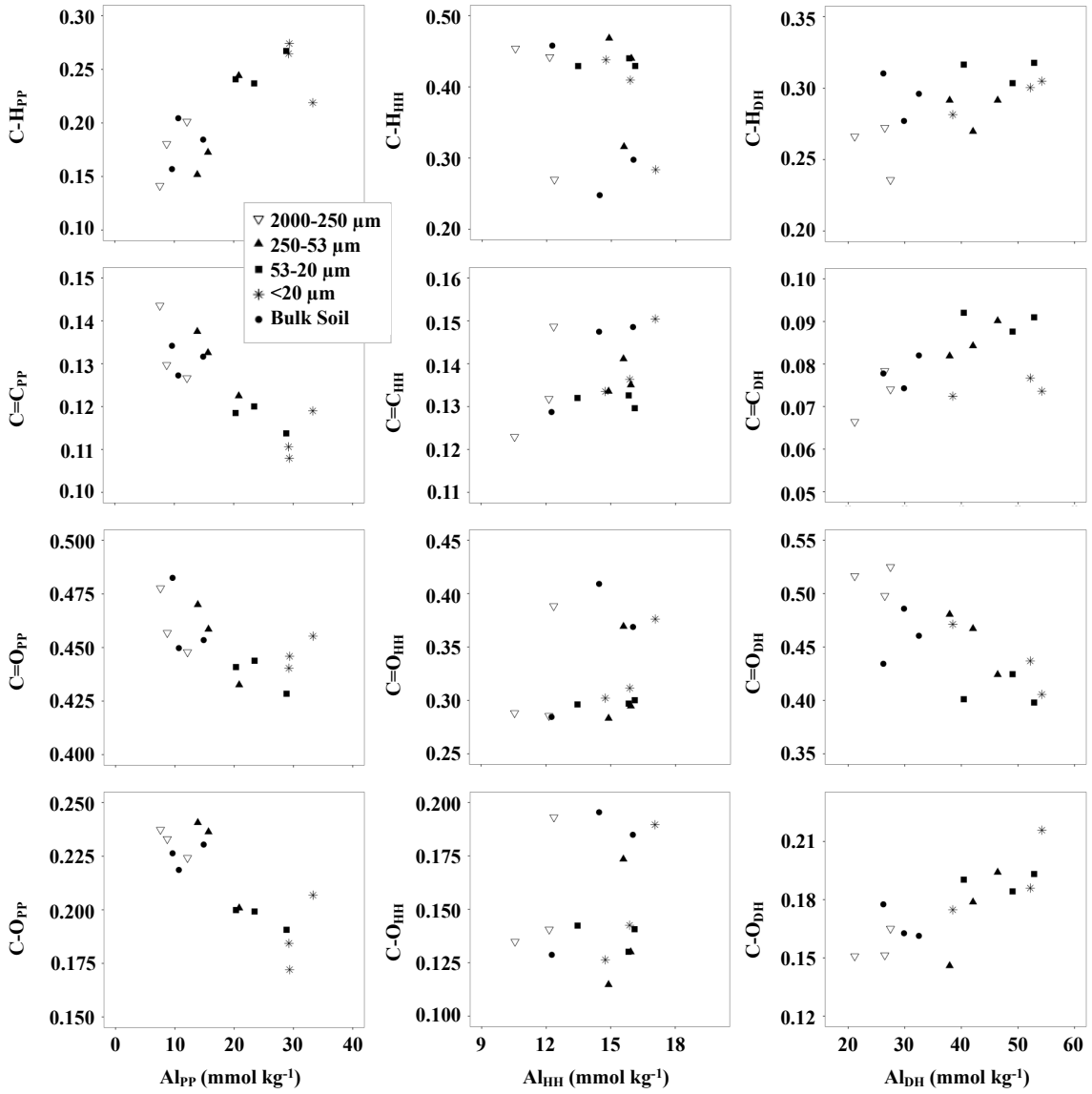

Figure S3-1. Comparisons between relative peak areas of C functional groups or structure and extractable Al concentrations.

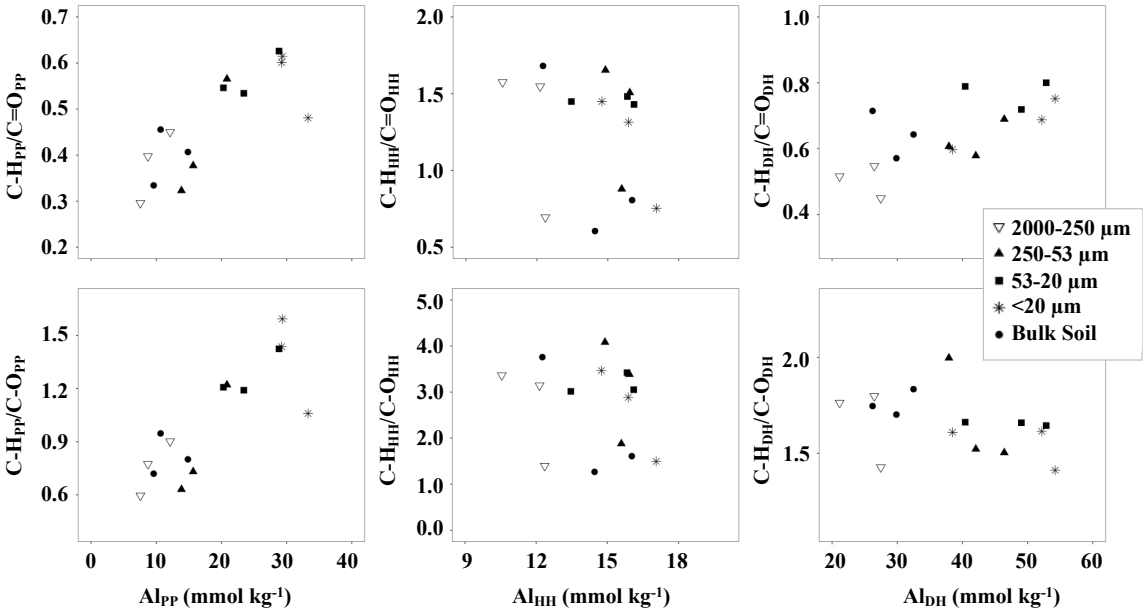

Figure S3-2. Correlations between ratios of aliphatic C-H to carbonyl C=O or carboxyl C-O and pedogenic Al in PP (left panel), HH (middle panel), and DH (right panel) extractable fractions.

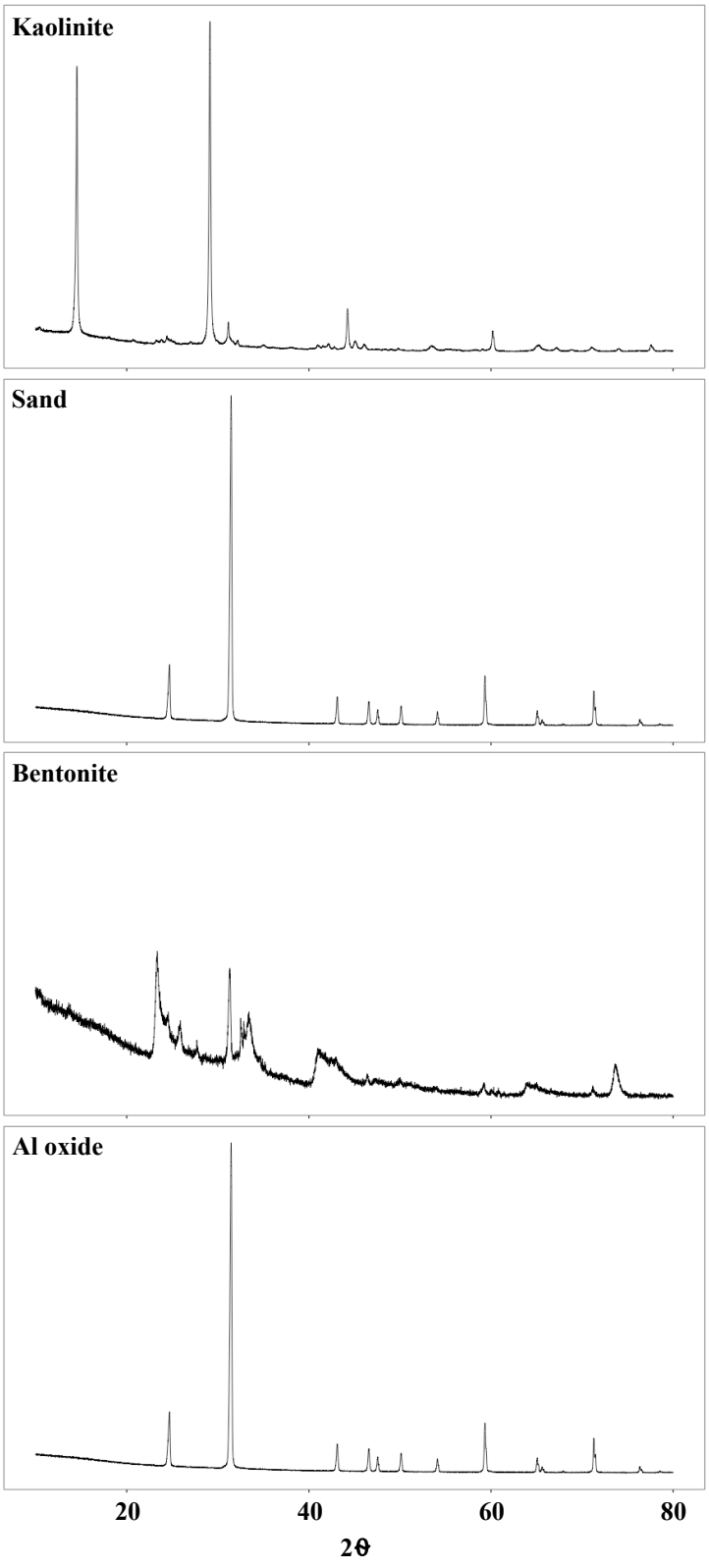

Figure S4-1. XRD results for minerals used to create artificial soils.

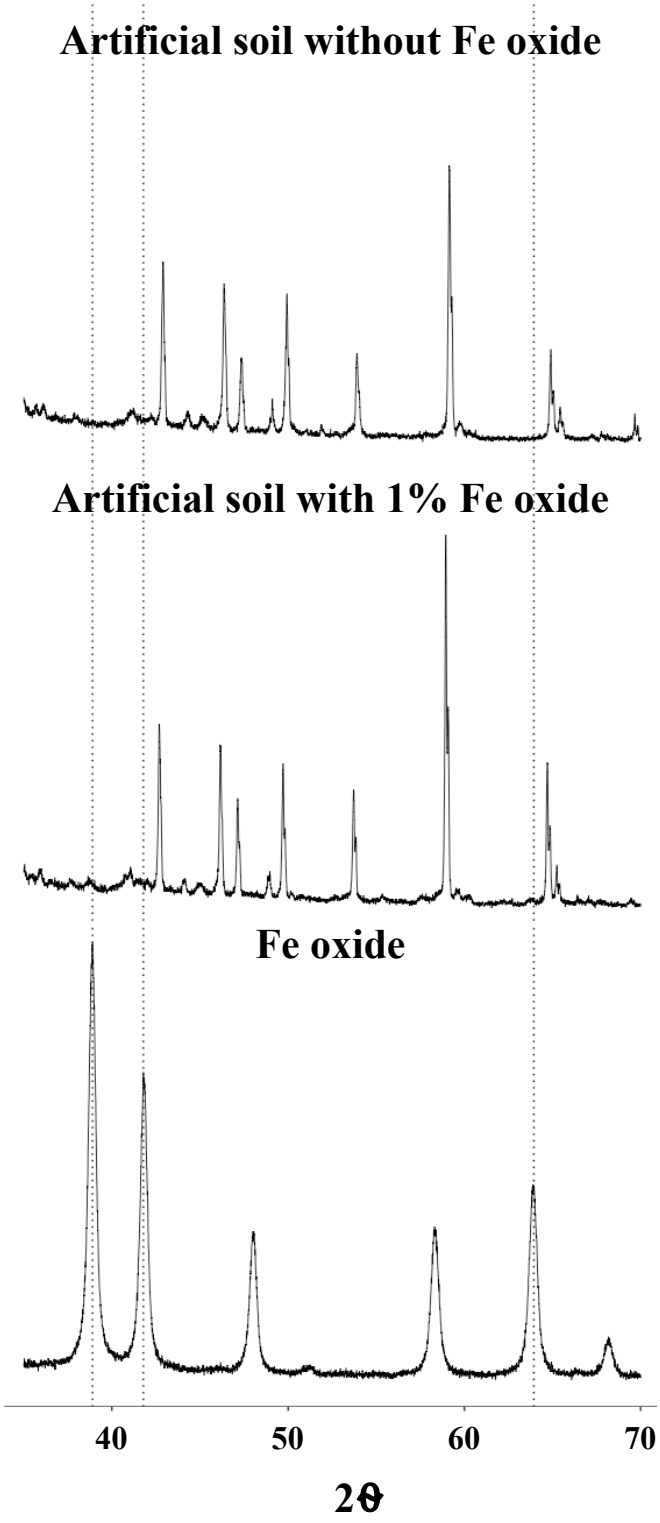

Figure S4-2. XRD results for artificial soils with and without Fe oxides.

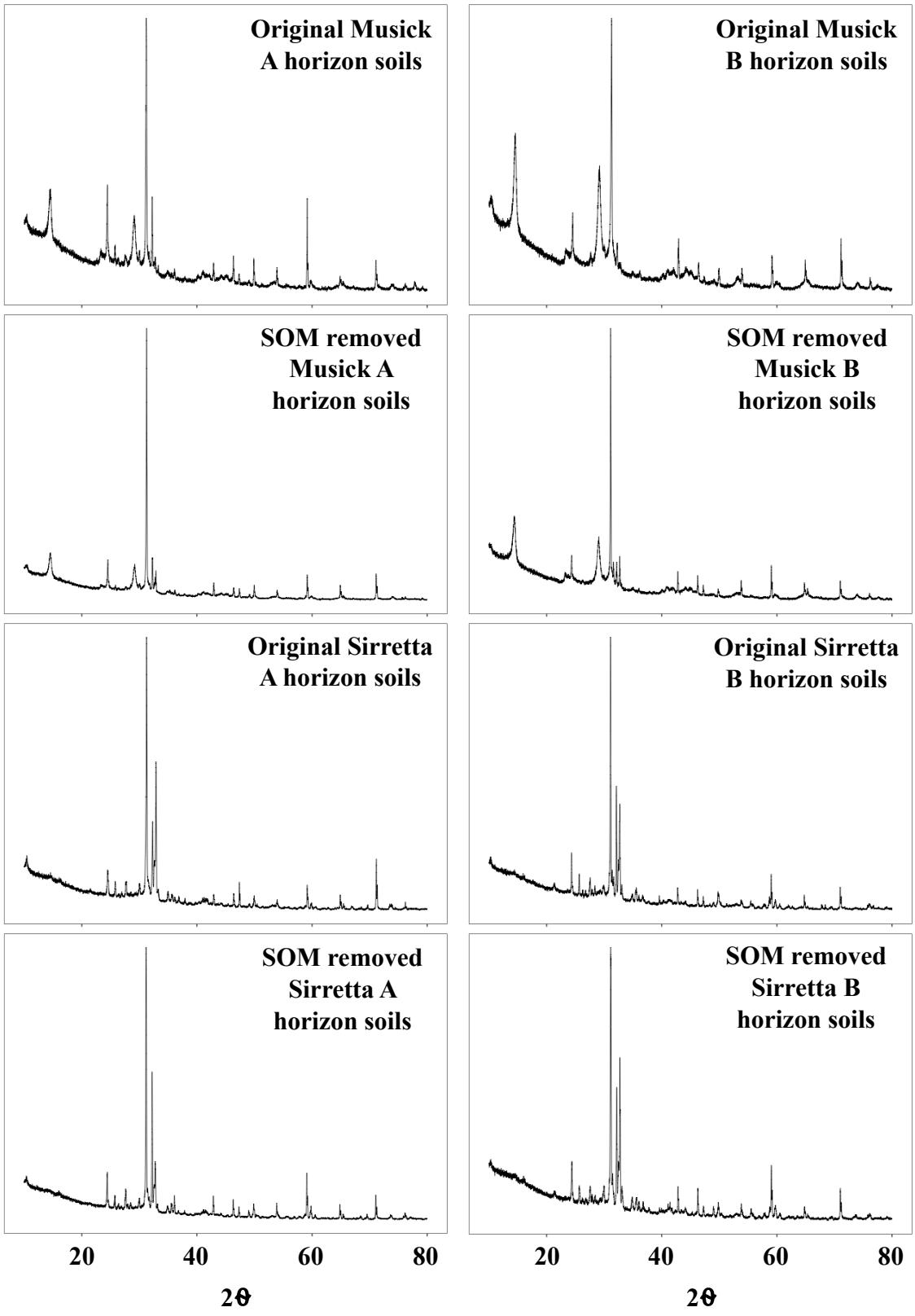

Figure S4-3. XRD results for original and SOM removed natural soils.